Final Report
Agreement T2695, Task 30
Cotton Duck Pad Design

Cotton Duck Bearing Pads: Engineering Evaluation and Design Recommendations

by

Dawn E. Lehman, Charles W. Roeder, Russell Larson, and Kevin Curtin

Department of Civil and Environmental Engineering
233B More Hall
University of Washington, Box 352700
Seattle, Washington 98195-2700

Washington State Transportation Center
University of Washington, Box 354802
1107 NE 45th Street, Suite 535
Seattle, Washington 98105-4631

Washington State Department of Transportation
Technical Monitor
Ralph Dornsife
Bridge Design Section, Bridges and Structures

Prepared for

Washington State Transportation Commission
Department of Transportation
and in cooperation with
U.S. Department of Transportation
Federal Highway Administration

November 2003

TECHNICAL REPORT STANDARD TITLE PAGE

1. REPORT NO.	2. GOVERNMENT ACCESSION NO.	3. RECIPIENT'S CATALOG NO.
WA-RD 569.1		

4. TITLE AND SUBTITLE	5. REPORT DATE
COTTON DUCK BEARING PADS: ENGINEERING EVALUATION AND DESIGN RECOMMENDATIONS	November 2003
	6. PERFORMING ORGANIZATION CODE
7. AUTHOR(S)	8. PERFORMING ORGANIZATION REPORT NO.
Dawn E. Lehman, Charles W. Roeder, Russell Larson, Kevin Curtin	
9. PERFORMING ORGANIZATION NAME AND ADDRESS	10. WORK UNIT NO.
Washington State Transportation Center (TRAC) University of Washington, Box 354802 University District Building; 1107 NE 45th Street, Suite 535 Seattle, Washington 98105-4631	11. CONTRACT OR GRANT NO. Agreement T2695, Task 30
12. SPONSORING AGENCY NAME AND ADDRESS	13. TYPE OF REPORT AND PERIOD COVERED
Research Office Washington State Department of Transportation Transportation Building, MS 47372 Olympia, Washington 98504-7372 Keith Anderson, Project Manager, 360-709-5405	Research Report 14. SPONSORING AGENCY CODE

15. SUPPLEMENTARY NOTES

This study was conducted in cooperation with the U.S. Department of Transportation, Federal Highway Administration.

16. ABSTRACT

Cotton duck bearing pads (CDP) are sometimes used to support loads and accommodate movements and rotations at bridge bearings. CDP are preformed elastomeric pads consisting of thin layers of elastomer interlaid with fabric, and they are manufactured under military specifications with limited guidance from the AASHTO. The behavior of these CDP bearing pads was experimentally evaluated to establish design models for predicting this behavior, to determine the variation in behavior expected with different bearing pad manufacturers, and to develop design recommendations. This research is a follow-up study of an earlier research program sponsored by Arkansas State University.

CDP bearing pads from three different manufacturers were tested, and the test program included dynamic and static (or monotonic) tests of bearings in shear, compression, and rotation. In general, the static tests were used to evaluate strength, stiffness, deformation limits, and general pad behavior. The dynamic tests examined durability and performance under repeated loading and deformation.

The results of this test program were used to develop design recommendations, and an appendix includes a draft of proposed wording for modification of the AASHTO LRFD Specifications to include these design recommendations. In addition, a spreadsheet was developed in Microsoft EXCEL to accomplish the calculations necessary to complete the design.

17. KEY WORDS	18. DISTRIBUTION STATEMENT
Cotton duck bearing pads, CDP, bridge bearings, bridge design,	No restrictions. This document is available to the public through the National Technical Information Service, Springfield, VA 22616

19. SECURITY CLASSIF. (of this report)	20. SECURITY CLASSIF. (of this page)	21. NO. OF PAGES	22. PRICE
None	None		

Disclaimer

The contents of this report reflect the views of the authors, who are responsible for the facts and the accuracy of the data presented herein. The contents do not necessarily reflect the official views or policies of the Washington State Transportation Commission, Department of Transportation, or the Federal Highway Administration. This report does not constitute a standard, specification, or regulation.

Contents

Figures

Tables

EXECUTIVE SUMMARY

Cotton duck bearing pads (CDP) may be used to support bridge loads while accommodating translational movements and rotations. CDP are preformed, elastomeric pads consisting of thin layers of elastomer interlayed with fabric, and they are manufactured under Military Specifications with limited guidance from AASHTO Specifications. To improve the understanding and engineering of CDP, an experimental research study was undertaken to develop design guidelines and to establish the variation in behavior expected with different bearing pad manufacturers.

The test program evaluated the response of CDP to dynamic and static (or monotonic) tests in shear, compression and rotation. CDP bearing pads from three different manufacturers were tested. Forty-four static, 17 cyclic, and 10 long duration (creep) compression tests were completed. Seventeen static rotation, 28 dynamic rotation, 10 static shear, and 8 dynamic shear tests were performed. In general, the static tests evaluated strength, stiffness and deformation limits, while dynamic tests examined durability under repeated loading. These research data, combined with data from an earlier research program sponsored by Arkansas State University, were used to develop design recommendations and a proposal for modification of the AASHTO LRFD Specifications.

The research showed that CDP tolerates significant compressive stress and rotation but limited shear deformation. These capacities depend upon the stiffness and deformation capacity of the CDP and vary from manufacturer to manufacturer. To assure adequate performance from CDP, quality control testing measures were developed. Pads that meet these quality control standards develop maximum compressive strains due to compression and rotation of approximately 0.25 in/in before sustaining diagonal shear fracture.

Delamination or secretion of oil and wax from the CDP are the common serviceability limit states for CDP. To control delamination, compressive stress limits of 3000 psi for maximum stress due to total dead plus live load and 2000 psi for stress due to live load are recommended. Dynamic, or cyclic, rotation, which induces uplift or partial separation of the pad from the load surface, may cause delamination and reduced service life. Uplift damage depends upon the maximum total rotation, as well as the

rotation range caused by the live load variation, and separate rotation limits are provided. Shear deformation is limited for CDP because interlayer splitting occurs at larger shear strains, but this limitation is frequently overcome by the addition of a PTFE sliding surface.

CHAPTER 1
INTRODUCTION

1.1. INTRODUCTION

Bridge bearings support large loads while accommodating translational movements and rotations. Loads are induced by structural weight, truck traffic, braking and acceleration, wind, and earthquakes. Movements and rotations are caused by deflections due to dead and live loads, construction tolerances, creep, shrinkage, and seismic deformations. Support of loads requires significant stiffness and resistance, but movements and rotations require flexibility. As a result, bridge bearing design requires a balance of multi-directional movements and restraint forces. Loads may be supported in one direction, while movements are permitted in others.

Cotton duck bearing pads (CDP) are sometimes used to meet these diverse requirements (Van Lund 1996). CDP are preformed elastomeric pads consisting of thin layers of elastomer interlaid with fabric, and they are manufactured under military specifications (MIL-C-882-E 1989) with limited guidance from the AASHTO Specifications (AASHTO 1994, AASHTO 1996). The fabric may be cotton or polyester, and CDP bearings are stiff with large compressive load capacity. However, CDP-specific design rules are incomplete because of the limited knowledge of their behavior.

Historically, CDP design was based on rules developed for unreinforced elastomeric bearing pads (PEP) and modified to account for the larger compressive stress capacity and bearing pad stiffness. The translational movement and rotational capacity of CDP are limited in the AASHTO LRFD (AASHTO 1994) and Standard Specifications (AASHTO 1996). The limit on translational movement capacity may be overcome by adding a polytetrafluorethylene (PTFE) sliding surface. The limit on rotation has historically been severe, but a slight relaxation was permitted in the 2001 Interim LRFD Specifications because of a review of recent research (Roeder 1999).

A more recent research study on CDP was sponsored by the Arkansas State University (Roeder, Lehman, and Larsen 2002), and it showed that CDP have significant compressive stress and rotational capacities. However, this previous test program was limited to pads

of a single manufacturer. This report describes a follow-up study that was developed to understand the variation in performance expected from different CDP manufacturers and to develop design recommendations.

1.2. BACKGROUND AND OVERVIEW

Design methods have been developed for reinforced elastomeric bearings (Stanton and Roeder 1982, and Roeder and Stanton 1983), and these methods have been adapted to PEP and CDP. Elastomers are flexible materials without adequate natural stiffness to support large gravity loads. Compressive load resistance is achieved by reinforcing the rubber layer, as illustrated in Figure 1.1. An unreinforced elastomer would deform outward when subjected to a compressive load, as illustrated in Figure 1.1a, but the stiff reinforcement layer restrains the outward movement of the elastomer, as shown in Figure 1.1b. Thus, the deformation of a reinforced elastomeric bearing is the superposition of figures1.1a and 1.1b to produce the stress and strain state illustrated in Figure 1.1c.

The restraint provided by reinforcement may stiffen the bearing in compression by many orders of magnitude. The shape factor, S, of the bearing provides an index of this stiffening effect and is given in Equation 1.1.

$$S = \frac{\text{Plan Area}}{\text{Perimeter Area of Layer}} = \frac{L\,W}{2\,(L+W)\,t} \qquad \text{(Eq. 1.1)}$$

In the expression, L and W are the length and width of the plan dimensions of a rectangular bearing, and t is the elastomer layer thickness. The bulging deformation induces shear strain, which depends on the shape factor and the compressive load. Thus, elastomeric bearing design consists of limiting the elastomer shear strain by controlling the shape factor to achieve the required strength and stiffness.

CDP has many closely spaced layers of fabric reinforcement, and it is sometimes claimed that the shape factor does not apply to the design of CDP (Fabreeka 2002, Blake and Pfeifer, 1997, and Roeder, 1999). The CDP fabric resists the outward deformation of the elastomer and stiffens the bearing, but the fabric is more flexible than the steel layers of reinforced elastomeric bearings. Furthermore, CDP also have an overall shape factor effect due to friction at the stiff loading surfaces. These competing influences obscure the proper definition of S for CDP and the influence of shape factor for CDP. The most realistic

definition of S for CDP bases S on the total pad thickness and recognizes the increased stiffness caused by closely spaced fabric layers as a material stiffening effect. This approach is used in this report.

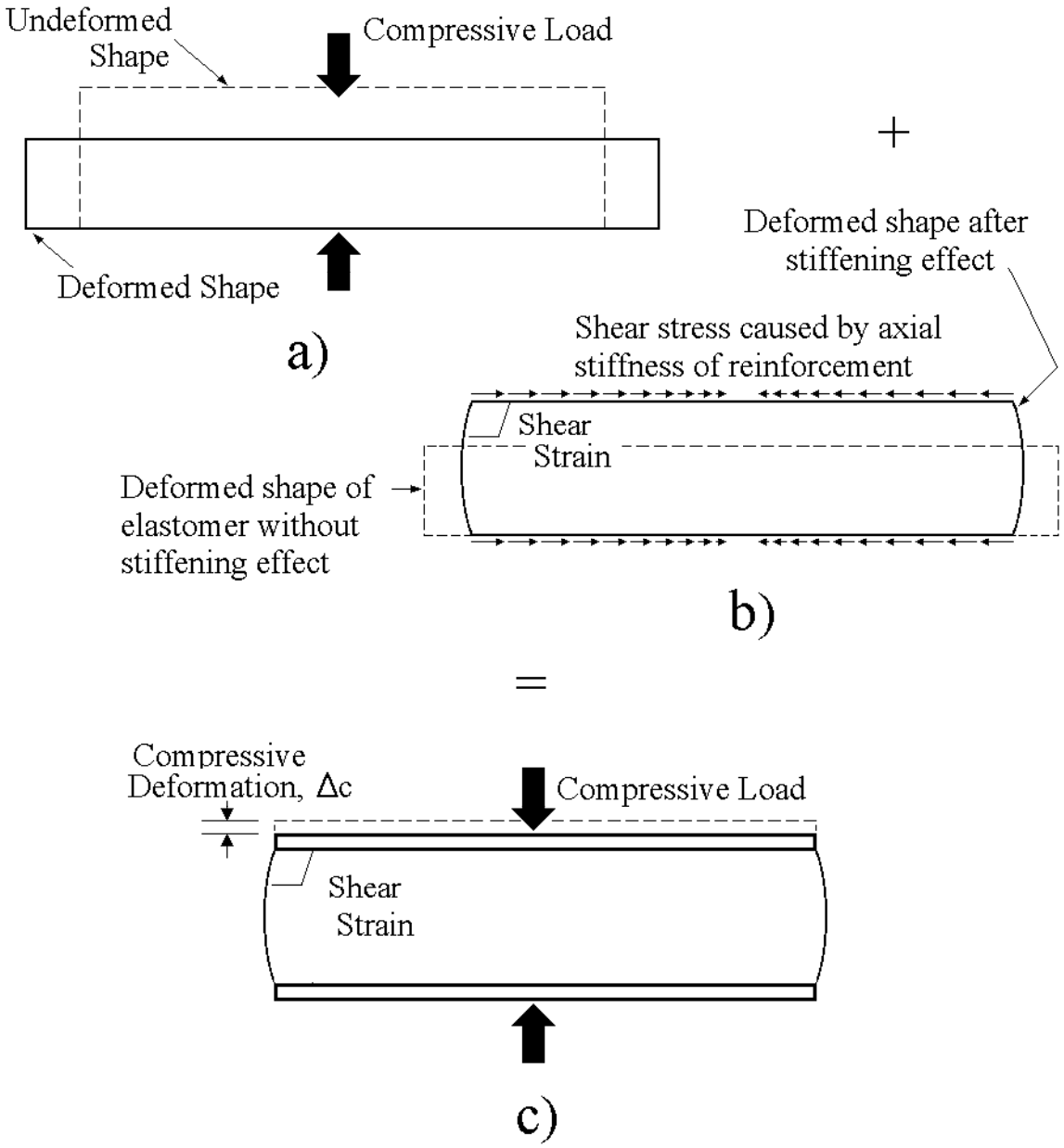

Figure 1.1 Deformation of Elastomeric Bearing Under Gravity Loads
a) Deformation of an Unreinforced Elastomer Layer; b) Shear Stress and Deformation Caused by Reinforcement; and c) Final Deformation of Reinforced Elastomer

For steel reinforced elastomeric bearings, bridge movements are accommodated by shear deformation of the elastomer, as illustrated in Figure 1.2. The reinforcement has

little influence on the shear stiffness of the elastomer. The layers of CDP are closely spaced, and there are many of them. These closely spaced layers provide a significantly larger shear stiffness and smaller shear deformation capacity than noted for other elastomeric bearing types. As a consequence, translational movement capacity for CDP cannot be based on the research findings and design guidelines for plain or steel reinforced elastomeric bearings.

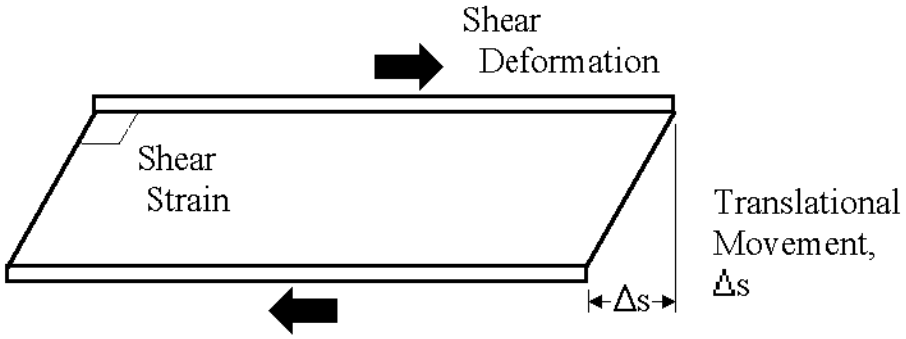

Figure 1.2. Deformation of Elastomeric Bearing Under Translational Movement

Rotation of reinforced elastomeric bearings deforms the rubber, as illustrated in Figure 1.3, and the rotational capacity is limited by the maximum shear strain in the elastomer and uplift of the superstructure from the bearing. This shear strain depends on the material properties and geometry of the reinforced bearing [(Gent and Meinecke, 1970, Stanton and Roeder, 1982)]. Uplift may overload one edge of the bearing while simultaneously unloading the opposing edge. Hydrostatic tensile stresses are damaging to elastomers and may occur at the unloaded edge. As a consequence, the present procedure for preventing uplift of reinforced elastomeric is conservatively defined as follows [(AASHTO 1996)]:

$$\theta \leq \frac{2\,\Delta_c}{b}. \qquad \text{(Eq. 1.2)}$$

where Δ_c and θ are the average compressive deformation and the rotation per layer, respectively, and b is the dimension of the bearing pad in the plane of rotation. The rotation of PEP is handled in a similar manner, but the shear strains and Δ_c are inherently larger for PEP than for reinforced elastomeric bearings because of their reduced stiffness.

The rotation of CDP follows a similar line of reasoning, but the mechanics of the rotation of CDP are not well understood.

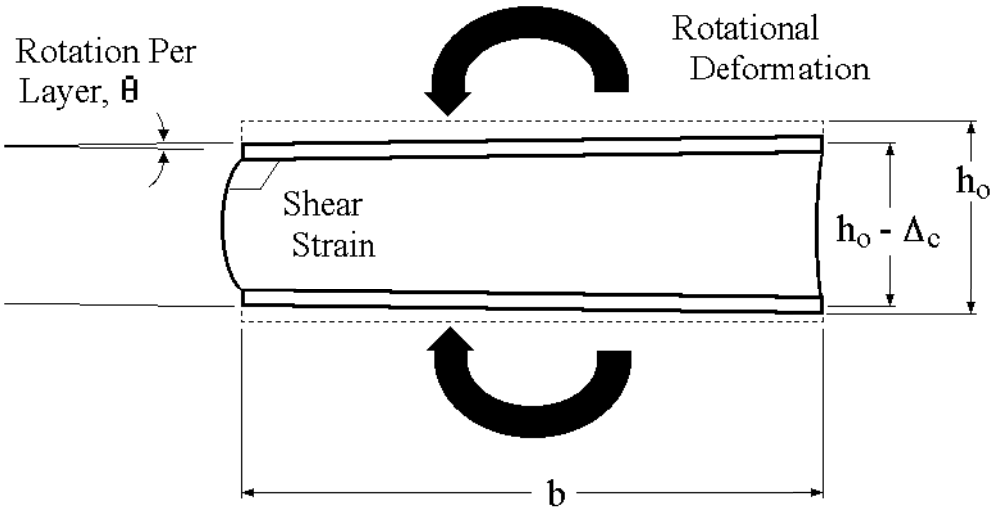

Figure 1.3. Deformation of an Elastomeric Bearing Subjected to Rotation

1.3. PREVIOUS RESEARCH RESULTS FOR CDP

Reinforced elastomeric bearing behavior is well understood, but the limitations in understanding the behavior of CDP are quite severe because of limited experimental data. Monotonic compression tests (Blake and Pfeifer 1997) were performed on CDP bearing pads in the mid-1990s. Those tests showed that the compressive load capacity of CDP is large in that the ultimate compressive stress exceeded 10 ksi. The influence of shape factor is much less pronounced for CDP than for steel-reinforced elastomeric bearings and PEP, as seen by comparing figures 1.4a, b, and c. Little information on shear or rotation was provided. This limited information was synthesized to develop improved AASHTO design provisions, which were adopted into the 2001 Interim AASHTO Specifications (Roeder, 1999).

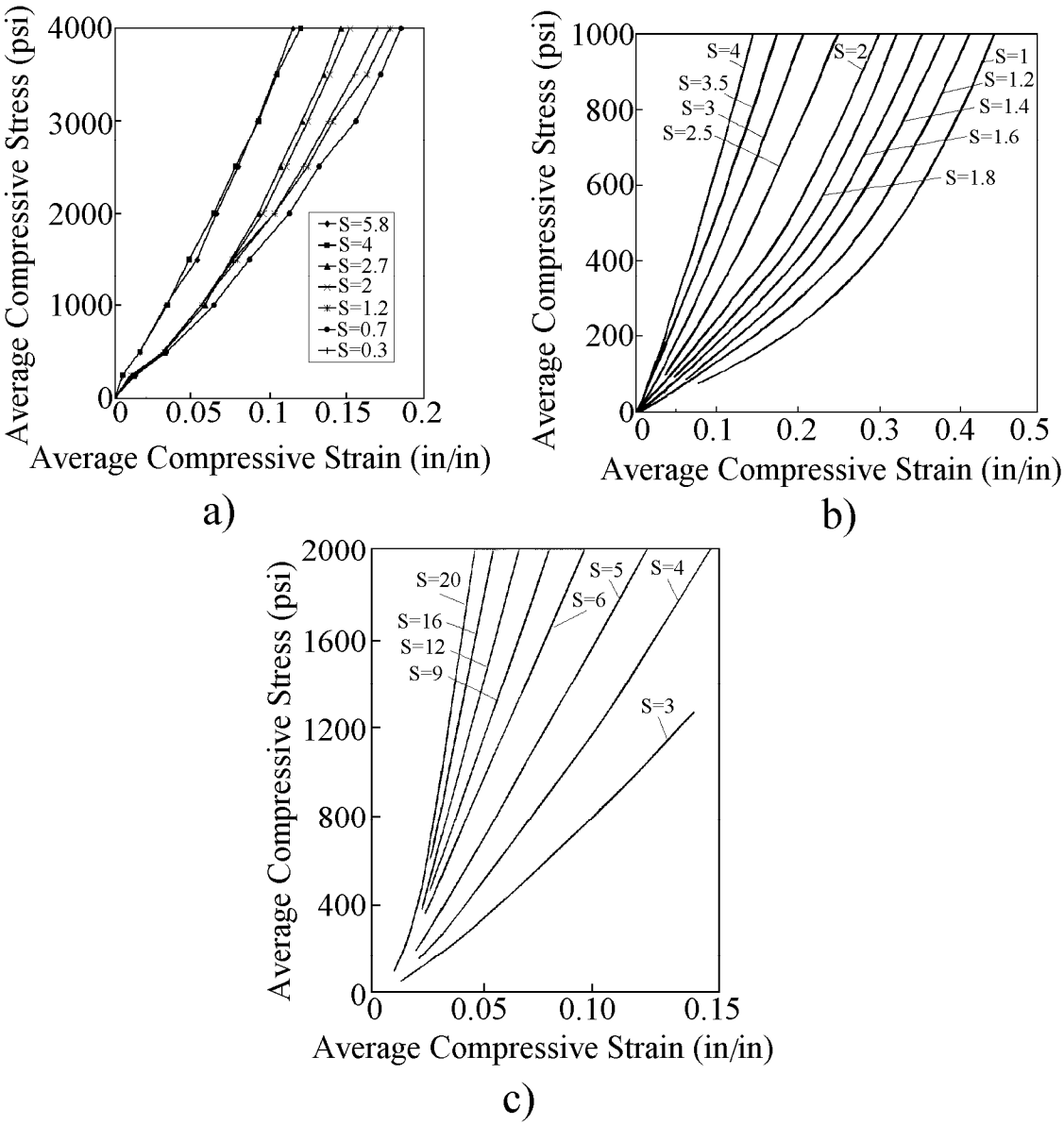

Figure 1.4. Average Compressive Stress and Strain as Function of Shape Factor; a) CDP , b) PEP, and c) Steel Reinforced Elastomeric Bearings

A more recent comprehensive research study (Roeder, Lehman, and Larsen 2002) was completed on CDP bearing pads provided by a single manufacturer. Eighteen static compression tests and ten cyclic compression tests were completed; six of the static compression tests were long-duration tests to evaluate creep and relaxation. Nine static shear and eight dynamic shear tests were completed. Seventeen static rotation and sixteen cyclic rotation tests were completed. The static tests were used to evaluate strength, stiffness, and deformation limits. The dynamic tests examined durability and

performance under repeated loadings and deformations. The intermediate and final damage states from these tests were as follows:

- Category A - No observable damage (see Figure 1.5a).
- Category B - No damage other than secretion of oil or wax (see Figure 1.5b).
- Category C - Delamination of CDP layers (see Figure 1.5c).
- Categories D and E - Fracture, cracking or splitting (see figures 1.5 d, e, and f).

Category A behavior occurred at lower stress, stress range, strain and deformation. Category B behavior was commonly noted on bearings that were subjected to somewhat greater stress and longer duration of loading than the Category A bearings. Both Category A and B bearing pads were fully functional after testing was complete. Category C represented intermediate damage with varying degrees of deterioration without immediate loss in resistance or deformation capacity. This delamination occurred during dynamic or repeated loading, and the damage was usually more severe on pads subjected to a larger cyclic stress range and maximum stresses or strains. Damage in categories D and E consisted of cracking, fracture, or splitting of the CDP, and this damage was strongly influenced by the maximum strain level. Bearings with D and E damage were not functional after testing and would require immediate replacement.

The short-term static compression test specimens developed at least 10 ksi compressive stress before failure, and many achieved compressive stresses in excess of 14 ksi. The compressive stress-strain behavior was nonlinear. Pad thickness interacted with the shape factor and also affected bearing pad behavior. The thicker, 1.5- and 2-inch pads were stiffer and tended to have different failure modes than the thinner, 0.75-inch pads. Category D fractures were noted at compressive strains in excess of 0.25 in/in. These were dramatic, brittle fractures where diagonal cracks propagated through the pad in a zigzag pattern. The creep tests commonly exhibited oil secretion or Category B behavior. The ratio of the steady state, long-term compressive strain to the short-term compressive strain for the same given stress level varied between 1.8 and 2.4. Specimens subjected to dynamic compressive loading typically exhibited only Category A, B, or C

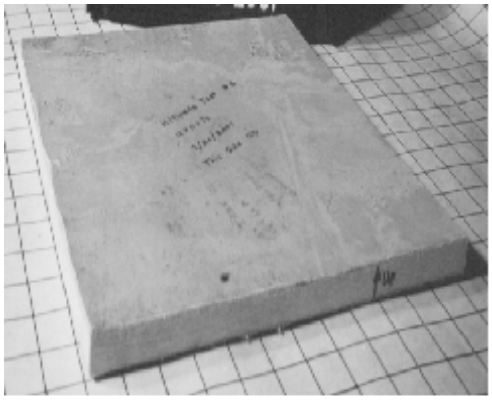

a) Category A - No Visible Damage

b) Category B - Secretion

c) Category C - Delamination

d) Category D - Diagonal Fracture

e) Category D - Diagonal Fracture

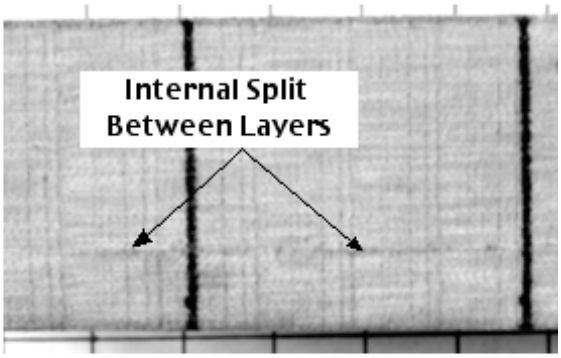

f) Category E - Shear Splitting

Figure 1.5. Typical CDP Bearing Pad Damage

damage, with several sustaining significant Category C delamination and Category B oil secretion. Delamination and oil secretion increased as the maximum compressive stress level and cyclic stress range increased. Dynamic strains under repeated loading were significantly larger than the short-term loading strains, but they were conservatively bound by the creep test results.

The shear tests were influenced by slip, and the coefficient of friction between steel and CDP was approximately 0.2. In some tests, restrainer or keeper bars were used to prevent this slip and permitted development of large shear deformations for some tests, but the increased strains precipitated internal splitting or cracking (Category D) failures at larger strain levels.

Rotation experiments showed that CDP have significant rotational capacity, and the moment-rotational behavior is quite stable under dynamic and repeated loading. Category D fractures were noted when the combined compressive strain due to rotation and axial compression exceeded 0.25 in/in. These fractures were similar to the compression fractures in that they initiated at a corner and progressed diagonally through the pad, but the rotation fractures were less extensive than those noted in the compression tests. Category C delamination was noted in some dynamic rotation tests in regions where cyclic uplift was noted as a result of bearing rotation.

1.4. MANUFACTURE OF COTTON DUCK BEARING PADS

As noted earlier, CDP are manufactured under Military Specification MIL-C-882-E (MIL-C-882-E 1989). This specification provides basic geometry, layer spacing, fabric orientation, and manufacturing tolerances; however, it does not specifically relate to bridge bearings nor does it discuss or address bridge bearings. The specification is relatively vague in many requirements, in that it has no material requirements for the elastomer compound and rather broad requirements regarding the properties of the fabric.

The specification has some very clear quality control requirements in that random sample selection and testing requirements are defined. The specification requires testing of samples from manufactured lots of CDP and prescribes acceptable variability and acceptance requirements for the finished product. The military specification requires testing of 2- x 2-inch pads under a controlled test procedure, which is also defined. The

acceptance criteria require that the test pads fall between a minimum and maximum stiffness range. The acceptable strains vary slightly with pad thickness, but Figure 1.6 shows the approximate range of acceptable behavior. The specification also requires that tests be completed to establish the acceptable permanent set of the CDP under compressive load. These quality control tests were evaluated as part of this research study; however, it is unclear that these tests are presently being completed on every production lot of CDP because the tests are not presently required by the AASHTO Specifications. Furthermore, it is not clear that the military specification is in force for military applications.

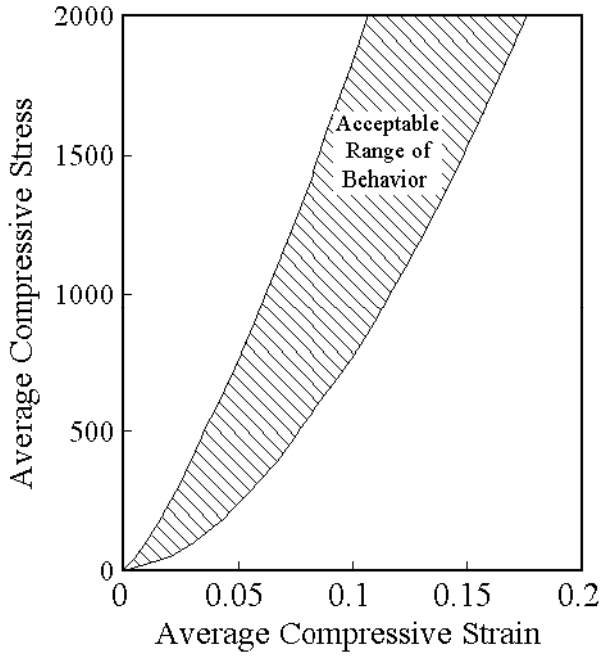

Figure 1.6. Stress-Strain Limits for CDP from Military Specification

Several manufacturers produce CDP in the U.S., but the pads are normally marketed to bridge engineers through a distribution company. Voss Engineering, Inc, of Lincolnwood, Illinois, is one such distribution company. Mr. Glenn Adams of Voss Engineering provided advice on the size selection of bearing pads for this study. The test bearing sizes and geometries were selected to reflect the full range of variation commonly expected in current bridge applications. Mr. Doug Martin of this same firm

provided continuing advice to the research team regarding the use of CDP in bridge applications, and he coordinated the supply of bearings for the research. The bearings were provided by three of the largest manufacturers in the U.S. at no cost to the research program. The research was a blind test in that the researcher team did not know the identity of the individual producers. These manufacturers are identified as Manufacturer A, Manufacturer B, and Manufacturer C in this report. Figure 1.7 shows a photo of similar pads provided by each of the three manufacturers.

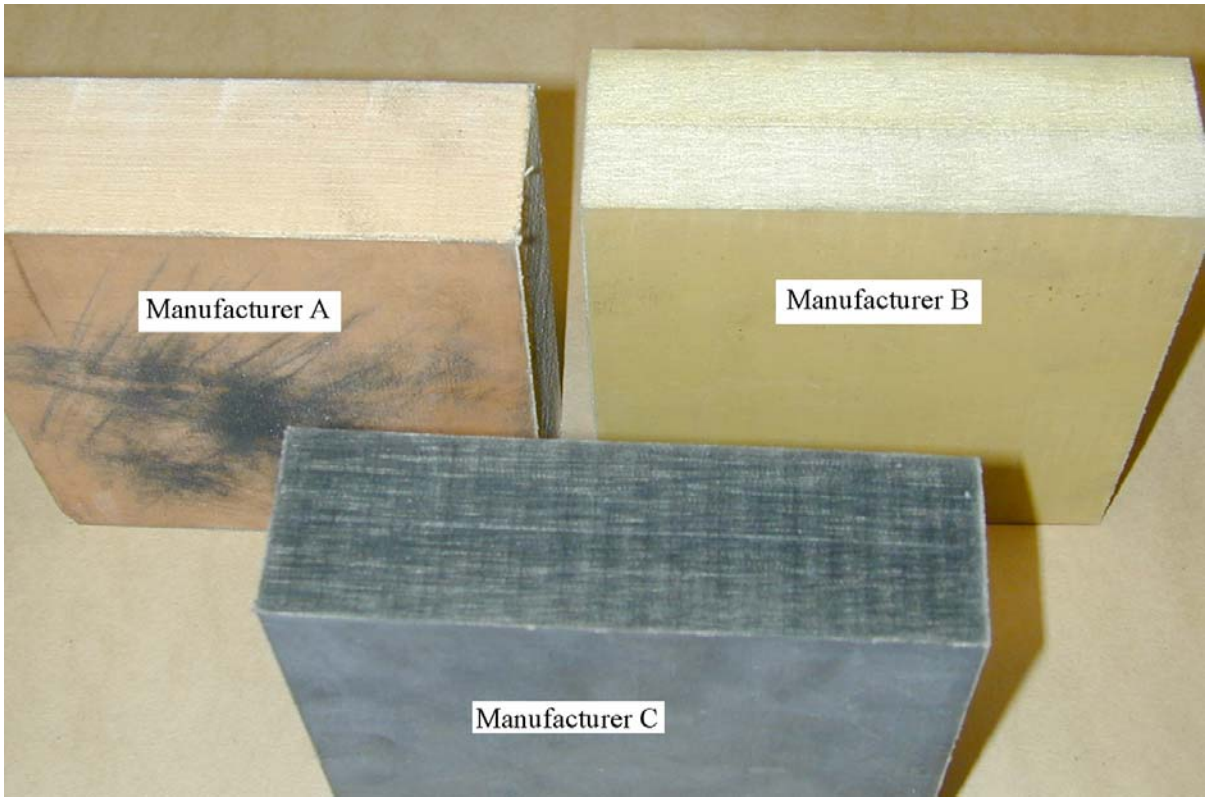

Figure 1.7. Typical Test Bearing Pads

The pads were inspected and measured before testing, and there were some clear similarities and differences among the individual products. All manufacturers employed similar layer structure and layer thickness. Manufacturer A produced light colored pads, which were made as a single unit up to the maximum 2-inch thickness used in this research program. Manufacturers B and C both produced pads of up to 1-inch thick as a single unit, but thicker pads were formed by bonding thinner layers together. This bond surface was viewed as a new potential failure surface and was closely monitored during

testing. However, none of the test bearings failed at this bonded surface, although a few test bearings exhibited deformation patterns that were influenced by the bonded surface. Manufacturer B provided light colored pads, which were a similar color to those provided by Manufacturer A. Manufacturer C provided pads that were close to black in color, which may be caused by the use of a different filler (such as carbon black) in the elastomer compound. The bearings of all three manufacturers were tested for identical loads and deformations and compared to illustrate the variation in bearing pad performance. A much larger number of Manufacturer A bearing pads were tested under a wider range of load and deformation conditions so that the full variation and basic models of behavior could be developed for CDP bearings.

1.5. OBJECTIVES OF THE RESEARCH PROGRAM

This research study was funded by the Washington State Department of Transportation (WSDOT). The research was aimed at developing widely applicable design recommendations and tools for more extensive use of CDP as bridge bearings. The research extended work completed during a previous research study (Roeder, Lehman, Larson 2002) of bearings supplied by Manufacturer A. This previous study suggested that expanded applications of CDP were possible, and so the specific research objectives of this follow-up study were as follows:

1) to verify that the research results from the previous limited test program are applicable to CDP manufactured by other companies
2) to develop design recommendations and expressions for CDP bridge bearings
3) to develop a spreadsheet-based tool to facilitate the design of CDP.

1.6. SCOPE OF THE REPORT

This report summarizes the research results from this experimental study. Chapter 2 discusses the experimental results from the compression tests, including the short-term and long-term static tests and the dynamic tests. Chapter 3 summarizes the rotation tests, and Chapter 4 describes the shear tests. Chapters 5 evaluates these individual research results and combines them into coherent and rational design

recommendations. Chapter 6 provides a summary and conclusions to the overall research program.

CHAPTER 2
COMPRESSION TESTS

2.1. INTRODUCTION

Bridge bearings are subjected to compression loads that are primarily caused by the weight of the superstructure, as well as the weight and dynamic impact from trucks and other vehicles. The weight of the bridge superstructure is categorized as a dead load in that it remains nearly constant during the life of the bearing and the structure; creep and long-term strain of the pad are of concern because of the long-duration nature of the loading. Vehicle loads are short-duration loads. They are dynamic in nature and may be repeated many millions of times during the life of the structure. However, the magnitude of these dynamic loads varies widely. Because of the long-term nature of the vehicle loading, the durability of these bearing pads is of concern. Stress and strain limits are needed to assure durability and to prevent deterioration of the bearing pad.

A portion of the experimental research program evaluated the response of cotton duck bearing pads (CDP) to different compressive loading conditions. The compressive test program modeled gravity-induced bridge loads that result from the weight of the bridge structure (dead load) and traffic loading (live load). Three types of test were conducted: short-term static, long-term static (or creep), and cyclic dynamic tests. The monotonic compression tests evaluated the compressive stress or strain capacity and the stress-strain response of CDP. The creep tests were conducted to establish the effects of constant long-term loading on the damage state and the strain demand. The dynamic tests were conducted to evaluate the effects of repeated cyclic loading on the pads and to establish the occurrence of different damage states and strain limits. The dynamic tests were accelerated relative to the anticipated loading in the field. During testing a relatively small number (typically 2 million or less) of relatively large load cycles were used to simulate the hundreds of millions of truck-load cycles expected during the bridge life. This acceleration permitted completion of a durability test within several weeks rather than the 50 to 100 years required for actual bridge bearing.

The strain and deformation of the bearing pad are critical parameters for all aspects of compressive load evaluation. Figure 2.1 illustrates the deformed shape and shear strains in a steel-reinforced elastomeric bearing subjected to compressive load. The loading induces compressive and lateral (bulging) deformations. As described in Chapter 1, the shape factor provides an index for modeling this behavior. Other elastomeric bearing pads exhibit similar behavior, but these other pads commonly rely upon friction to provide the bulging restraint. Frictional capacity is quite variable, and this variability adversely affects the performance of some other elastomeric bearing pads. As discussed in Chapter 1, CDP are expected to be stiff in compression, and the presence of closely spaced cotton duck fabric layers stiffens the elastomeric pad against bulging restraint. These issues raise questions as to whether the shape factor should be employed and, if so, how it should be defined. If sufficient frictional capacity exists between the pad the loading plate, local shear strains will develop at the top and bottom edges of the bearing pad, as depicted in Figure 2.1. During testing, it is important to monitor these deformation modes.

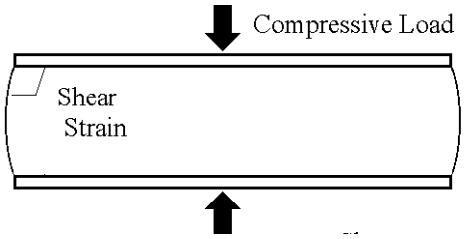

Figure 2.1. Elastomeric Bearing Pad Subjected to Compressive Loading

The compression test series studied these issues. Within each test category (i.e., short-term static, long-term static (or creep), dynamic), a test matrix was developed to study the influence of important parameters, including the following:

- pad shape factor
- pad thickness
- manufacturer
- maximum and minimum compressive stresses
- stress range.

The following sections summarize the test matrix, test set-up and procedure, observations, and results for each test series. In addition, the final damage state for each pad is indicated. Damage states relevant to compressive loading are described in Table 2.1 and illustrated in Figure 1.6. The damage states include (A) No Damage, (B) Oil Secretion, (C) Delamination Damage (degree of delamination is noted by numbers 1-3), and (D) Fracture. These damage states are indicated for the pads subjected to short-term monotonic loading, long-term monotonic loading, and dynamic loading. The delamination initiates from the edits of the bearing pad, and the degree of delamination is based on the percentage of the bearing length where delamination was noted.

Table 2.1. Pad Damage States

Designation	Description
A	No Damage
B	Oil Secretion
C1	Damage within 5% of Edge
C2	Damage within 10% of Edge
C3	Damage within 15% of Edge
D	Pad Fracture

2.2. TEST SETUP AND OPERATION

Two different test apparatuses were used for the short-term static and the creep and dynamic tests. The pads that were subjected to short-term static loading were tested to failure, and therefore, the capacity of the testing rig had to exceed 10,000 psi for the largest pad area. The creep and dynamic tests were subjected to lower levels of stresses, and a different test setup was used to impose the required cyclic histories. The following sections describe the testing frame and instrumentation for each of the test series.

2.2.1. Short-Term Static Tests

The static compression tests were conducted with the University of Washington Civil and Environmental Engineering Department's Structures Lab Baldwin 2.4-million-pound testing machine, shown in Figure 2.2. Before testing, the test pad was placed between two 24-inch-square, 2-inch-thick steel plates. These plates were used to transfer the compressive load from the Baldwin load head to the test pad. To increase

accessibility and facilitate placement of the instrumentation, the lower plate was raised with large steel blocks.

The pads were instrumented to measure vertical and horizontal displacements at several locations on the pad. The measured displacements were used to interpret strains in the pad. A sketch of the instruments is shown in Figure 2.3. The instruments used were 1.5-inch Duncan linear potentiometers. Two potentiometers, labeled Ch0 and Ch1 and located at opposite corners of the test pad, recorded compressive displacements. Four other potentiometers, labeled Ch2, Ch3, Ch4, and Ch5, recorded the lateral bulge of the pad on the front and right sides. Compressive force data were provided from the Baldwin digital load display.

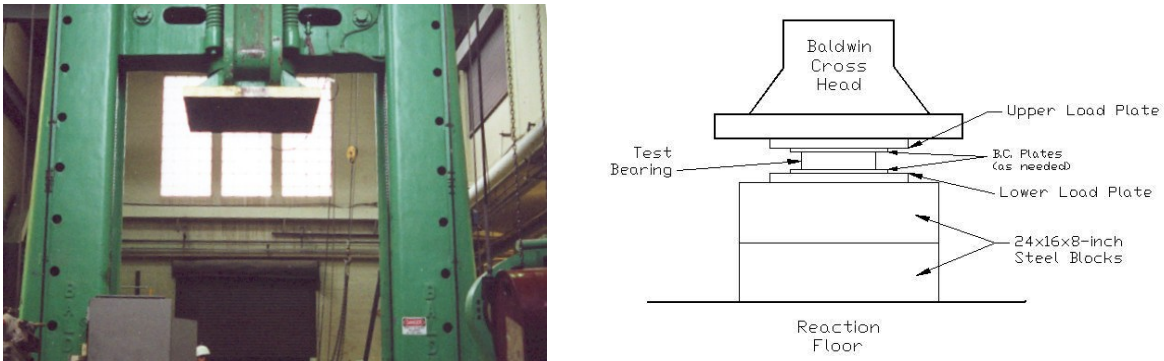

Figure 2.2. Testing Apparatus for Monotonic Compression Tests

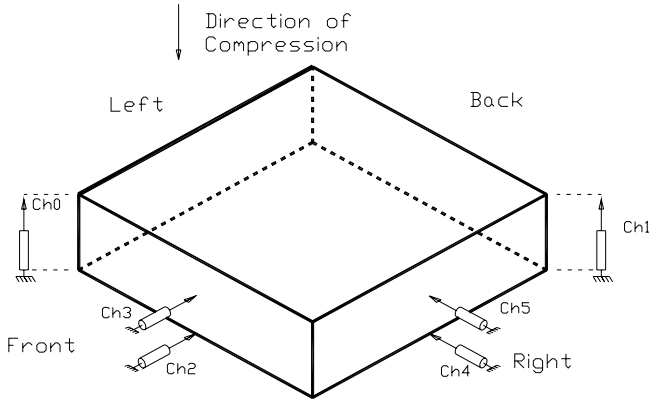

Figure 2.3. Instrumentation for Short-Term Static Tests

Test setup consisted of centering the steel blocks and load plates under the Baldwin and attaching the potentiometers. During each test, the pad was monitored for crack formation and other damage states. Several tests were videotaped for later review. During testing, the potentiometer and load readings were recorded with a Hewlett Packard (HP) data acquisition system. The instruments were calibrated by standards traceable to the U.S. National Bureau of Standards within the 12 months prior to testing. All measurements were scanned at a rate of 1 cycle per second, and the recorded data were immediately transferred to a computer and stored on disk. The load was applied slowly at a rate of 2 kips/second. This load rate required approximately 10 to 30 minutes for application of the 650- to 2,000-kip load to the various specimens.

2.2.2. Creep and Dynamic Tests

A special testing frame was constructed to test the pads under compressive creep and dynamic compression loading. The frame was self-reacting and equipped with a 300-kip, double acting hydraulic actuator, which allowed the pads to be subjected to high cyclic axial stresses. Figure 2.4 shows a sketch and photograph of the frame.

The testing frame was 144 inches high and was placed vertically in the lab, as shown in the photograph. The primary load carrying members were two vertical W14x90 sections and two horizontal pairs of MC18x58 sections placed back-to-back. Each test pad was placed between a 4-inch end plate on the actuator and a 4-inch reaction plate that was attached to the upper pair of channels. A smaller, ¾-inch sensor mounting plate was attached between the actuator end plate and the test pad. This plate held the testing pad and sensors, which measured the pad deformation.

The instruments were placed to measure vertical and lateral displacements. The number of instruments was increased relative to the static tests to increase the reliability and usefulness of the data. Figure 2.5 shows the instrumentation layout. Two instruments were placed on diagonally opposite corners to measure vertical displacements. A total of 12 instruments were placed to measure the lateral deformation of the pad. Placement of instruments on opposite faces permitted differentiation of rigid-body pad translation and pad deformation. Three horizontal instruments were placed on each face to provide a rough estimate of the shape of the bulging of each face.

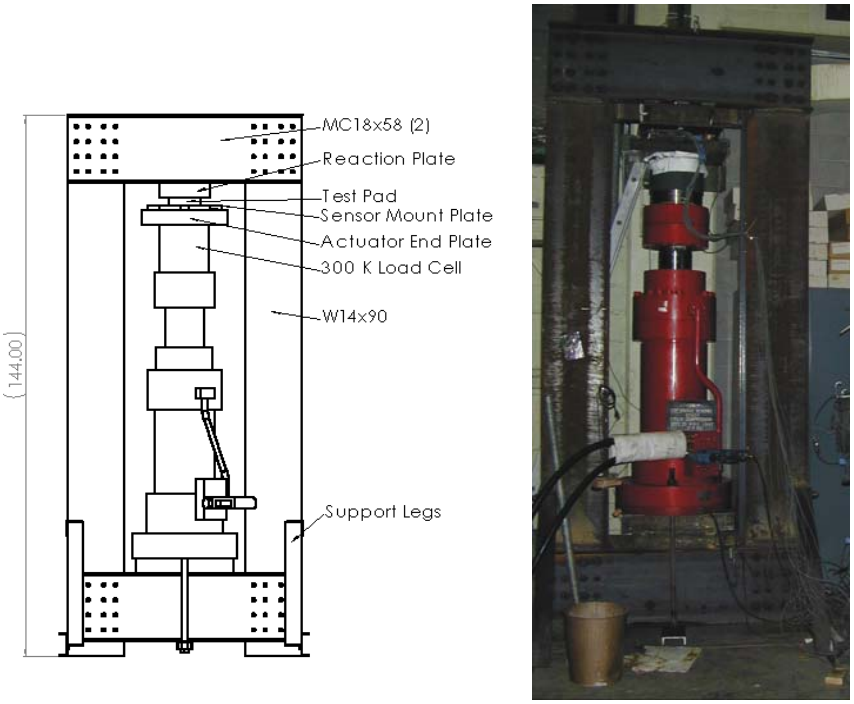

Figure 2.4. Sketch and Photograph of Test Frame

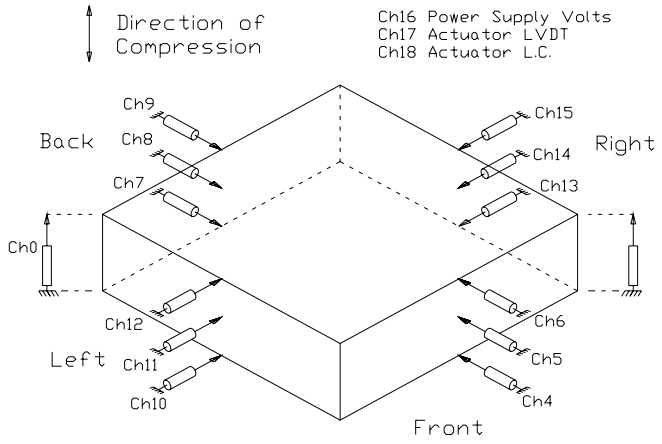

Figure 2.5. Layout of Instrumentation for Creep and Dynamic Tests

Actuator servo-control was provided by an MTS 442 controller. The controller was configured to operate under force control, that is, the servo-valve of the actuator displaced the piston to achieve a target force level. An MTS 410 Digital Function

Generator controlled the variation of actuator force. A National Instruments data acquisition system was used to read the data from the load cell and potentiometers. Using the Labview software program, test-specific data acquisition was developed for this testing series. The system collected the readings from each sensor channel in real time after a prescribed cycle increment. Test data were saved to an ANSI tab-delimited file for later analysis.

Before testing, the dimensions of the test pad were measured. The pad was placed on the sensor mount plate, and the lateral and compressive deformation potentiometers were attached. To seat the pad and initialize the test, a pretest load of 2 to 3 kips was applied, and the sensors were initialized to zero. All subsequent potentiometer readings were relative to this initialization point.

2.3. STATIC COMPRESSION TESTS

The short-term static compression tests (designated as series CS) were conducted to establish the maximum compressive load capacity and stress-strain response of CDP. The effects of pad thickness, shape factor, boundary conditions, and manufacturer were studied. (All of the test specimens for each series are listed in Table 2.2.)

As noted in Chapter 1, the three manufacturers were designated as A, B, and C. Likewise, the three sub-series were designated CS-A, CS-B, and CS-C, to denote the manufacturer. Test Series CS-A formed the basis of the evaluation, and 28 tests were conducted, as indicated in Table 2.2. The results for Test Series CS-B and CS-C were used to compare the Test Series CS-A findings; eight pads were tested for each of those test series.

Within Test Series CS-A, a selected group of tests was conducted to establish the influence of the condition of the boundary between the pad and the loading surface on the stress-strain response. Three boundary conditions were considered: a steel plate, a sand-blasted plate, and a greased plate.

During testing, pad damage was monitored. Data were collected to evaluate the effective modulus and the stress and strain capacities of cotton duck pads subjected to short-term monotonic loading.

Table 2.2. Short-Term Static Compressive Load Tests

Test/ Series	Bearing Geometry		Test Conditions		Results				
	Pad Size (in. x in. x in.)	Shape Factor	Test Date (M / Y)	Boundary Condition	Peak Stress (ksi)	Peak Strain (in./in.)	Max Strain (in./in.)	E_{0-3} (ksi)	Damage State
CS-A1	8x8x2	1.00	Mar-01	Steel	10	0.185	0.185	38.5	D
CS-A2	8x8x0.75	2.67	Mar-01	Steel	20.3	0.329	DNF	37.0	D
CS-A3	8x8x2	1.00	Mar-01	Steel	12.4	0.214	0.215	33.4	D
CS-A4	12x12x2	1.50	Mar-01	Steel	11.7	0.23	0.243	37.2	D
CS-A5	10x10x1.5	1.67	Mar-01	Steel	11.7	0.225	0.232	30.3	D
CS-A6	12x12x0.75	4.00	Mar-01	Steel	11.6	0.286	DNF	17.5	C1
CS-A7	10x10x2	1.25	Mar-01	Steel	11.5	0.207	0.222	17.3	D
CS-A8	10x10x0.75	3.33	Mar-01	Steel	12.8	0.304	DNF	17.9	A
CS-A9	8x8x1.5	1.33	Mar-01	Steel	12.1	0.252	0.268	30.3	D
CS-A10	18x6x2	1.13	Mar-01	Steel	12	0.217	0.226	33.5	D
CS-A11	18x6x1.5	1.50	Mar-01	Steel	13.4	0.246	0.263	33.9	D
CS-A12	12x12x1.5	2.00	Mar-01	Steel	12.7	0.257	0.221	22.3	D
CS-A13	6x6x2	0.75	Jun-02	Steel	11.1	0.248	0.248	12.7	D
CS-A14	6x6x0.75	2.00	Jun-02	Steel	14.9	0.358	0.355	24.3	D
CS-A15	6x6x0.75	2.00	Jul-02	Steel	7.3	0.282	DNF	23.1	A
CS-A16	10x10x0.75	3.33	Jul-02	Steel	8.5	0.294	DNF	27.6	A
CS-A17	6x6x2	0.75	Jul-02	Steel	10.3	0.244	0.244	18.9	D
CS-A18	10x10x2	1.25	Jul-02	Steel	10.8	0.229	0.236	13.8	D
CS-A19	8x8x1.5	1.33	Jul-02	Steel	11.4	0.2	0.248	18.0	D
CS-A20	8x8x0.75	2.67	Aug-02	Grease	6.4	0.338	DNF	13.6	A
CS-A21	8x8x2	1.00	Aug-02	Grease	12.8	0.288	0.288	21.0	D
CS-A22	8x8x2	1.00	Aug-02	Sand Blast	11.5	0.281	0.298	37.5	D
CS-A23	8x8x2	1.00	Aug-02	Steel	9.9	0.248	0.248	34.6	D
CS-A24	8x8x0.75	2.67	Aug-02	Steel	9.3	0.308	DNF	39.4	A
CS-A25	8x8x0.75	2.67	Aug-02	Sand Blast	9.2	0.352	DNF	22.6	A
CS-A26	8x8x0.75	2.67	Aug-02	Grease + Mill	10	0.31	DNF	36.2	A
CS-A-27	8x8x0.75	2.67	Oct-02	Grease	13.4	0.412	0.447	22.1	D
CS-A-28	8x8x1.5	1.33	Oct-02	Grease	14.1	0.322	0.322	32.1	D
Mean Values (Steel B.C. only)					11.7	0.26	0.24	29.5	
CS-B1	6x6x2	0.75	Mar-03	Steel	9.89	0.246	0.246	27.3	D
CS-B2	8x8x0.75	2.67	Jan-03	Steel	17.30	0.311	0.311	33.0	D
CS-B3	8x8x1	2.00	Jan-03	Steel	12.27	0.278	0.278	26.2	D
CS-B4	8x8x1.5	1.33	Mar-03	Steel	13.30	0.285	0.285	26.7	D
CS-B5	8x8x2	1.00	Jan-03	Steel	10.40	0.245	0.245	26.8	D
CS-B6	12x12x0.75	4.00	Jan-03	Steel	15.40	0.300	0.300	25.1	D

Test/ Series	Bearing Geometry		Test Conditions		Results				
	Pad Size (in. x in. x in.)	Shape Factor	Test Date (M / Y)	Boundary Condition	Peak Stress (ksi)	Peak Strain (in./in.)	Max Strain	E_{0-3} (ksi)	Damage State
CS-B7	12x12x1	3.00	Jan-03	Steel	13.40	0.287	0.287	26.6	D
CS-B8	12x12x2	1.50	Jan-03	Steel	8.93	0.214	0.214	28.8	D
Mean Values					12.61	0.27	0.27	27.6	
CS-C1	6x6x2	0.75	Mar-03	Steel	8.08	0.163	0.163	38.8	D
CS-C2	8x8x0.75	2.67	Mar-03	Steel	10.80	0.150		47.5	A
CS-C3	8x8x1	2.00	Mar-03	Steel	11.40	0.184	0.213	45.0	D
CS-C4	8x8x1.5	1.33	Mar-03	Steel	8.83	0.143	0.143	47.9	D
CS-C5	8x8x2	1.00	Mar-03	Steel	8.48	0.153	0.153	41.9	D
CS-C6	12x12x0.75	4.00	Mar-03	Steel	14.50	0.161		47.6	A
CS-C7	12x12x1	3.00	Mar-03	Steel	12.90	0.163	0.17	56.4	D
CS-C8	12x12x2	1.50	Mar-03	Steel	8.83	0.154	0.154	43.0	D
Mean Values					10.48	0.16	0.17	46.0	

2.3.1. Test Matrix

The test matrix was developed to study the influence of shape factor and thickness on the monotonic compressive response, including the effects of different pad manufacturers, pad geometries, and boundary conditions. The pad dimensions were chosen to provide experimental data over a wide range of values of the study parameters. In plan, the pads were either 6 x 6 in., 8 x 8 in., 10 x 10 in., 12 x 12 in. or 18 x 6 in. The pads were 0.75-inch, 1.0-inch, 1.5-inch, or 2-inch thick. Table 2.2 summarizes the test matrix, including the pad geometry, shape factor, boundary conditions, and salient results.

2.3.2. Test Observations

Each static test was conducted until the pad exhibited compressive failure (indicated by formation of diagonal fracture), or the limiting stress or deformation of the test setup was reached. Testing was stopped at a load corresponding approximately to 15 ksi since larger stresses and deformations would damage the test setup. In particular, the top load plate suffered plastic deformation due to irregularities in the load head, and large compressive strains damaged the potentiometers. In all cases, the 1.0-inch, 1.5-inch, and 2-inch thick pads were tested to failure. Within Test Series CS-A and CS-C, most of the 0.75-inch thick pads were not tested to failure.

The typical failure pattern of pads with shape factors of 2 or less was characterized by distinct crack formation, as shown in Figure 1.5d and sketched in Figure 2.6. As the pad was compressed, lateral bulging resulted in local shearing stresses and strains at the top and bottom, as depicted in Figure 2.1. The crack pattern initiated when the principal tensile strain perpendicular to the crack, which resulted from the compressive, lateral, and shearing strains, reached a limiting value. Videotape footage of several of the tests verified this crack initiation sequence. After the initial crack had formed, the stress state in the pad caused the crack to propagate at an angle through the pad. Once the crack reached the opposite face of the pad, conditions of high shear strain developed there, and a new crack initiated and propagated to the opposite face, resulting in the zigzag crack pattern depicted in figures 2.6 and 1.5d.

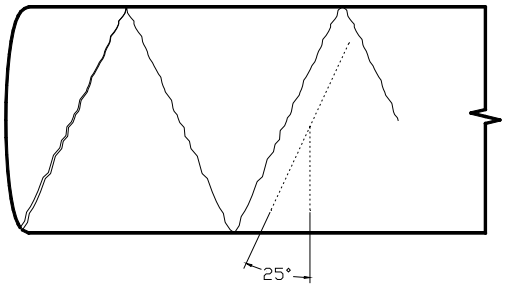

Figure 2.6. Crack Pattern at Failure

The cycle of zigzag crack formation continued until the reduced area of the pad could tolerate the applied compressive strain. Each time the square pads with shape factors of 2 or less were tested, the failure pattern followed the theorized zigzag crack formation pattern as described. In the case of a rectangular pad, the damage on the short face of the pad followed the zig-zag pattern; damage on the long face was primarily limited to horizontal cracking and delamination.

The Manufacturer A and B 0.75-inch thick pads with shape factors greater than 3 were able to sustain larger compressive stresses and strains than the thicker pads. In these cases, the load and deformation limits of the test setup were reached. The damage of these pads with larger shape factors was limited to delamination around the perimeter of the pad, which most likely resulted from variation in lateral strain within the pad.

2.3.3. Results

Data were recorded to evaluate the full stress-strain response of the pads. Figure 2.7 describes a typical stress-strain response of a cotton duck pad subjected to monotonic compressive loading. The initial response was approximately linear and was followed by a highly nonlinear response until the peak stress and strain, σ_{peak} and ε_{peak}, were reached. The post-peak response depended on the manufacturer and stiffness. For some pads, the maximum strain, ε_{max}, exceeded the peak strain; for others post-peak degradation was not noted. These values are provided in Table 2.2 for all of the pads tested.

The results showed that the response of the pads was strongly influenced by the manufacturer and boundary conditions. Figure 2.8 shows the measured stress-strain response for three 8x8x2 pads, one from each manufacturer. Those results are typical of all pad sizes and show that the Manufacturer C pads had reduced stress and strain capacities and an increased stiffness relative to the other two manufacturers. In general, the stiffness of the Series B pads was less than the 1.5- and 2.0-inch pads from Manufacturer A.

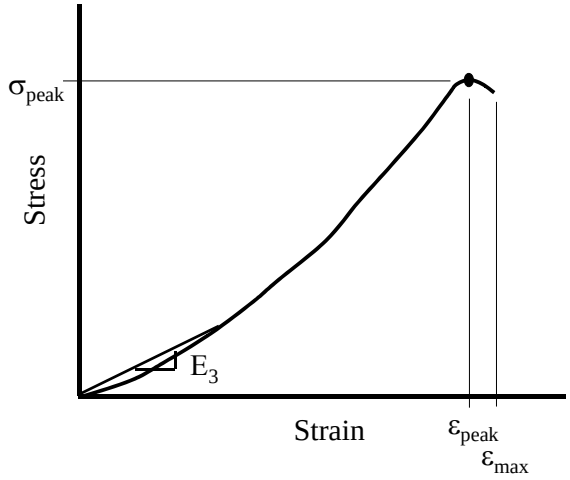

Figure 2.7. Typical Monotonic Stress-Strain Curve

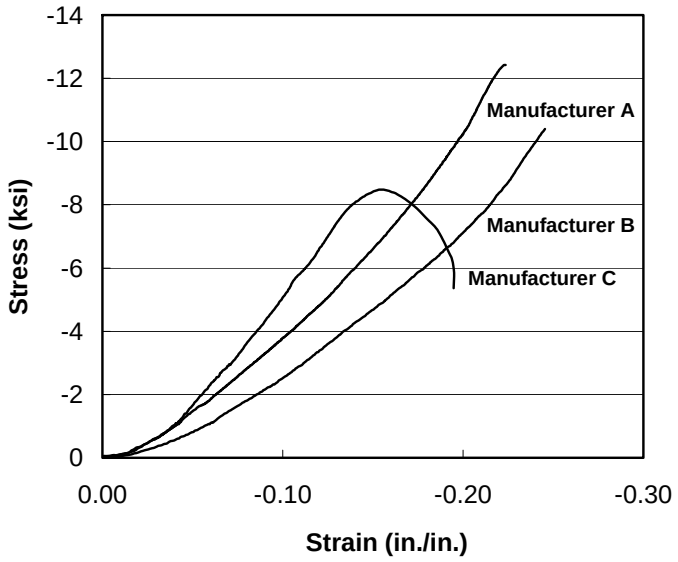

Figure 2.8. Measured Stress-Strain Responses for 8x8x2 Pads from Each Manufacturer

Differences in the stress-strain response were also noted to result from the condition of the boundary between the pad and the loading surface. Reduced-friction boundary conditions (i.e., greased) resulted in a reduction in pad stiffness and an increase in strain capacity.

The differences in the response did not appear to depend on the shape factor as much as they depended on the other study parameters. It is worthwhile noting that the variation in the shape factor was small (1 to 4). Differences in behavior due to shape factor in neoprene bearing pads were demonstrated on pads with shape factors varied from 3 to 16 (Dupont 1983) in Figure 1.6. Therefore, more notable differences in the behavior might have resulted from a greater variation in the shape factor.

The results from the static compression tests were used to establish the strength and deformation capacities of the pads. In addition, approximations to the pad stiffness were made. The following discusses the influence of the study parameters, including the manufacturer, shape factor, and boundary conditions, on these values.

Secant Modulus Values

The stress-strain response of cotton duck pads is highly non-linear. To accurately describe the full stress-strain response, a series of complex mathematical expressions

would be required. Since these types of expressions are normally not practical for engineering design, a secant modulus was used to describe the compressive behavior under normal service-load conditions. Here, the pad stiffness was approximated using the secant modulus from 0 to 3 ksi (denoted E_3). The stress level of 3 ksi was likely to provide an upper-bound to the service load stress. Values of the secant modulus for each test pad, E_3, are provided in Table 2.2.

The results for secant modulus are plotted in Figure 2.9. Only the CS-A test specimens tested with the steel boundary conditions were used. Differences resulting from the manufacturer, and therefore likely the manufacturing process and fabric properties, were apparent. In general, the influence of the shape factor was not apparent. The Series CS-C tests indicated that the pad stiffness increased with an increase in the shape factor; the results from the Series CS-A and CS-B test did not show a trend. In the figure, the Series CS-A 0.75-inch pads were plotted separately from the Series CS-A 1.5-inch and 2-inch pads. The differences in the stiffness values may appear to be due to the shape factor, but it is speculated that the differences were due to the manufacturing process as well, since manufacturers indicate two different methods for producing thinner bearing pads.

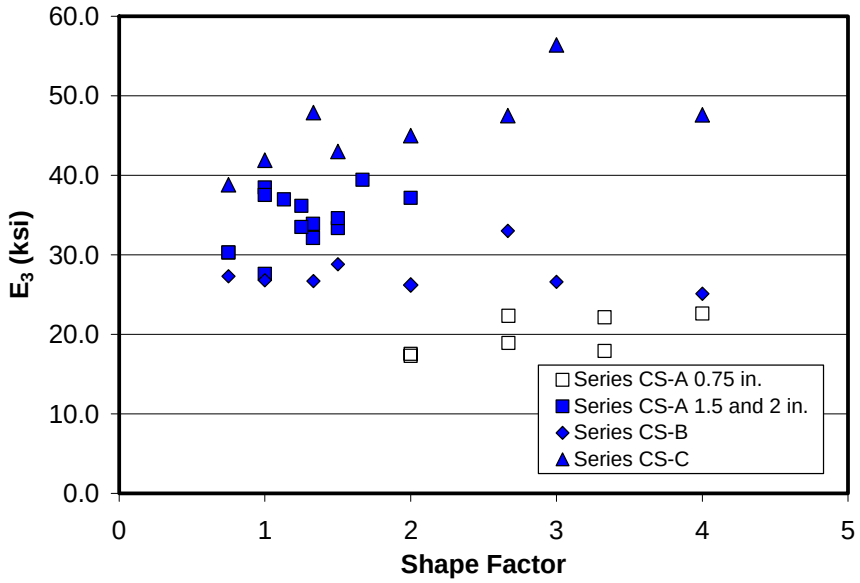

Figure 2.9. Values of E_3 as a Function of Shape Factor and Manufacturer

Within Test Series A, a sub-series of tests were conducted to establish the influence of the boundary condition on the stress-strain response. Figure 2.10 shows the influence of the boundary condition on the pad stiffness. As shown in the plot, the initial stiffness of the pad depended on the boundary condition. However, at large stress demands, the difference diminished.

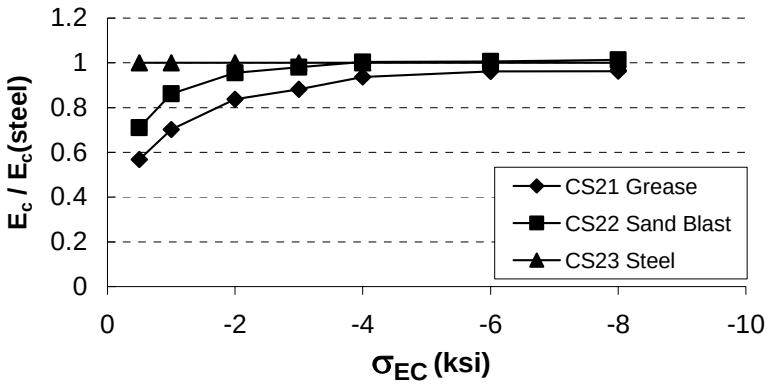

Figure 2.10. Normalized Elastic Modulus vs. Stress

Peak Stress

The peak stress of the pad, σ_{peak}, was measured for each pad. Values are provided in Table 2.2. On average, the peak strength of the Manufacturer B pads was the highest (12.6 ksi), and the strength of the Manufacturer C pads was the lowest (10.5 ksi). Note that approximately half of the Manufacturer C pads fell below the 10 ksi strength limit implied by the Military Specifications.

Figure 2.11 further illustrates the difference in pad strength as a function of both manufacturer and shape factor. Here an influence of the shape factor is apparent in that the peak strength increased with an increase in the shape factor for all of the pads. In addition, it is noted that the peak strength was influenced by the pad boundary condition. Figure 2.12 shows that the pad strength also increased with a reduction in the coefficient of friction at the pad/loading surface boundary.

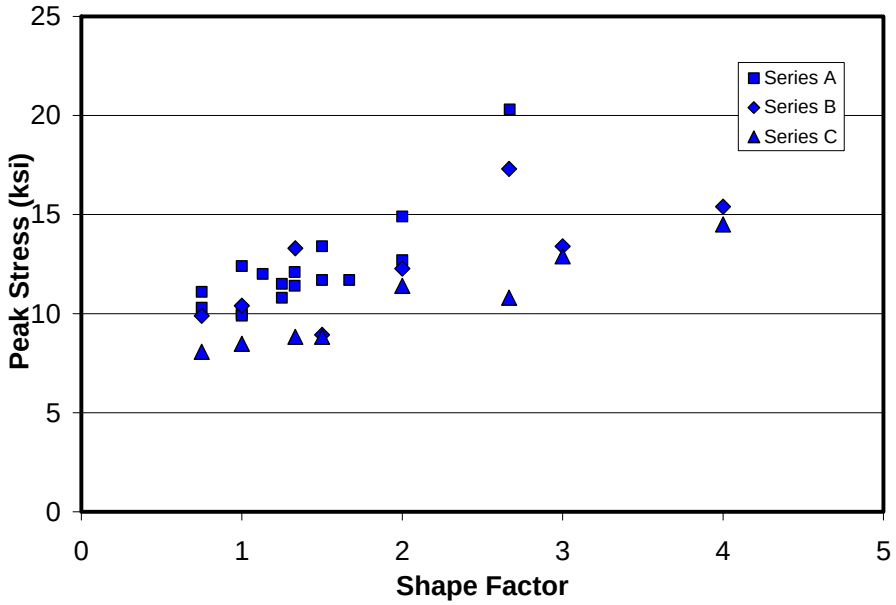

Figure 2.11. Relationship between Peak Stress and SF for Pads Tested to Failure

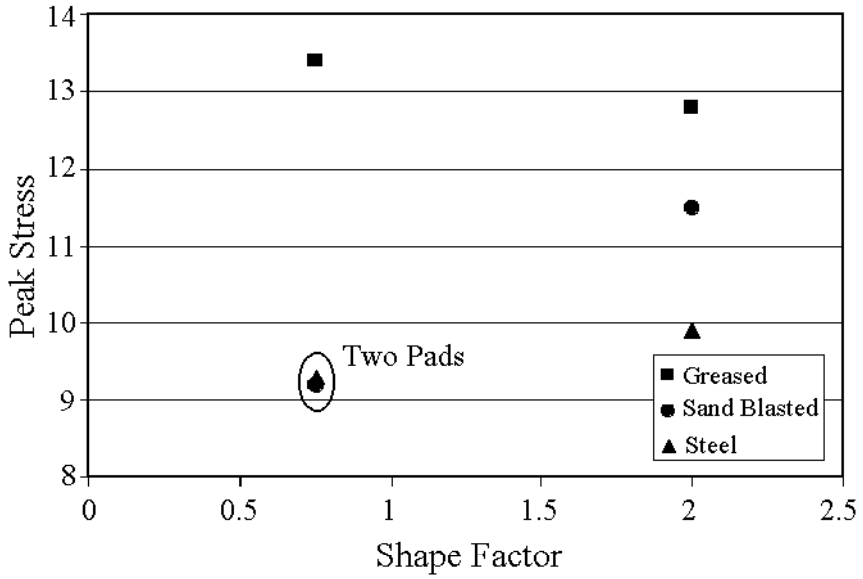

Figure 2.12. Relationship between Peak Stress and Boundary Condition

The results shown in figures 2.11 and 2.12 are not contradictory but instead indicate that the influence of the shape factor on the pad response relates to the frictional resistance of the surface, or the ability of the pad to slip, which minimized the shear strains at the edge of the pad. Research into the response of bonded rubber has shown that

the shear strains are maximal near the edge and zero at the center of the bearing (Gent, 1974). On the basis of this observation, an elastic theory was developed to predict the magnitude of the maximum shear stress under this compressive load. This theory suggests that

$$\tau_{max} = \sigma_{avg} \frac{b}{\kappa t} \quad \text{(Eq. 2.1)}$$

where b is the base dimension of the bearing, t is the pad or layer thickness, and κ is a constant that depends on the plan dimensions of the bearing and the magnitude of the slip restraint. The maximum shear stress, τ_{max}, is a function of the frictional capacity and therefore is limited by the compressive stress, σ_{avg}, and the coefficent of friction, μ, between the steel and the bearing pad. Therefore,

$$\tau_{max} = \sigma_{avg}\, \mu < \sigma_{avg} \frac{b}{\kappa t} \quad \text{(Eq. 2.2)}$$

and so slip will occur if

$$\mu < \frac{b}{\kappa t} \quad \text{(Eq. 2.3)}$$

The b/t ratio is invariably larger for thin pads, and so thin pads require a larger coefficient of friction to prevent slip. In particular, the coefficient of friction needed to prevent slip and provide bulging restraint for a 0.75-in. pad is twice as large as that needed for a 1.5-in. pad and 2.7 times as large as that needed for a 2-in. pad. The coefficient of friction is inadequate to restrain the bulging, and the pads respond closer to a "greased" boundary condition and, therefore, decrease the shear strain demand, which permits a larger stress to be reached.

Failure Strain

The strain capacity of a CDP depends on the shape factor, manufacturer, and boundary condition. Table 2.2 provides and Figure 2.13 shows the measured maximum strains values. On average, the maximum strain was 0.24 in./in. for Manufacturer A, 0.27 in./in. for Manufacturer B, and 0.17 in./in. for Manufacturer C. None of the Manufacturer C pads reached the average strain capacities measured for the CS-A and CS-B series.

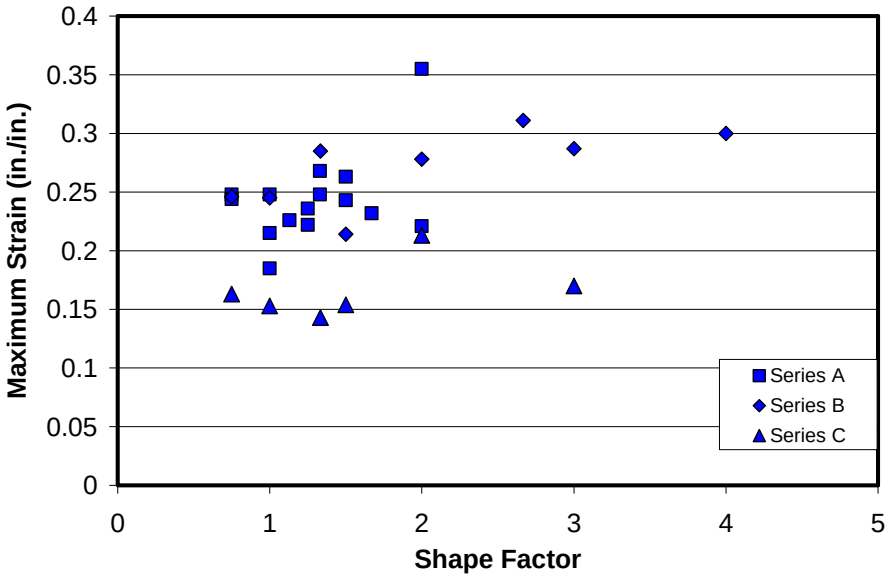

Figure 2.13. Maximum Strain vs. Shape Factor for Each Manufacturer

In general, the maximum strain capacity was linked to the shape factor, where a larger shape factor generally resulted in a larger strain capacity. This difference resulted from the shearing stresses on the top surface of the pad, which were found to limit the strain capacity in a manner similar to which they limited the stress capacity. Test boundary conditions also had an impact on the strain capacity because specimens with greased pads had consistently larger strain capacity than other pads.

Trends in the data indicated that the maximum strain decreased with an increase in pad stiffness, as shown in Figure 2.14. A linear regression of the data indicated that the strain capacity may be approximated for the measured stiffness using Equation 2.4

$$\varepsilon_{max} = 0.41 - 0.005E_3 \qquad \text{(Eq. 2.4)}$$

This relationship may be used to determine the adequacy of a pad in that the pad may be tested to determine its initial stiffness, and the resulting stiffness may be used to determine the pad strain capacity.

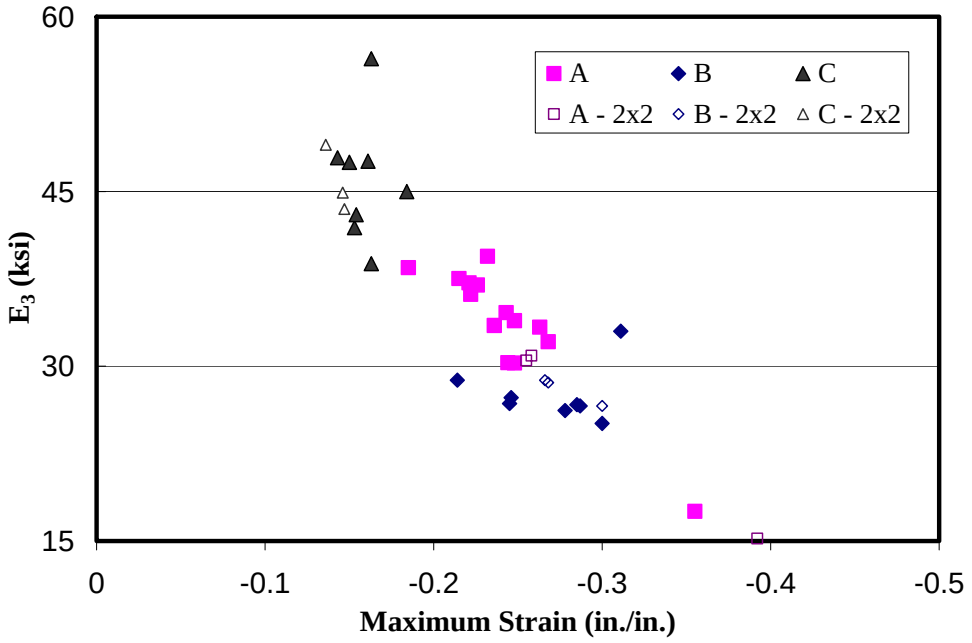

Figure 2.14. Secant Modulus as a Function of Maximum Strain

Cyclic Response

In addition to the monotonic static tests, Specimens CSA-7 and CSA-12 were subjected to a static cyclic loading history. The results for Specimen CSA-12 are shown in Figure 2.15. The results indicated that the response followed the monotonic envelope, the unloading and loading curves were highly nonlinear, and that the full strain was not recovered after full unloading. The residual strain was measured and found to be 13 percent to 35 percent of the maximum strain sustained by the pad during the loading cycle; on average the residual strain was 25 percent of this maximum strain. A cyclic compressive constitutive model was developed to approximate the response, and the results are shown in the figure. The mathematical expressions for the analytical representation are provided elsewhere (Larson 2003).

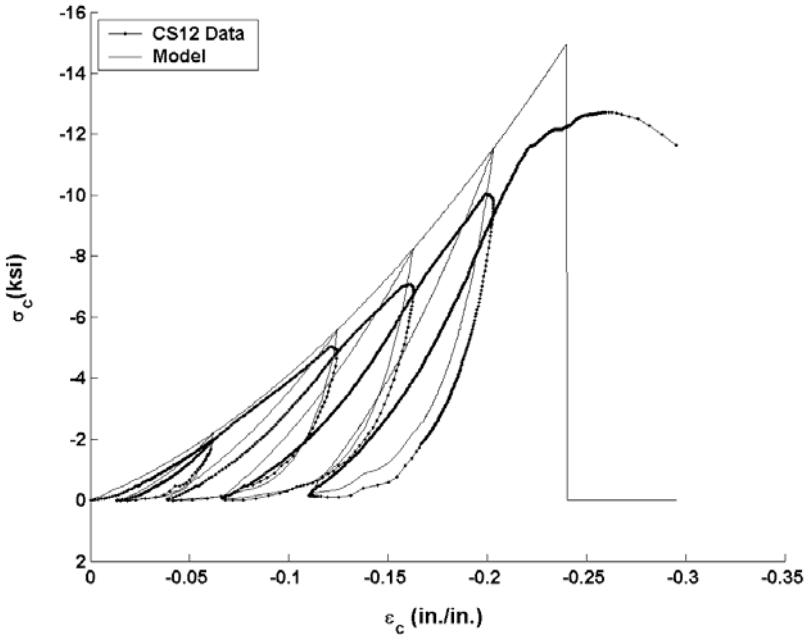

Figure 2.15. Cyclic Response of CS-A12

2.4. COMPRESSIVE CREEP TESTS

In the field, bearings are subjected to long-term compressive loading resulting from the dead load on the bridge. Neoprene bearing pads have been found to exhibit an increase in strain of 25 percent to 45 percent relative to their initial deflection under sustained compressive load (Dupont 1983). Therefore, this type of loading is important to the engineering design of cotton duck bearing pads.

To establish the effect of long-term loading on pad response, compressive creep tests were conducted with the rig shown in Figure 2.5. In addition to the instruments used for the short-term static tests, instruments were placed on all sides of the pads to better monitor lateral deformations. Testing was initiated by applying the predefined axial stress to the pad. The load was sustained for a minimum of 14 days to ensure that the steady-state long-term strain was approximated. Tests on neoprene pads have indicated that the majority of creep strain (80 to 90 percent) develops within the first two weeks of testing (Dupont 1984). The pad was monitored during the test to evaluate pad damage and oil excretion. Upon completion of the test, the pad was removed, photographed, and measured. After testing, the pad thickness was recorded daily for one week after test completion to document pad thickness recovery.

2.4.1. Test Matrix

The test series was developed to evaluate the influence of pad geometry, including shape factor and thickness, axial stress, and the manufacturer on the creep response. A total of six A specimens, two B specimens, and two C specimens were tested, as shown in Table 2.3. All pads were 8 x 8 inches and were 2, 1.5, or 0.75 inches thick. Three axial stresses were used 1, 2, and 3 ksi. This range was chosen to reflect the maximum and minimum compressive stress.

Table 2.3. Pads Subjected to Long-Term Monotonic Compressive Loading (Creep)

Test Specimens	Pad Size *l x w x t (in.)*	Shape Factor	Peak Stress (ksi)	Damage State	$\varepsilon_{steadystate}$	$\frac{\varepsilon_{steady\ state}}{\varepsilon_{static}}$
CC-A1	8x8x0.75	2.67	1.0	A	0.11	2.0
CC-A2	8x8x0.75	2.67	2.0	B	0.20	1.8
CC-A3	8x8x1.5	1.33	1.0	A	0.10	2.4
CC-A4	8x8x1.5	1.33	2.0	B	0.17	2.4
CC-A5	8x8x1.5	1.33	3.0	B	0.21	2.2
CC-A6	8x8x2	1.00	1.0	A	0.08	2.0
CC-B1	8x8x0.75	2.67	2.0	B	0.14	2.0
CC-B2	8x8x1.5	1.33	3.0	B	0.19	1.7
CC-C1	8x8x0.75	2.67	2.0	A	0.018	1.8
CC-C2	8x8x1.5	1.33	3.0	A	0.017	1.3

2.4.2. Test Observations and Results

Oil secretion was observed for the Series CC-A and CC-B pads that had experienced axial stresses of 2 ksi or larger. The pads that were subjected to a long-term axial stress of 1 ksi did not secrete oil during testing. The oil secretion data for all of the creep and the dynamic compression tests are presented in Section 2.5.

The compressive creep tests were conducted, in part, to establish the influence of several study parameters, including applied axial stress and pad thickness. As described previously, the effects of the axial stress, pad shape factor, and thickness were not found to be significant (Roeder, Lehman, and Larson 2002). Figure 2.16 shows three CC-A series 8- x 8- x 1.5-inch pads subjected to long-term axial stresses of 1, 2, and 3 ksi. The normalized plots for CS-A series pads that were subjected to different axial stress ratios are shown.

(To differentiate the contribution of the long-term loading effect and the axial stress effects, the plots were normalized to the axial strain resulting from instantaneous compressive loading, as presented in Section 2.2.) The normalized strain-time curves for the three 8- x 8- x 1.5-inch pads subjected to different axial stresses were similar, indicating that differences in their responses were primarily due to the increase in axial load rather than a coupled axial load-sustained load effect. For the three pads, the ratio of the steady-state strain to the monotonic strain was approximately 2.1

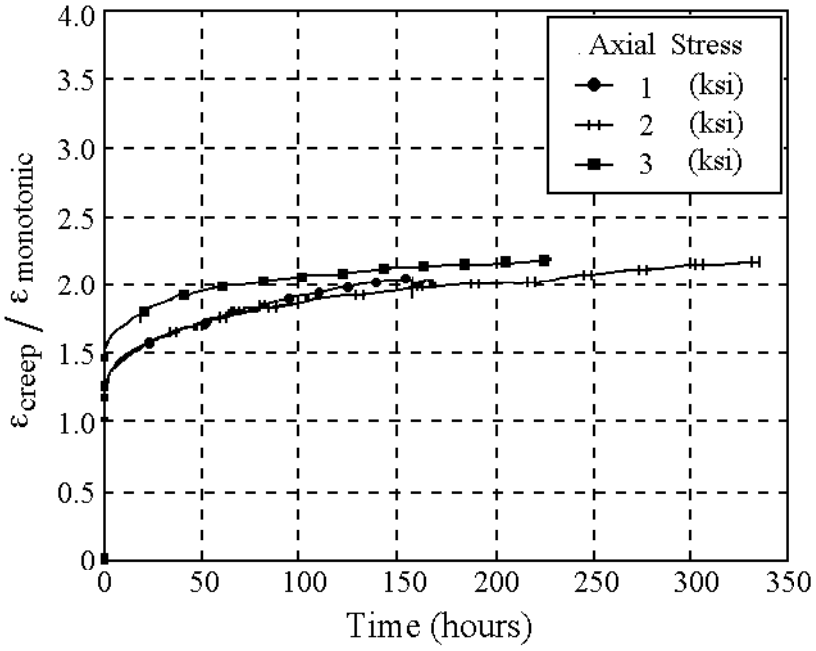

Figure 2.16 Normalized Response to Long-Term Compressive Loading: Axial Stress

The shape of the axial strain-time curve was similar for all of tests. Initial application of the compressive load resulted in an initial strain equal to the strain that would be achieved under short-term monotonic loading. In addition, as expected, long-term compressive loading resulted in creep and, therefore, an increase in the compressive strain. The most significant increase took place within 50 hours of testing. After two weeks, the strain-time curves were relatively flat, and the creep strains had nearly reached their long-term steady-state strain. Note that the sharp vertical dips seen on the plots

resulted from removal of the load to monitor the pad or test rig. It is of interest to note that for most of the tests, when the load was removed, the strain sustained by the pad was approximately equal to the strain that would be induced under short-term monotonic loading.

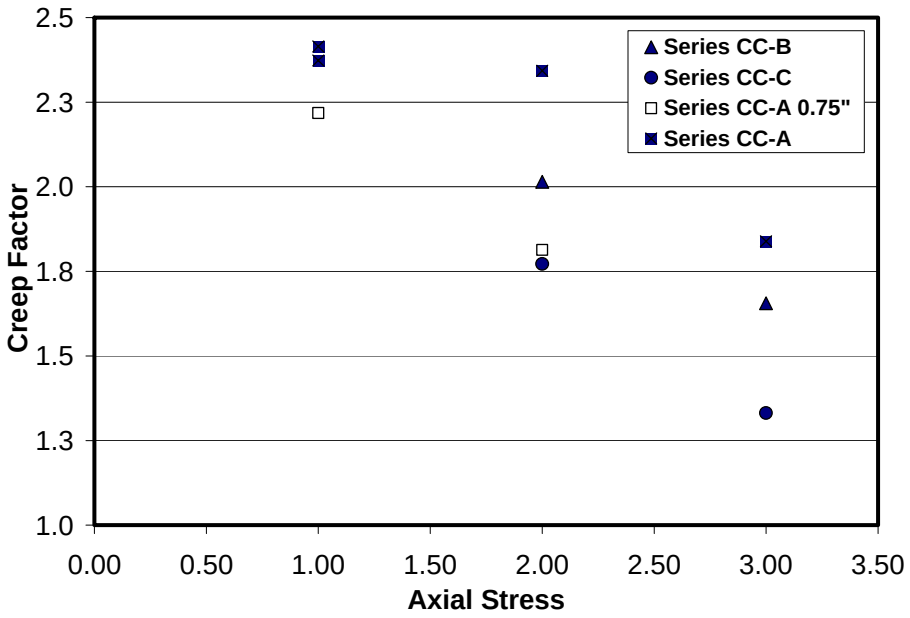

Figure 2.17. Creep Factor vs. Applied Axial Stress

In Table 2.3, the ratio of the steady-strain strain to the monotonic strain is provided for all of the specimens. The normalized strain ratio, or creep factor, was between 1.3 to 2.4. The variation in the factor is shown graphically in Figure 2.17. The lowest factor was calculated for the Series CC-C specimens. A trend of a decrease in the creep factor with an increase in the axial stress ratio was evident. It was expected that the sustained stress (dead load) would range from 1 to 2 ksi in practical bridge applications. For the pads tested, the average creep factors were 2.1 and 2.0 stresses of 1 and 2 ksi, respectively. An amplification factor of 2 is recommended to calculate the deflection due to the sustained load.

2.5. DYNAMIC COMPRESSION TESTS

The dynamic compression tests were intended to simulate the response of cotton duck bearing pads to dead load and traffic loading and to result in design

recommendations for this type of loading condition. Under these conditions, these time-varying loads result from live load effects that vary the maximum stress and the stress range on the bearing. The minimum load depends on the dead load and therefore is a function of the construction material (e.g., steel bridges tend to result in smaller dead load stresses). The stress range depends primarily on the statistical distribution of the live load.

The dynamic compression test matrix was developed to examine the effects of stress range, peak stress, shape factor, pad thickness, and pad manufacturer on pad stiffness and durability. With the results from the dynamic tests, compressive stress or strain limits can be developed to prevent undue fatigue-induced damage.

2.5.1. Test Matrix

The test matrix was developed to evaluate the effect of dynamic loading on the pad response, including the progression of damage and failure mode. Therefore, the pad had to be subjected to a realistic number of cycles to model the pad response over its lifetime. However, since hundreds of millions of truck-load cycles are possible within a normal bridge life, only the cycles resulting from heaviest trucks, which cause the majority of the damage, were modeled. On the other hand, the experimental load history was more intensive than an actual loading and therefore may have been more taxing.

To model the response, approximately 2 million cycles were applied with a loading rate of 1.5 Hz. A reasonable loading rate was used to test in an effective manner without causing harmful heat build-up in the pad. (Note that a reduced loading rate of 0.75 Hz was used for a pad measuring 12 x 6 x 2 inches and subjected to a peak stress of 4 ksi and a stress range of 3 ksi, since the heat build up in that pad exceeded the acceptable limits.) The loading regime permitted completion of the tests in a timely manner; the majority of the tests were completed in 16 days.

After completion of the tests, the pads were subjected to several compressive load cycles at a frequency 0.05 Hz to investigate possible rate-dependent effects on pad stiffness. In addition, some of the specimens were tested to failure under static load to determine the influence of the dynamic load on stress and strain capacities.

The test matrix consisted of 17 specimens, as presented in Table 2.4. The matrix included 13 tests on pads from Manufacturer A (Series CD-A), three tests on pads from

Manufacturer B (Series CD-B), and one test on a pad from Manufacture C (Series CD-C). For each test, the table indicates the pad geometry, shape factor, number of dynamic cycles that were applied, and information about the stress range, including minimum stress, σ_{min}, maximum stress, σ_{max}, and stress range, σ_{max}-σ_{min}. Pads to which fewer than 2 million cycles were applied are highlighted. The effect of pad thickness was assessed by comparing specimens with the same applied stresses. In a similar manner, the effects of stress range, minimum stress, and maximum stress were evaluated by comparing specimens of similar sizes.

Table 2.4. Dynamic Compression Tests

Test	Pad Size	Shape Factor	Peak Stress (ksi)	Stress Range (ksi)	Total Cycles	S.S. Strain (in./in.)	Max. Strain (in./in.)	Residual Strain (in./in.)	Damage State
CD-A1	8x8x1.5	1.33	1.00	0.50	2 M	0.06	0.064	0.000	A
CD-A2	8x8x1.5	1.33	2.00	1.00	2 M	0.13	0.135	0.032	C1, B
CD-A3	8x8x2	1.00	2.00	1.00	2 M	0.14	0.146	0.021	C1, B
CD-A4	8x8x0.75	2.67	2.00	1.00	2 M	0.21	0.212	0.038	A, B
CD-A5	10x10x2	1.25	3.00	1.00	2 M	0.17	0.174	0.060	C1, B
CD-A6	6x6x2	0.75	6.00	3.00	2 M	0.27	0.278	0.130	C3, B
CD-A7	6x6x2	0.75	4.00	2.00	2 M	0.24	0.247	0.080	C2, B
CD-A8	10x10x0.75	3.33	3.00	1.00	300 K	NA			A
CD-A9	10x10x0.75	3.33	3.00	2.00	2 M	0.22	0.229	0.050	C1, B
CD-A10	8x8x1.5	1.33	4.00	1.00	400 K	NA			A, B
CD-A11	8x8x1.5	1.33	4.00	1.00	2 M	0.21	0.213	0.062	A, B
CD-A12	8x8x1.5	1.33	4.00	3.00	2 M	0.20	0.215	0.092	C3, B
CD-A13	12x6x2	1.00	4.00	3.00	1.3 M	0.23	0.245		C3, B
CD-B1	8x8x2	1.00	2.00	1	2 M	0.16	0.157		B
CD-B2	10x10x2	1.25	3.00	2	2 M	0.20	0.195		C1
CD-B3	6x6x2	0.75	6.00	3	1 M	0.28	0.275		D
CD-C1	8x8x2	1.00	2.00	1	2.1 M	0.11	0.105		A,B

The dynamic compression tests were conducted with the custom self-reacting testing frame described in Section 2.2 and shown in Figure 2.4. The dynamic tests were subjected to a cyclic sine-wave force history. Testing was conducted by placing the mean operating load on the pad. The amplitude of cyclic loading was applied to meet preset values, and the test continued until completion of the target number of cycles. Data were recorded with the Labview data acquisition system at 15 samples per second. All load

cycles were monitored, but only selected cycles were recorded. The measured cycles were completed for pre-selected cycle increments. Additional measurements were selected for points where possible changes had occurred. Photographs of the test specimen were taken during the test to document pad damage and the progression of oil excretion. The temperature of the test specimen was also monitored to guard against damaging heat buildup. Upon completion of the test, the pad was removed, photographed, and measured. The pad thickness was then recorded daily for one week after test completion to document pad recovery.

2.5.2. Test Observations and Results

During testing the pads were visually monitored to observe the progression of pad damage. The damage states during and at the end of testing are noted in Table 2.4. For the pads with the most significant damage states, the progression of damage was initial secretion of oil (Damage State B) followed by pad delamination. Three degrees of pad delamination were noted: State C1 delamination within 5 percent of edge, State C2 delamination within 10 percent of edge, and State C3 delamination within 15 percent of edge. Examples of the damage state categories are shown in Figure 1.5.

As indicated for the creep tests and in earlier reports [(Roeder, Lehman, and Larson 2003)], oil secretion was observed in pads that were subjected to long-term monotonic or dynamic loading of 2 ksi or larger. The onset of oil secretion was related to the peak stress and the stress range. For a given peak stress, pads with a higher stress range exuded oil earlier (note that the stress range was zero for the creep tests). This effect was relatively linear with respect to time, i.e., the onset of oil secretion displayed a roughly linear relationship between peak compressive stress and time. An increase in stress range (denoted by different marker shapes) also resulted in earlier oil secretion.

Figure 2.18 indicates the final damage state for each of the pads that were subjected to dynamic compressive loading. The results indicated that the final damage state was a function of the maximum stress and the stress range. Although an increase in the maximum stress increased the damage, the stress range had a more significant effect. This effect can be seen by comparing the pads that were subjected to a maximum stress of 4 ksi (Figure 2.18). Of that data set, the pad with the smallest stress range, 1 ksi, sustained damage that was limited to oil secretion. The pads that were subjected to larger

stress ranges of 2 and 3 ksi sustained significantly more damage. Therefore, to limit damage to the pads, it is recommended that the stress range be less than or equal to 2 ksi. Note that it was expected that the maximum stress would not exceed 3 ksi. This region is marked “damage limited” in the figure.

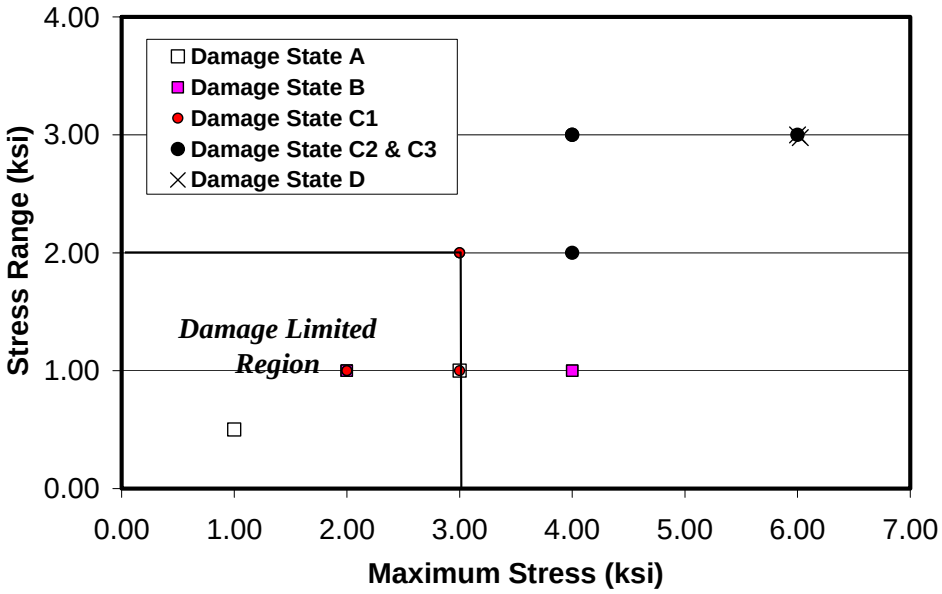

Figure 2.18. Damage to CD Series Pads

The damage state influences the residual strain, which is the strain sustained by the pad after loading. After testing, pad recovery was monitored until the measured strain was approximately constant over time. Table 2.4 reports residual strain measurements for some of the CD-A series specimens. The results showed that the pads that had higher stress ranges, and therefore sustained more significant damage, had larger residual strain ratios, where the residual strain ratio is the ratio of the residual strain to the maximum strain. Residual strains were not sustained by Specimen CD2, which was the only pad that did not secrete oil during testing.

Previous analysis has indicated that that subjecting CDP to continuous dynamic compression loading increases the effective modulus of elasticity (Roeder, Lehman, and Larson 2002). As observed previously, the increased deflection, or strain, of the pads due to dynamic compression is similar to the creep amplification. However, as noted previously, the damage sustained by the pad is significantly influenced by both the stress range and

the maximum stress and, therefore, dynamic effects are important to assess the probable damage state. Additional details on those findings are available in elsewhere (Roeder, Lehman, and Larson 2002).

To determine the influence of the dynamic loading regime on the pad stress and strain capacities, some of the CD-A series pads were subjected to monotonic static load and tested to failure after completion of the dynamic tests. The measured peak stress and failure strain values were compared to a monotonic static compression test, presented in Table 2.2. The measured strain and stress values for the monotonic retest were normalized to the static test values. The stress and strain ratios are presented in the final two columns of Table 2.5. The results showed that the stress and strain capacities increased relative to the static test, which indicates that a failure strain of 0.25 in./in. may be too limiting for pads subjected to creep or dynamic loading.

Table 2.5. Monotonic Retest of Some Series CD-A Specimens

Test	Pad Size (in.)	Peak Stress (ksi)	Stress Range (ksi)	Peak Stress (ksi)	Failure Strain (in/in)	Static Test	Ratio of Retest to Static Peak Stress	Ratio of Retest to Static Failure Strain
CD-A1	8x8x1.5	1	0.5	12.7	0.29	CSA-19	1.11	1.17
CD-A2	8x8x1.5	2	1	13.3	0.33	CSA-19	1.17	1.33
CD-A3	8x8x2	2	1	11.3	0.3	CSA-23	1.14	1.21
CD-A4	8x8x0.75	2	1	12	0.35	CSA-24	1.29	
CD-A10	8x8x1.5	4	1	11.1	0.28	CSA-19	0.97	1.13
CD-A11	8x8x1.5	4	1	12.1	0.34	CSA-19	1.06	1.37
CD-A12	8x8x1.5	4	3	13.2	0.35	CSA-19	1.16	1.41

CHAPTER 3
ROTATION TESTS

Bridge bearings rotate because of deflections due to truck traffic and temperature gradient and because of construction tolerances and practices. Rotations due to construction tolerances and camber may remain nearly constant for the life of the bridge. Rotations due to vehicle load are dynamic and occur millions of times during the bridge life. Rotations are damaging to bridge bearings because concentrated compressive strains develop on one edge of the bearing, as illustrated in Figure 3.1a and b. Furthermore, rotation may cause uplift or local separation between the bearing and the bridge structure, as illustrated in Figure 3.1c. Uplift causes large local bearing strains and local damage on polytetrafluoroethylene (PTFE) sliding surfaces.

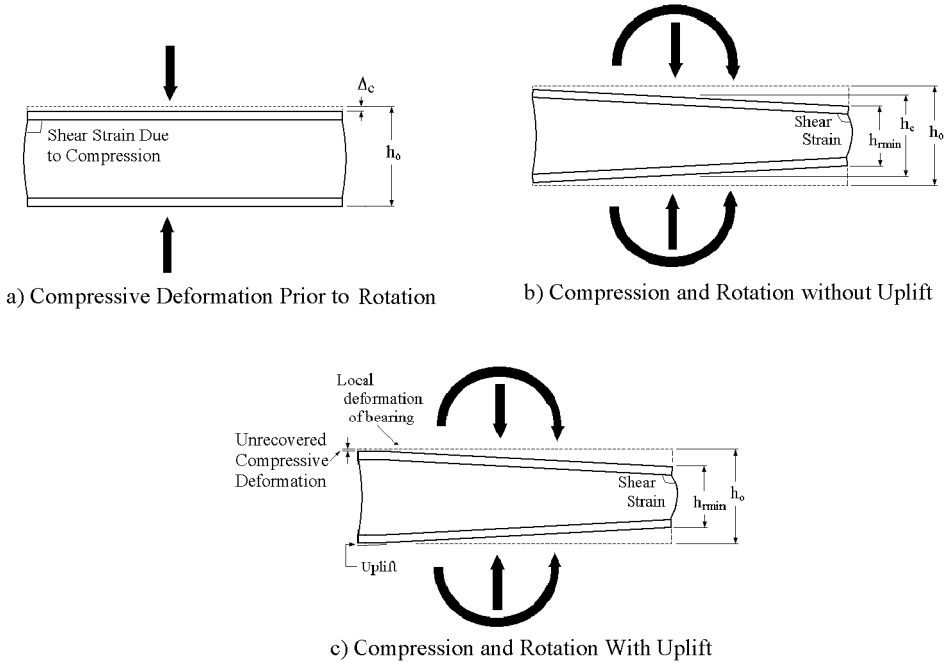

Figure 3.1. Rotational Strains and Deformation

CDP bearing pads, which were provided by three manufacturers, were tested under combined compression and rotation. These tests evaluated the strength, stiffness, deformation properties, and failure modes under both static and dynamic test conditions.

The static or monotonic tests (RS tests) were completed to establish the rotational stiffness, the relationship between uplift or separation, the relationship between rotation and strain, the influence of bearing geometry, and the failure modes. The RS tests aided in determining the maximum strain or deformation limits of the bearing pad. The dynamic or cyclic tests (RD tests) applied a large number of cycles of relatively large rotations to test pads of different sizes to provide an accelerated evaluation of the lifetime performance of CDP. These RD tests examined the fatigue life or durability of the bearing pad.

3.1. ROTATION TEST APPARATUS

Rotational experiments are difficult to perform on bridge bearings. Eccentric loading and tapered plates were used for many earlier bearing rotation tests, but these tests did not permit rational evaluation of rotational stiffness, uplift or separation, or the relationship between rotation and bearing strain. A specially designed testing apparatus shown in Figure 3.2 was designed to overcome these shortcomings [Stanton and Roeder, 1999, Roeder et al., 1995, Gilbert, 1991, Rodgers, 1991]. The apparatus is versatile, since it permits application of any magnitude of pure rotational deformation combined with compressive load. During testing, the rotation can be increased or decreased to evaluate the effect on bearing response, and a fixed shear force of modest magnitude can be applied.

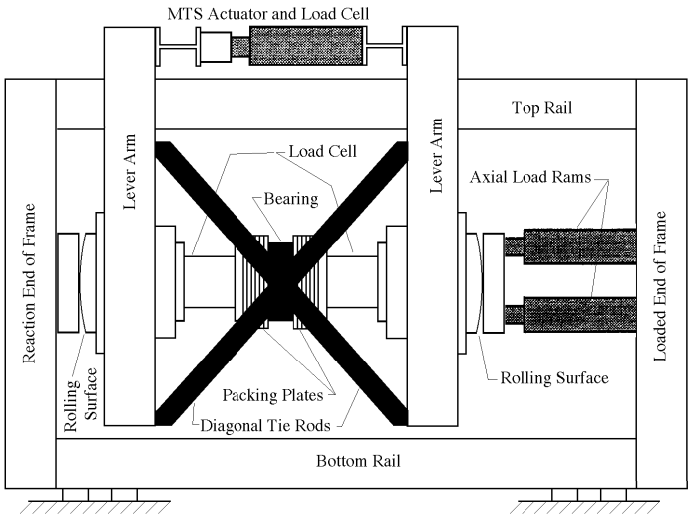

Figure 3.2. Schematic of Rotational Test Rig

With this test rig, the test bearing is placed in the center of a 51-inch diameter split cylinder with rotating arms, as shown in the figure. Moment and rotation are applied by the top servo-controlled actuator, and a wide range of monotonic and cyclic rotation histories can be applied. Compression loading on the bearing of up to 800 kips can be applied by the axial load rams.

CDP subjected to combined compression and rotation deform, as shown in Figure 3.1. Instrumentation was placed to monitor these behaviors, as shown in Figure 3.3. In the figure, potentiometers are represented by arrows and are designated a channel number (e.g., Ch3). Potentiometers 0 through 3 were located at the corners of the load plate to measure the separation between the cylinder halves and determine the rotational and compressive deformations.

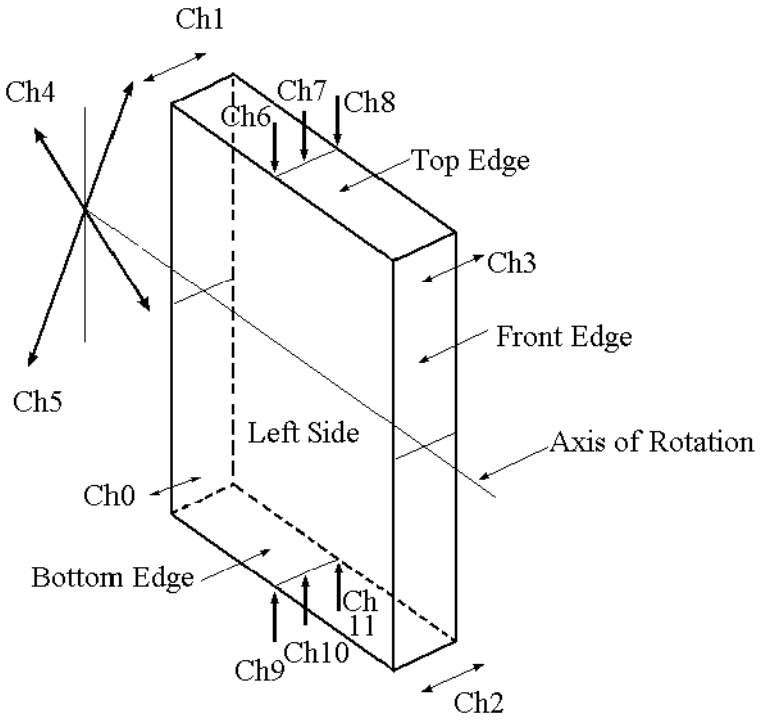

Figure 3.3. Instrumentation Plan

The internal LVDT on the actuator provided a redundant, approximate check of bearing rotation. Potentiometers 5 and 6 measured shear deformations of the pad. These shear deformations were expected to be zero, and these data checked the operation of the equipment. Potentiometers 6 through 11 measured pad bulge in the plane of rotation.

Compressive load on the bearing pad was measured with two 800-kip capacity load cells, shown in Figure 3.2. Moments on the bearing were calculated by using the dimensions from the actuator to the test pad (moment arm) and the horizontal actuator force that was monitored with a 100-kip load cell located on the actuator. Four load cells recorded the force in each of the diagonal bars. Bearing pad temperature was measured during the dynamic testing program.

All instruments were calibrated before testing by standards traceable to the National Bureau of Standards within the last year. Data from the potentiometers and load cells were collected and stored on computer disk with a Labview data acquisition system. Initial data were measured as voltages and converted to loads, displacements, and rotations through calibration factors and the geometry of the test setup.

During the RS tests, the rotational deformation was slowly applied, and all data were measured and recorded at 0.5-second intervals. For the RD tests, cyclic rotational deformations were imposed using a sine-wave displacement history with a 20-second period. This slow rate of cyclic deformation prevented heat build-up due to hysteretic behavior of the elastomer, but it was fast enough to permit timely completion of the test. Prevention of heat build-up is important, because elevated temperatures may change the material properties of the elastomer. Data recording was triggered with a cycle count timer for the RD tests. This timer counted a specific, predetermined number of cycles and then triggered data recording at 10 samples per second through one complete rotational cycle. The timer then reset and started a new cycle. Data measurements were also manually initiated when needed.

Before testing, specimen dimensions were measured, and the specimen was installed into the test rig. The installation of the test bearing and the positioning of the rotation arms required considerable care. After the bearing was properly oriented and temporarily blocked into position, initial zero voltages of the instruments were obtained. The pad compressive force and diagonal bar force were then increased to testing levels. The temporary blocking was removed, and the test proceeded. During testing, the pad was monitored to document pad uplift or damage. Visual observations and photographs were taken throughout the test.

3.2. ROTATIONAL TEST RESULTS

Manufacturer A provided the baseline tests for this study, and a total of 15 RS and 18 RD tests were completed for these bearing pads. This initial test program evaluated the effects of size and geometry, axial compressive stress, rotation range and magnitude, failure modes and general CDP bearing rotation performance, and these tests were described in an earlier report [Roeder, Lehman and Larsen 2002]. Additional tests were performed on pads supplied by Manufacturers B and C and compared to the previous work for this subsequent test program. The combined data provide a comparison of the range of variation in this behavior, and permit development of design recommendations for assuring good CDP performance. This chapter provides an overview of the complete test results, with emphasis on the variation in CDP behavior among different manufacturers and design recommendations. Tables 3.1 and 3.2 summarize the results from the RS and RD test programs, respectively, for all three manufacturers. Specimens are identified by manufacturer (A, B, or C) and the identification notation used in Chapter 2.

3.2.1 Static Test Results

The compressive stress level, bearing rotation, maximum compressive strain at the bearing edge due to combined rotation and compression, uplift information, and failure modes and test outcomes for the RS tests are noted in Table 3.1. Moment-rotation curves such as illustrated in Figure 3.4 were obtained for each test specimen. The typical moment-rotation response was slightly nonlinear, with softening behavior as illustrated in Figure 3.6.

Uplift was visually observed during testing, but initiation of uplift is difficult to precisely determine. In this study, a 0.003-inch feeler gauge was inserted between the bearing pad and the load surface to detect separation and uplift. The measured uplift distance, d_u, was measured as the distance where this feeler gauge fit into the uplift gap, as illustrated in Figure 3.5, and d_u was tabulated as a function of a specific rotation, θ, in Table 3.1.

Table 3.1. RS Test Program

Test Specimen	Pad Size	Axial Stress (ksi)	Maximum Rotation (radians)	Maximum Compressive Strain (in./in.)	Uplift Region, d_u	Rotational Stiffness (kip-in/rad)	Test Outcome
RS-A1	12 x 12 x 2	1.5	0.02	0.13	1.5" @ 0.02 rad	55,000	No Failure
RS-A2	12 x 12 x 2	2.0	0.02	0.15	No Uplift	62,500	No Failure
RS-A3	12 x 12 x 2	1.0	0.02	0.13	1.0" @ 0.02 rad.	42,500	No Failure
RS-A4	10 x 10 x 2	1.5	0.02	0.10	1.0" @ 0.02 rad.	31,250	No Failure
RS-A5	10 x 10 x 2	2.0	0.02	0.11	No Uplift	37,500	No Failure
RS-A6	10 x 10 x 2	1.0	0.02	0.09	1.0" @ 0.02 rad.	25,000	No Failure
RS-A7	12 x 12 x 2	1.5	0.02	0.12	1.75" @ 0.02 rad.	54,000	No Failure
RS-A8	18 x 6 x 2	1.5	0.02	0.11	No Uplift	10.000	No Failure
RS-A9	18 x 6 x 2	2.0	0.02	0.14	No Uplift	15,000	No Failure
RS-A10	18 x 6 x 2	2.0	0.03	0.15	No Uplift	15,000	No Failure
RS-A11	10 x 10 x 2	3.0	0.02	0.21	No Uplift	42,500	No Failure
RS-A12	10x10x1 1/2	2.0	0.02	0.19	1" @ 0.02 rad.	37,500	No Failure
RS-A13	10 x 10 x 2	4.0	0.027 @ fail	0.23 @ fail.	No Uplift	61,700	Shear fracture
RS-A14	10x10x1 1/2	4.0	0.033 @ fail.	0.24 @ fail.	1.0" @ 0,033	61,700	Shear Fracture
RS-A15	12x12x1 1/2	3.0	0.035 @ fail	0.24 @ fail.	1.0" at 0.025	85,300	Shear fracture
RS-B 1	10 x 10 x 2	4	0.036 @ fail.	0.295 @ fail	No Uplift	56,750	Shear fracture
RS-C1	10 x 10 x 2	4	.0223 @ fail	0.207 @ fail.	No Uplift	71,400	Shear fracture

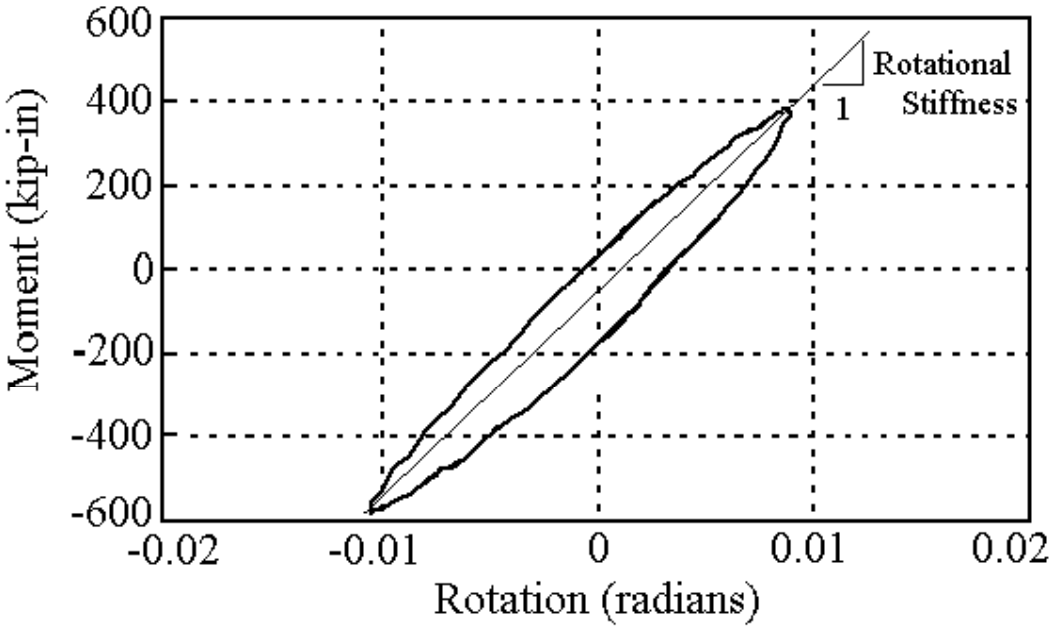

Figure 3.4. Typical Moment-Rotation Curve and Stiffness Determination

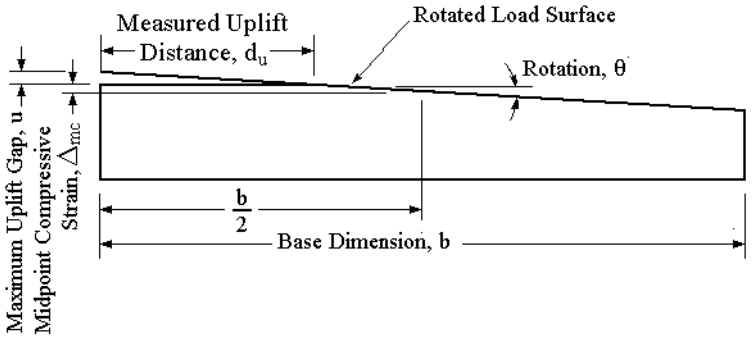

Figure 3.5. Determination of Uplift Rotation

3.3.2. Dynamic Test Results

For RD tests, the compressive load was applied, and several thousand cycles of repeated rotation were employed to simulate the long-term durability of the bearing pad under repeated cyclic rotations. The moment-rotation behavior was continually monitored, and selected cycles were recorded for later data analysis. Table 3.2 summarizes the compressive stress level, cyclic rotation, maximum compressive strain

Table 3.2. RD Test Program

Test Specimen	Pad Size (in.)	Axial Stress (ksi)	Cyclic Rotation (rad.)	Total Number of Cycles	Compressive Strain Range (in/in)	Observed Performance and Final Condition
RD-A1	12x12x2	1.5	±0.001	21,497	0.005	No damage
RD-A2	12x12x2	1.5	±0.01	58,729	0.070	C3 and B damage levels
RD-A3	12x12x2	1.5	±0.01	6,404	0.064	C3 damage level
RD-A4	12x12x2	1.5	±0075	6,300	0.050	C2 damage level
RD-A5	12x12x2	1.5	+.006 to +0.014	6,378	0.024	No damage
RD-A6	10x10x2	3.0	±0.01	6,706	0.053	C2 damage level
RD-A7	10x10x2	2.0	±0.01	6,400	0.057	C3 damage level
RD-A8	10x10x2	1.0	±0.01	6,300	0.060	C3 damage level
RD-A9	12x12x2	2.0	+.011 to +0.019	6,400	0.023	C2 damage level
RD-A10	18x6x2	1.5	±0.01	7,080	0.033	No damage
RD-A11	18x6x2	2.0	+.011 to +0.019	6,400	0.014	No damage
RD-A12	18x6x2	2.0	±0.02	6,530	0.070	C2 damage level
RD-A13	10x10x2	2.0	+.015 to +0.025	6,616	0.032	No damage
RD-A14	10x10x2	2.0	+.025 to +0.035	6,465	0.034	No damage
RD-A15	10x10x2	3.0	+.025 to +0.035	1,815	0.026	Fracture @ 300 cycles
RD-A16	10x10x1$^{1}/_{2}$	2.0	+.01 to +0.02	100,000	0.033	C3 and B damage levels

RD-A17	10x10x2	1	±0.02	4,589	0.107	C3 damage level
RD-A18	10x10x2	2	±0.02	5,450	0.108	Fracture @ 2260 cycles
RD-B1	10x10x2	2	+.025 to +0.035	6585	0.021	A1 - Ridge formed near layer bond @ 50 cycles
RD-B2	10x10x2	2	±0.01	6540	0.055	A1 - Ridge formed near layer bond @ 15 cycles
RD-B3	10x10x2	2	+.015 to +0.025	7077	0.023	A1 - Ridge formed near layer bond @ 60 cycles
RD-B4	10x10x2	3	+.025 to +0.035	285	0.021	Fracture @ 282 cycles
RD-B5	10x10x2	1	±0.01	6900	0.052	A1 - No uplift - ridges formed after 200 cycles
RD-B6	10x10x2	1	±0.02	5909	0.105	Shear fracture
RD-B25	10x10x2	2	±0.02	895	0.106	Fracture @ 895 cycles
RD-C1	10x10x2	2	+.025 to +0.035	24	0.020	Fracture @ 4 cycles
RD-C2	10x10x2	2	±0.01	856	0.068	Fracture @ 320 cycles
RD-C3	10x10x2	2	±0.005	6563	0.029	Oil secretion but otherwise no damage

and strain range at the edge of the bearing, failure modes, and test outcomes for the RD tests.

Figure 3.6 shows the moment-rotation curve for the initial, the 100th, the 1000th, the 2500th, and the 5000th cycles of a typical specimen. This variation in behavior was typical of that observed for all other test specimens. Each cycle displayed hysteretic behavior, and the area within each hysteresis loop was the magnitude of this work for a given load cycle. For RS tests, the work and heat build-up caused by the hysteretic behavior was not a concern, because the heat build-up in a single cycle was small. However, the RD tests were accelerated durability tests, and large rotation cycles were applied much more frequently than is expected under normal service conditions. Under these conditions, the heat build-up could have increased the bearing pad temperature during testing, and the increased temperature could have adversely affected the material properties of the elastomer and the pad. As a result, both the energy input per cycle and the temperature of the bearing were monitored, and the rate of dynamic loading was controlled to avoid excessive heat build-up. During these tests, the temperature did not increase more than a few degrees for any test. This modest temperature increase would not cause significant changes in the elastomer or bearing pad properties (Roeder and Stanton 1983, Stanton and Roeder 1982).

Specimen stiffness was computed for each cycle of each dynamic test by the method illustrated in Figure 3.4. During testing, changes in stiffness were relatively small, as can be seen in Figure 3.6. Later cycles had somewhat larger stiffnesses than the initial cycles, but the difference was normally less than 10 percent to 20 percent.

Four basic outcomes or end damage categories were noted from the rotation tests. These damage categories or failure modes were similar to those described for the compression tests and are shown in Figure 1.5. Category A resulted in no observed damage, and Category B resulted in excreted oils and waxes during testing but no other physical damage. Some thick specimens were formed by bonding two thin pads together, and in some cases a pronounced lateral deformation was observed at the bonded interface, as illustrated in the photo of Figure 3.7. These pads did not fracture at the bonded surface, nor did they demonstrate any deterioration in resistance or stiffness. As a result, the outcome illustrated in Figure 3.7 was defined as Category A1. Specimens

that sustained damage states A and B were regarded as completely serviceable bearings at the end of the test program, and bearings with these outcomes had

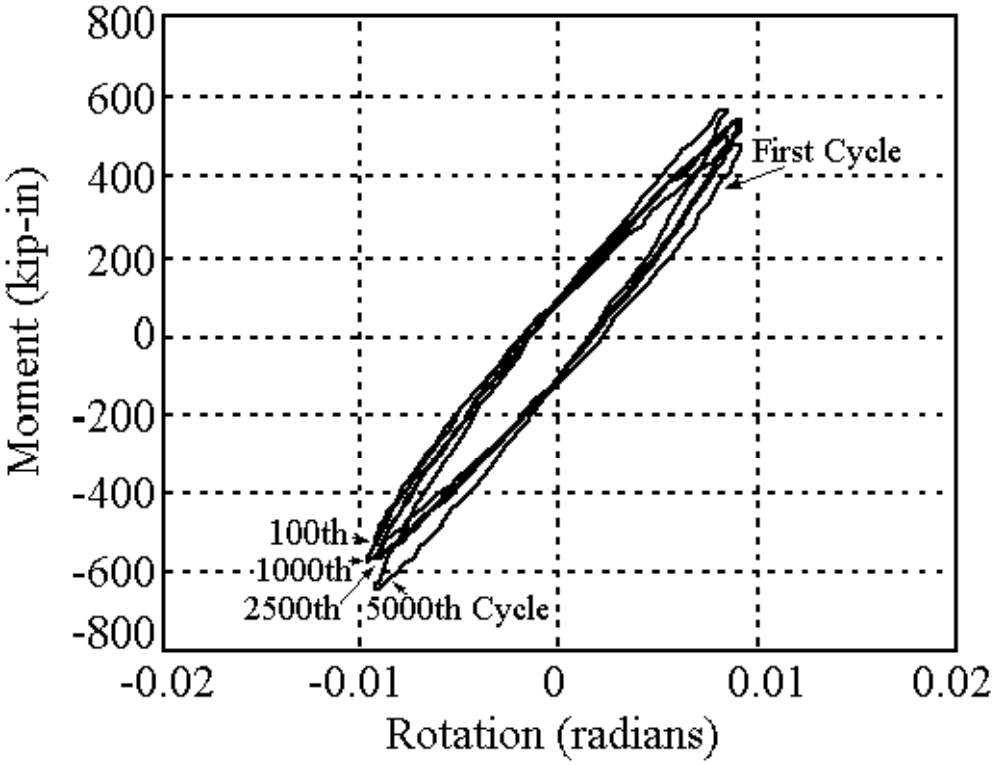

Figure 3.6. Typical Moment-Rotation Curves for Specimen RD-A2

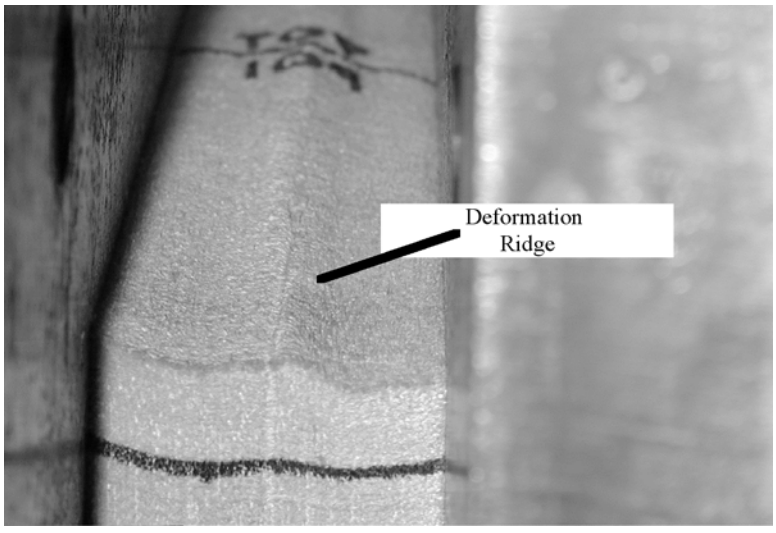

Figure 3.7. Ridge of Deformation at the Bonded Layer

- maximum compressive strains smaller than the fracture strain threshold, ε_{cr}
- no observable uplift during cyclic rotation (or were subject to no cyclic rotation).

Category C resulted in delamination and separation of the layers of the CDP. Delamination initiated on the top and bottom layers of the CDP specimen near the extreme edge of the bearings where the rotational shear strain was largest. Delamination displayed a range of severity, and three different damage levels for Category C were noted:

- Category C1 had relatively minor damage confined within 5 percent of the plan dimension at the edge of the bearing.
- Category C2 had damage greater that Category C1, but damage was confined to 10 percent of the plan dimension at the edge of the bearing.
- Category C3 had damage greater than Category C2.

Figure 1.5c is a photo of typical delamination damage. It is clear from the photograph that even severe delamination does not represent a complete bearing pad failure, but severe delamination clearly results in deterioration of the long-term performance and service life of the bearing pad.

Category D damage consisted of a brittle diagonal fracture initiating from the highly strained bearing edge, as illustrated in Figure 1.5e. This fracture represents a clear bearing failure, and in the field immediate replacement would be required should this failure occur. Category D damage was noted only when the maximum compressive strain exceeded the failure strain, ε_{cr}. As noted in Chapter 2, this failure strain depends on the properties and manufacturing methods of the CDP pads. Figure 3.8 plots the maximum compressive strain due to combined compression and rotation versus the maximum rotation level for all RS and RD test results, and it shows the final damage condition of the test specimens. This figure illustrates all levels of behavior (Categories A, B, C, and D). Specimens provided by Manufacturers A, B, and C are identified as diamonds, squares, and circles, respectively. Specimens with no damage are identified as hollow symbols. Specimens with fracture are identified as solid black symbols, and

intermediate delamination damage is indicated by shaded symbols. Specimens with shaded areas indicate delamination or Category C behavior.

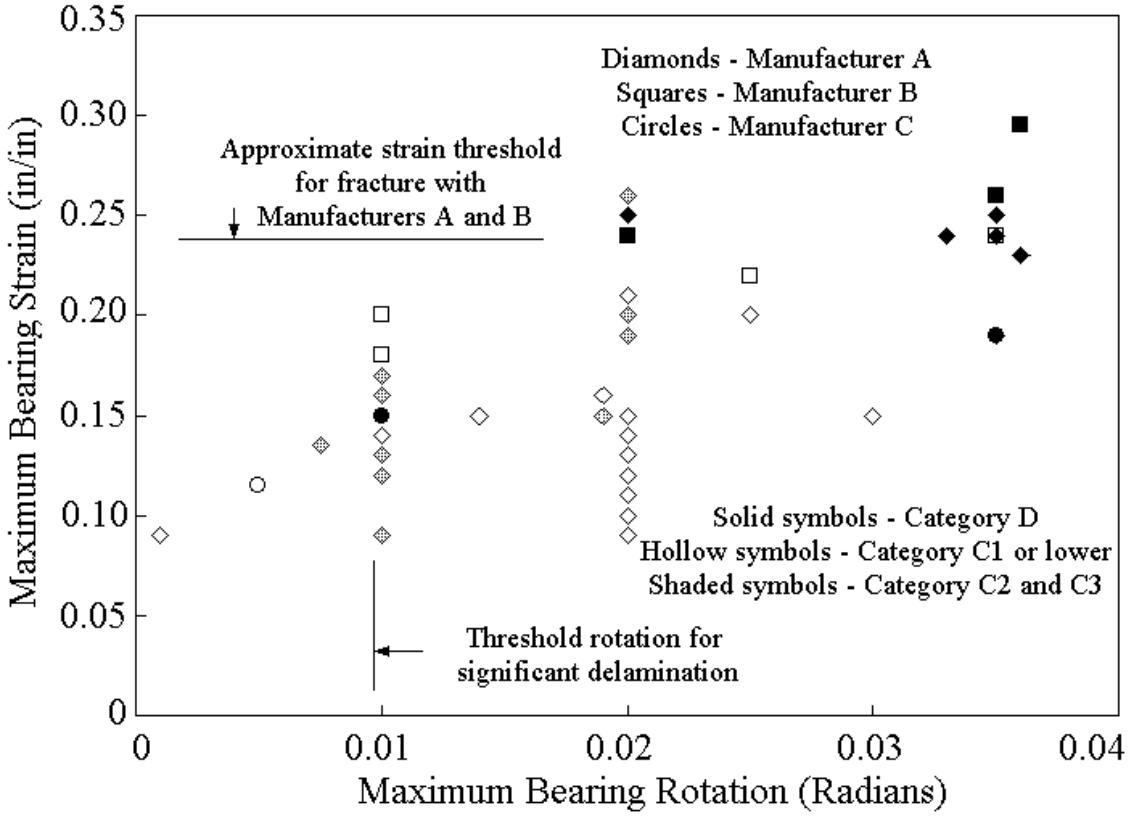

Figure 3.8. Rotation Damage Level as Function of Maximum Rotation and Strain for Different Manufacturers

The figure shows that maximum strain may be a weak indicator of delamination (Category C) damage, but it is a strong indicator of fracture (Category D damage). Delamination damage associated with smaller maximum bearing rotations always occurred with cyclic rotation and uplift or separation between the bearing pad and the load surface. Therefore, delamination and rotation limits must distinguish between static and dynamic rotations and must give consideration to uplift. However, fracture due to rotation (Category D damage) is related to a threshold compressive strain level, as noted for compressive loading in Chapter 2. Manufacturers A and B consistently achieved a maximum strain of approximately 0.25 before this fracture occurred, whereas Manufacturer C's specimens fractured at maximum compressive edge strains as small as 0.15. Behavior such as that provided by Manufacturers A and B were sought in the

design recommendations developed during this research program because this behavior permits significant increases in the design capacity of CDP bearing pads. Behavior such as that provided by Manufacturer C should be avoided, since it would severely restrict possible design limits. Chapter 5 discusses quality assurance measures prescribed to assure that these goals are achieved.

3.3. DESIGN LIMITS AND VARIATION IN BEHAVIOR

The ultimate goal of this research study was to determine the variation in behavior achieved with CDP provided by different manufacturers and to establish design limits that can be used to assure good bearing performance within this context. The rotation tests demonstrated three major design requirements for CDP bearings:

- A maximum compressive strain limit, ε_{cr}, must be defined to prevent fracture and Category D damage.
- Uplift under cyclic load causes delamination (Category C) damage. As noted earlier, Category C damage is limited damage, but it must be controlled to guarantee long-term serviceability.
- Bearing rotation is directly associated with a bearing moment, as illustrated in figures 3.4 and 3.6. This moment is transferred to structural elements of the bridge, and so it is necessary to predict the magnitude of this moment as a function of bearing rotation.

These three design requirements are discussed below.

Tables 3.1 and 3.2 and Figure 3.8 show 12 specimens that exhibited Category D failure, or diagonal fracture. Figure 3.6 shows that these fractures were most strongly related to a maximum compressive strain limit, ε_{cr}, rather than a maximum rotation limit. The strain limit was also consistent with similar failures at similar measured strain capacities for CDP bearings in compression. Five of the eleven bearings were provided by Manufacturer A, four were provided by Manufacturer B, and three were provided by Manufacturer C. Manufacturers A and B had similar average strain limits. The mean values of ε_{cr} were 0.255, 0.259, and 0.182 in/in for Manufacturers A, B, and C, respectively. Furthermore, the standard deviations of Manufacturers A and B of 0.0229 and 0.0259 in/in, respectively, were quite similar, and these pads provided comparable

bearing performance. As a result, they were grouped to provide a more reliable estimate of bearing pad performance.

Category D failure is the most serious failure noted with CDP pads, and it clearly should be avoided under all practical consequences. However, this failure is not likely to be disastrous in that the bearing will still support gravity load after failure occurs. As a result, it is anticipated that a design beta factor of 2.5 is appropriate for this application, and therefore, Equation 3-2 provides a limiting strain for design. Using the results from Manufacturers A and B, a compressive strain limit was derived. A mean and standard deviation of 0.257 and 0.0228 in/in, respectively, were used.

$$\varepsilon_{cr} = 0.257 - 2.5\ (0.0228) = 0.20 \text{ in/in} \qquad \text{(Eq.3-2)}$$

This design limit excludes the data from Manufacturer C because of its product's very limited strain capacity. This exclusion is based on the material properties of the CDP, and the limits of the exclusion are discussed in Chapter 5.

Prediction of uplift is also an issue of concern because cyclic rotations with uplift cause delamination of the bearings pads. As noted earlier, very small amounts of uplift may be tolerable because delamination damage increases with increasing uplift rotation and uplift distance. Figure 3.5 and Equation 3.1c show that uplift deformation exceeds Δ_{mc}. Section 2.3 of Chapter 2 shows that the full compressive strain and deformation are not recovered when a compressive stress is removed from CDP, and a residual strain of 13 percent to 32 percent of the maximum strain occurs when compressive stress is removed from CDP. The loading and unloading stiffness values are approximately the same before uplift, and a 20 percent residual strain is an intermediate value. As a result, the recovered strain may be calculated as

$$\varepsilon_{recovered} \leq (1 - .2)\ \varepsilon_c = 0.80\ \varepsilon_c \qquad \text{(Eq.3-3a)}$$

where $\varepsilon_c = \dfrac{\sigma_s}{E_3}$

and the rotation at uplift, θ_{uplift}, may be approximated as

$$\theta_{uplift} \approx 0.80\ \frac{2\ t\ \varepsilon_c}{b} \qquad \text{(Eq.3-3b)}$$

Prevention of any uplift requires that the total rotation, θ_T, be limited to

$$\theta_T \leq 0.80 \frac{2\, t\, \varepsilon_c}{b} \qquad \text{(Eq.3-3c)}$$

The experiments showed that uplift without cyclic rotation does not usually cause bearing delamination. As a result, cyclic rotations, θ_R, are the issue of concern for delamination and may cause delamination at rotations smaller than indicated by Equation 3-3c. Figure 3.9 shows the delamination damage noted with various bearings as a function of the dimensionless cyclic rotation and total rotation range of the bearing pad. The figure shows that bearings with θ_R larger than approximately $0.30 \frac{2\, t\, \varepsilon_c}{b}$ may have delamination damage at a smaller total rotation.

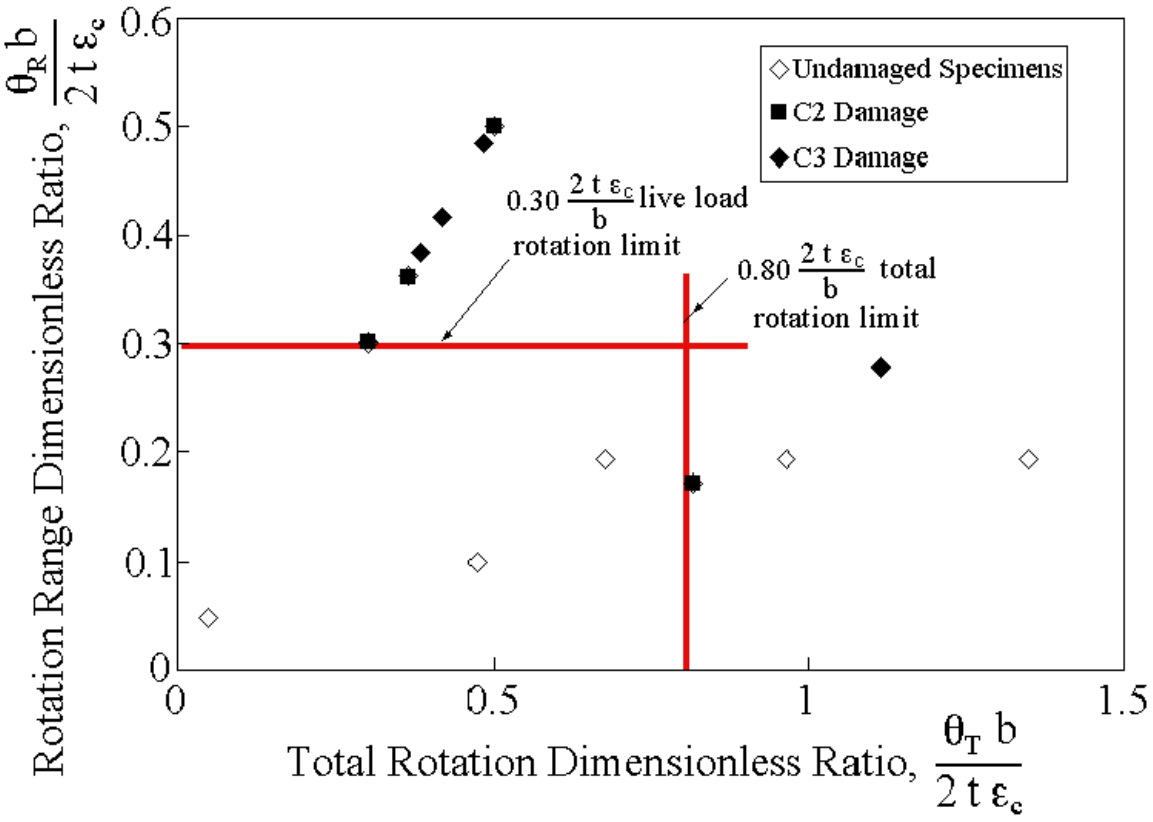

Figure 3.9. Dimensionless Rotation Range for Delamination Damage

This analysis suggests that the limit on θ_R should be

$$\theta_R < 0.30 \frac{2\,t\,\varepsilon_c}{b} \qquad \text{(Eq. 3.6)}$$

and combined with Equation 3-3c to provide conservative limits to avoid delamination damage due to repeated, cyclic loads. Figure 3.9 shows that a substantial number of bearings tolerated larger rotations than suggested by the rotation limits of equations 3.3 and 3.6. (The number of specimens plotted on this figure is larger than readily apparent because several tests are plotted over one another.) This two-level design approach is similar to the recommended limits provided for the live load and total compression stress limits in Chapter 2. Furthermore, the motivation for those limits is also similar to that of the rotation limits derived here. However, there is one clear difference. The compression fatigue tests employed 2,000,000 cycles of cyclic stress at a stress level that is appropriate for application with the AASHTO truck load because this design truck load is larger than most trucks on the highway system. However, the accelerated testing employed for the compression durability tests could not be used for the rotation tests. The rotation tests required very slowly applied rotations because of the potential heat buildup. As a result, the normal RD test had 6,000 to 60,000 cycles of rotation. Thus the cyclic rotation in Equation 3.6 is larger than the rotation associated with bridge live loads. To account for this difference, it is suggested that θ_R be 1.5 times the live load rotation, θ_L. Therefore,

$$\theta_R = 1.5\,\theta_L < 0.30 \frac{2\,t\,\varepsilon_c}{b} \qquad \text{(Eq. 3.7a)}$$

$$\text{or} \quad \theta_L = 0.2 \left(\frac{2\,t\,\varepsilon_c}{b} \right) \qquad \text{(Eq. 3.7b)}$$

Rotational stiffness, K_θ, is needed for some design applications. For example, K_θ is needed to define the moment transferred by CDP bearings when they are subjected to an applied rotation. K_θ was determined as a secant stiffness from the measured moment-rotation data, as shown in Figure 3.4. Simplified theory suggests that K_θ should depend upon the bearing thickness, t, the second moment of inertia of the plan area, I, and the elastic stiffness of the pad under compressive load, E_c. Since E_c increases with increasing compressive stress, larger compressive stress should also result in greater stiffness. The

measured values of K_θ are expressed in a dimensionless rotational stiffness shown in Equation 3.8.

$$\text{Dimensionless Rotational Stiffness} = \frac{K_\theta \, t_p}{E_c \, I} \qquad \text{(Eq. 3.8)}$$

The resulting ratio is plotted in Figure 3.10 as a function of shape factor, S. The dimensionless ratio always lies between 1.5 and 4.0, and the ratio is somewhat larger for the smaller shape factors and larger compressive stress levels. There is scatter in the results, but this ratio can be reasonably represented by a linear relationship that is a function of these two parameters.

$$K_\theta = \{4.5 - 2.2\,S + 0.6\,\sigma\}\frac{E_c \, I}{t_p} \qquad \text{(Eq. 3.9)}$$

where σ is the average compressive stress on the bearing pad.

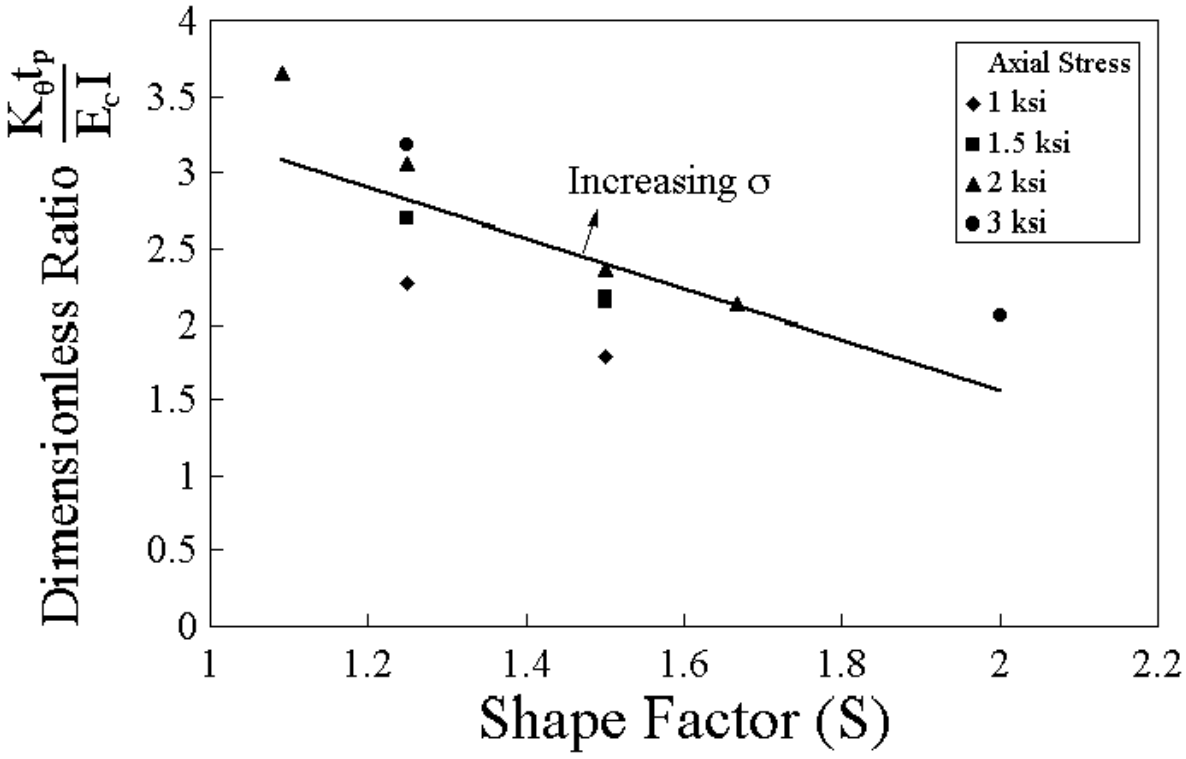

Figure 3.10. Dimensionless Bearing Pad Stiffness as a Function of Shape Factor

CHAPTER 4
SHEAR TESTS

4.1. INTRODUCTION

Bridge bearings accommodate translational movement caused by thermal effects, creep and shrinkage of the bridge superstructure, and dynamic loading. Elastomeric bearings normally accommodate these translational movements through shearing deformation of the elastomer as illustrated in Fig. 4.1a. Previous research [Roeder, Lehman and Larsen 2002] showed that CDP bearings are relatively stiff and have limited strain capacity in shear deformation. As a result, CDP bearings subject to significant translational movement should be built with a polytetraflourethylene (PTFE) sliding surface at the top of the bearing, as shown in the cutaway section of Figure 4.1b.

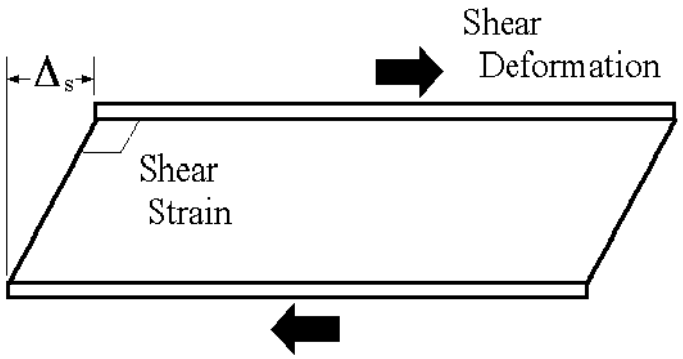

a)

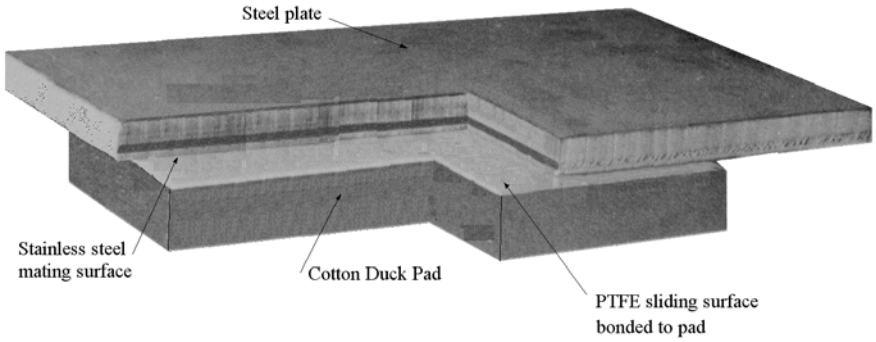

b)

Figure 4.1. Translation of Bridge Bearings a) Shear Deformation of an Elastomeric Bearing Pad and b) PTFE Low Friction Sliding Surface with CDP

In a PTFE application, a polished stainless steel mating surface is attached to the superstructure. The PTFE sheet may be bonded directly to the elastomer, or it may be recessed into a steel plate that is bonded to the bearing pad. The latter approach is beneficial because recessed PTFE has greater resistance to cold flow. PTFE sliding surfaces that are subjected to rotation experience edge bearing stress. The edge stresses must also be evaluated for cold flow or creep of PTFE. In some cases, this edge loading due to the moment associated with rotation may control the CDP bearing pad design.

PTFE sliding surfaces can tolerate both large and small translational movements with little lateral resistance. The lateral resistance is controlled by friction, which depends on the compressive stress level, type of PTFE, lubrication and surface finish, cleanliness or contamination, and temperature and environmental conditions (Campbell and Kong, 1987 and 1988). The CDP bearing must develop adequate shear force and deformation to overcome the static frictional resistance of the sliding surface, and proper anchorage of the bearing pad may also be required to avoid slip, since slip or sliding of the bearing pad causes long-term wear or deterioration. Consequently, shear testing of CDP bearings was needed to establish shear stiffness and the expected coefficient of friction between CDP and the load surface, since this would provide minimum guidance on anchorage and attachment of CDP.

A comprehensive test program of CDP produced by Manufacturer A was conducted to evaluate the shear load and deformation properties as described in an earlier report[Roeder, Lehman and Larsen 2002] and is summarized here. This chapter provides a more detailed description of the shear stiffness and frictional characteristics of CDP produced by Manufacturers B and C with comparison to the results noted in the earlier study.

4.2. TEST APPARATUS AND INSTRUMENTATION

Figure 4.1a shows simple shear deformation of an elastomeric bearing pad, and the test setup shown in Figure 4.2 was designed to simulate this idealized state and the deformation commonly induced on bridge bearings. The test apparatus was a self-reacting steel frame with a matched pair of test bearings. A horizontal actuator deformed the pads in shear, and the load required to achieve this deformation was equally divided between the two bearing pads because of the symmetry of the arrangement. The actuator

operated under servo-hydraulic control of the displacement, and it applied its load through a central plate between the test specimens. As the test specimens deformed, the horizontal shear forces were transferred to a pair of steel reaction plates placed outside the bearing pads. These reaction plates were bolted to the end rail of the load frame through long slotted holes, which permitted height adjustment to accommodate different bearing pad thicknesses. Four manually tightened threaded rods (with separate load cells) applied compressive force to the test specimens. Packing bearings acted as elastomeric springs within this compressive load chain to maintain the compressive load as the large shear deformations were applied.

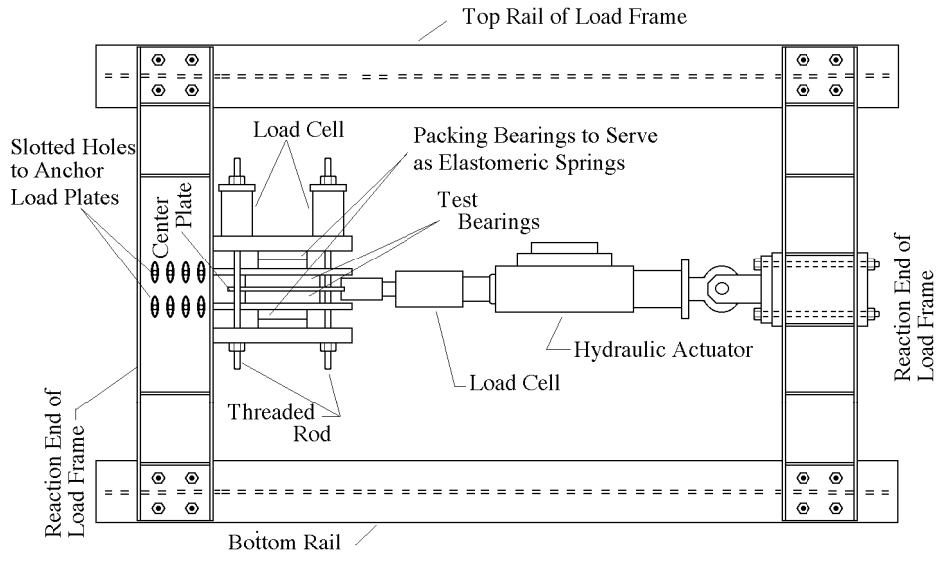

Figure 4.2. Schematic of the Shear Test Rig

The instrumentation (see Figure 4.3) was designed to measure all loads and deformations. Four potentiometers (labeled Ch0, Ch1, Ch2, and Ch3 in the figure) measured shearing deformation and horizontal slip of the pad. Four additional potentiometers (Ch4, Ch5, Ch6, and Ch7) measured compressive displacements. In addition, the applied shear was measured by a load cell within the actuator chain, and four custom load cells monitored the applied compressive load. The measured data were read and recorded with the National Instruments Labview data acquisition system and were interpreted with the MATLAB software program.

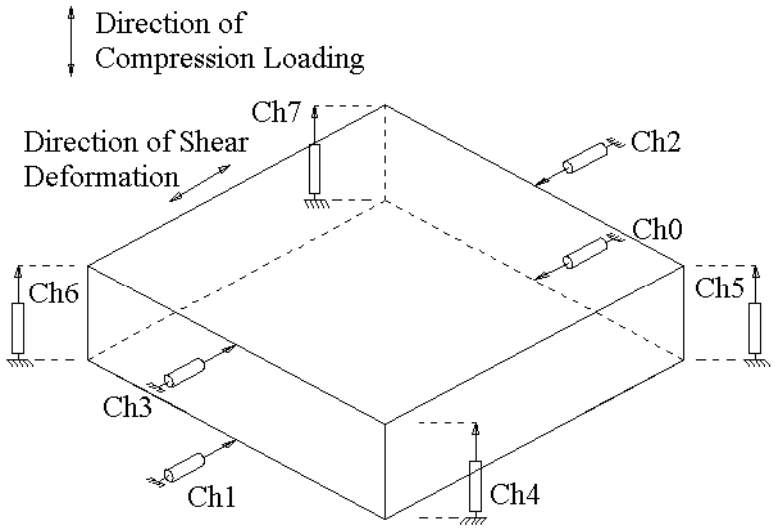

Figure 4.3. Shear Test Instrumentation

Both static shear tests (SS Tests) and dynamic shear tests (SD Tests) were performed on pads provided by Manufacturer A. These initial tests showed that CDP can not tolerate large shear deformation. The focus of the Manufacturer B and C tests were SS tests to determine shear stiffness and the coefficient of friction value of those pads. Thicker pads were tested because thicker pads permitted better resolution of the measured data.

The SS test results are summarized in Table 4.1. For these tests, monotonically increasing shearing deformations were applied at a strain rate of 0.002 in/in/sec under deformation control. Data for these tests were recorded at 1-second intervals, and the test specimens were observed to determine any slip between the pads and a load surface or damage to the test specimens. Photographs were taken to document important occurrences of damage.

The SD test results are summarized in Table 4.2. For the SD tests, the test pads were subjected to a cyclic sine wave of shear deformation (usually with a 20-second period). The amplitude of this deformation was selected on the basis of the specific test parameters, and the number of cycles were established to determine the durability of the CDP bearing pads under the specified deformation. For the SD tests, data were recorded at specified cycles intermittently throughout the test.

4.3. SHEAR TEST RESULTS

Several specimens were tested to failure. These specimens experienced increasing shear strains until a horizontal shear failure developed within the pad, as shown in Figure 1.5f or at a local strain concentration. The crack or separation initiated between laminate layers of the bearing pad, and a splitting type failure ultimately occurs. Under cyclic loading internal splits were noted within the bearing pad at strain levels that were significantly smaller than those noted for the rotation and compression tests. The observed failure mode may not be practical for many applications because pad slip will occur before these large strains develop. Unless slip of the pad is severely restrained for practical applications, this failure may not develop. Furthermore, these splits still occurred at shear forces that were larger than those normally expected with a good PTFE sliding surface.

Damage noted during the shear tests was categorized in a manner similar to that in the compression and rotation tests. Category D was modified to include the failure modes noted for the shear tests, and Category E was added. Therefore, the damage categories used for the shear tests are as follows:

- Category A - No damage.
- Category B - Secretion of oil or wax.
- Category C - Delamination confined at the edge of the bearing.
- Category D - Internal splitting or separation of layers.
- Category E- Edge splitting or cracking initiating from the keeper bars.

Table 4.2 summarizes the damage noted for each specimen and the cycles and strains at which initiation of damage was noted. Category C damage was not divided into sub-categories as was done for the dynamic compression and rotation tests.

Figure 4.4a shows a typical average stress-strain relationship. The initial stress-strain cycle is a softening curve with moderate hysteresis. The secant stiffness was used to define bearing stiffness, as illustrated in the figure, and these stiffness values are tabulated in tables 4.1 and 4.2. The secant shear modulus, G, which is defined as the slope of the straight line connecting the peaks of the first cycle, as shown in Figure 4.4a, was determined for each test and is shown in the tables.

Table 4.1. Summary of the Static Shear Test Program

Test Specimen	Pad Size	Compressive Stress (ksi)	Shear Strain (Radians)	Keeper Bars	Shear Modulus (ksi)	Coef. of Friction, μ	Test Outcome
SS-A1	8x8x2	1.5	To Slip	No	NA	0.18	Initiation of Slip; Coefficient of Friction
SS-A2	8x8x2	1.0	±0.40	Yes	1.9 ksi	NA	Determination of Stiffness
SS-A3	8x8x2	1.5	±0.20	Yes	2.6 ksi	NA	Determination of Stiffness
SS-A4	8x8x2	2.0	To Failure	Yes	NA	NA	Splitting of the elastomer initiating from keeper bars
SS-A5	8x8x1$^1/_2$	1.0	±0.20	Yes	2.2 ksi	NA	Determination of Stiffness
SS-A6	8x8x1$^1/_2$	2.0	To Failure	Yes	NA	NA	Splitting of the elastomer initiating from keeper bars
SS-A7	8x8x2	2.0	To Slip	No	NA	0.22	Initiation of Slip; Coefficient of Friction
SS-A8	10x10x1$^1/_2$	1.5	To Slip	No	NA	0.27	Initiation of Slip; Coefficient of Friction
SS-A9	8x8x2	1.0	±0.20	Yes	2.3 ksi	NA	Determination of Stiffness
SS-B1	8x8x2	1.5	To Slip	No	2.6 ksi	0.17	Determination of Stiffness and Friction
SS-C1	8x8x2	1.5	To Slip	No	2.2 ksi	NA	Determination of Stiffness

Table 4.2. Summary of the Dynamic Shear Test Program

Test Specimen	Pad Size	Compressive Stress (ksi)	Shear Strain Range (radians)	Mean Shear Strain (radians)	Total Number of cycles	Secant Shear Modulus (ksi)	Keeper Bars	Coeff. of Friction μ	Test Outcome
SD-A1	8x8x2	2.0	±0.25	0	218	NA	No	0.45 max	Type C damage noted at less the 218 cycles
SD-A2	8x8x2	2.5	± 0.12	0	4622	NA	No	0.45 max	Type C damage noted at less the 1000 cycles
SD-A3	8x8x2	2.0	± 0.10	0	10,103	4.0	Yes	NA	Type B and E damage. Initiated at 3970 cycles.
SD-A4	8x8x2	2.0	± 0.20	0	1,002	3.0	Yes	NA	Type D and E damage. Initiating at 690 cycles.
SD-A5	8x8x1$^1/_2$	2.0	0 to + 0.20	0.10	3,346	4.0	Yes	NA	Type B, D, and E damage. Initiating at 1,300 cycles.
SD-A6	8x8x1$^1/_2$	2.0	± 0.20	0	786	3.0	Yes	NA	Type D and E damage. Initiating at 80 cycles.
SD-A7	8x8x2	1.0	± 0.10	0	17,074	2.6	Yes	NA	Type B, D, and E damage. Initiating at 8,650 cycles.
SD-A8	10x18x1$^1/_2$	1.0	± 0.10	0	4,200	2.4	Yes	NA	Type E damage. Initiating at 280 cycles.

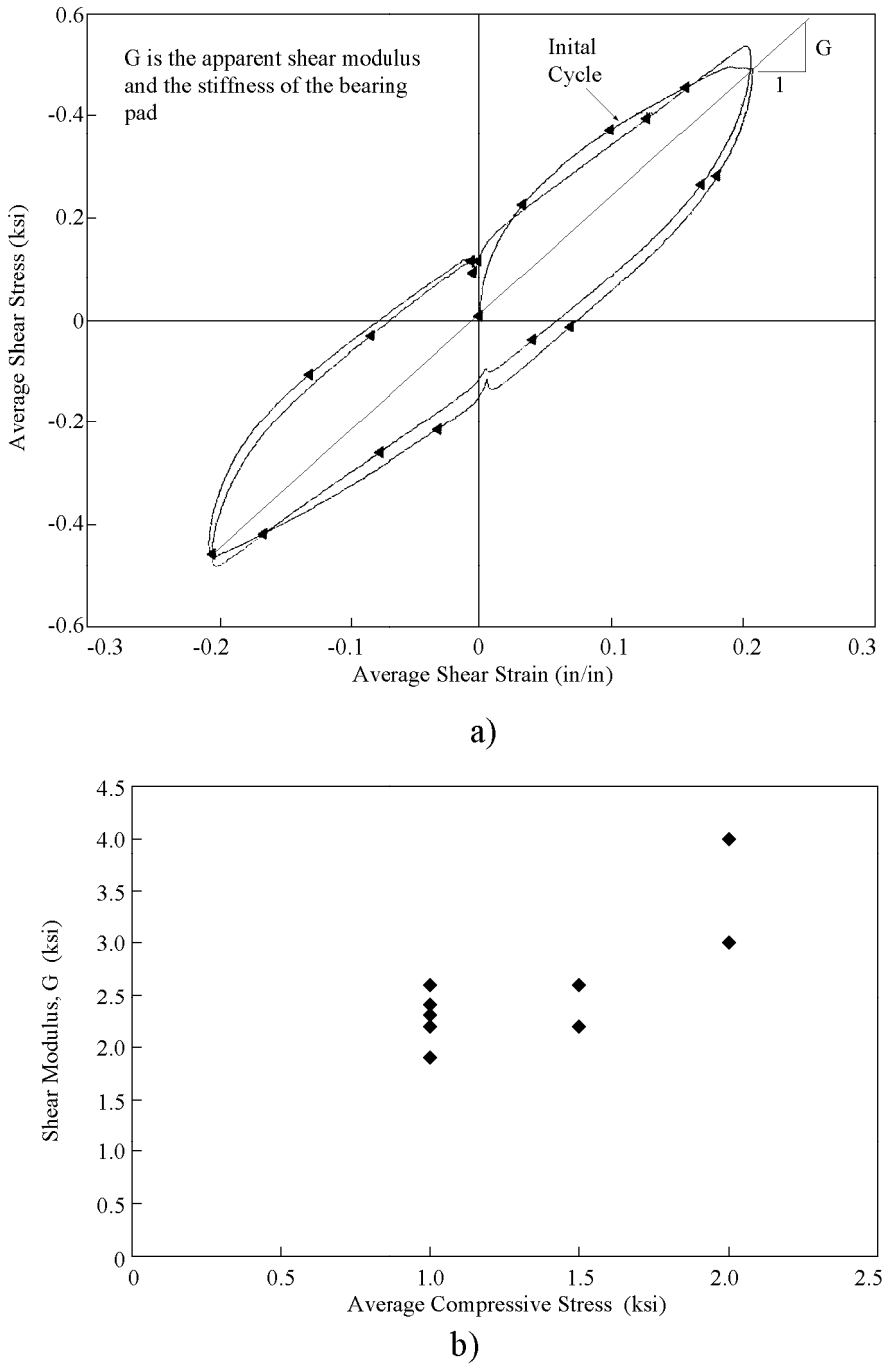

Figure 4.4. Shear Behavior: a) Typical Average Stress-Strain Curve from Static Shear Test and Definition of Shear Stiffness; b) Shear Stiffness as a Function of Compressive Stress

The results show that the value of G was smaller if it was measured at larger strain levels, and larger if it was measured at smaller strains. However, all of the

modulus values obtained in these tests corresponded to shear strains of 0.25 or smaller. Furthermore, this shear modulus was on the order of 10 to 25 times the shear modulus commonly measured for a steel-reinforced elastomeric bearing with 50 to 60 Shore A Durometer hardness. The value of G always exceeded 1.5 times the compressive stress level, and always exceeded 1.9 ksi regardless of the compressive stress level, as shown in Figure 4.4b. This indicates that CDP bearings will exert significantly larger forces on the bridge structure if subjected to the large shear strains commonly encountered in steel reinforced elastomeric bearings. It also indicates that the CDP bearing pad will have very small shear strains when the frictional resistance of the PTFE sliding surface is overcome because a well-designed PTFE surface should have a friction coefficient of approximately one order of magnitude smaller than this ratio.

Initiation of slip and the coefficient of friction between the test pad and the steel loading surface were evaluated. Slip originated from one edge of the bearing pad and progressed over the entire bearing surface. Subsequent slip occurred at a lower coefficient of friction after initial slip had occurred. The static coefficient of friction, μ_s, for initial slip between CDP and an unfinished steel loading surface varied between 0.18 and 0.27 for pads produced by Manufacturer A, with a mean value of 0.22. Tests on the other bearing pads suggested that similar coefficients are possible between CDP and smooth or finished concrete, and slightly larger coefficients are possible between CDP bearing pads and rough concrete surfaces. Cyclic slippage of the pad under service deformations is not tolerable because this slippage leads to delamination and deterioration of the pad, as noted with Category C damage in compression and rotation tests.

SD tests were not completed for Manufacturer B and C pads, but SD test data are briefly discussed because they are relevant to the development of design recommendations. The secant shear modulus, G, remained stable during the early cycles of the SD tests but decreased slightly during later cycles, as illustrated in Figure 4.5. This decrease in stiffness under repeated cyclic shear loading has been commonly noted for all elastomeric bearing types (Stanton and Roeder 1982), and it is not a deterioration in the material or bearing pad behavior.

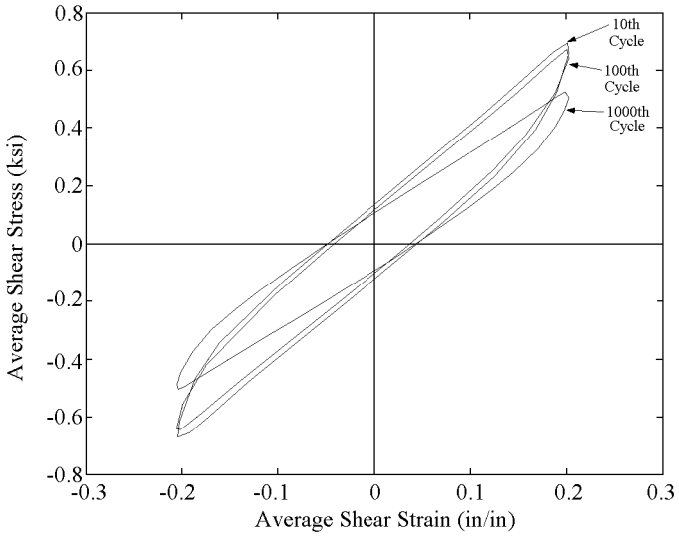

Figure 4.5. Dynamic Stress-Strain Curves

4.4. PROPOSED DESIGN LIMITS

The SS and SD tests showed that shear deformation is clearly damaging to CDP bearing pads. Internal cracking or separation of layers and splitting between layers from the outside, restrained edge of the bearing pad represent the more severe failure modes. However, neither of these failure modes resulted in the abrupt fractures noted with bearings that were subjected to compression and rotation. Because of their relatively large stiffness, cotton duck bearing pads may not be able to develop the large shear forces needed to develop the large shear strains. Slip may occur between the bearing and loading surface. This slip causes damage to the bearing pad and clearly reduces service life. Anchorage or restraint may reduce slip damage, but they increase the likelihood of splitting layers of the bearing pads.

The secant shear modulus, G, is needed to quantify the lateral force transmitted by the CDP bearing pad from the substructure to the superstructure for a given level of shear strain. For this purpose, G of CDP bearings can be taken as the larger of

$$G = 2\ \sigma \geq 2 \text{ ksi} \qquad \text{(Eq. 4-1)}$$

where σ is the average compressive stress on the bearing pad. Equation 4-1 provides a conservative estimate of the force to transfer and anchorage force required for the bearing pad.

Tests show that CDP may experience splitting type failures at large shear strains, γ, and so it is recommended that

$$\gamma \leq 0.10 \qquad \text{(Eq. 4-2)}$$

to control the adverse effects of this behavior. The static coefficient of friction, μ_s, between CDP and steel plates usually exceeded 0.2 for these tests. The coefficient between CDP and concrete would logically be expected to be larger. As a result,

$$\mu_s \leq 0.15 \qquad \text{(Eq. 4-3)}$$

is viewed as a conservative design limit. This limit may be used to avoid slip of the pad because the tests show that the slip causes rapid deterioration of pad performance. The large shear modulus combined with the observation that a well-designed PTFE sliding surface delivers coefficients of friction smaller than 0.1 means that the slip resistance and strain limit are unlikely to control the design of a CDP bearing pad when the pad is combined with a PTFE sliding surface.

CHAPTER 5
RECOMMENDATIONS FOR DESIGN AND QUALITY ASSURANCE

5.1. INTRODUCTION

Current provisions for the design of CDP are included in the AASHTO LRFD Bridge Design Specifications and the WSDOT Bridge Design Manual. In addition to those documents, quality control of CDP manufacturing process is largely defined in the Military Specification MIL-C-882E (dated January 1989). However, these specifications were implemented without experimental verification of the properties of CDP as required in the specification. Furthermore, the rationale behind the Military Specification control tests for bridge bearing applications is not documented or published.

The experimental research program described in this report was designed, in part, to evaluate and, where necessary, modify the current design and quality control provisions. The following sections present recommendations for design and quality control of cotton duck bearing pads used in bridge applications. Within a testing category, the experimental results have been distilled to develop design recommendations. Here these recommendations are compiled and presented to support modification of current specifications. A draft of the modified specification is provided in Appendix A. A design example using the proposed design expressions is also provided.

5.2. QUALITY CONTROL

Cotton duck bearing pads are manufactured under Military Specification MIL-C-882E (dated January 1989). The specification covers laminated cotton duck or cotton-polyester blend duck cloth that has been impregnated with oil resistant synthetic rubber. Within that document, the following material requirements are specified: composition and unit weight of the duck, construction tolerances, age, and density. In addition, load-deflection and permanent-set limits are specified and specific testing procedures are outlined. The permanent-set and load-defection tests are conducted on small (2 x 2-inch) sample pads. Two sets of samples are to be taken from each lot (using different strips). Before testing, the samples are inspected to evaluate defects, and the specimens are to be conditioned for 4 hours at room temperature.

Of particular interest during this research effort was a study of the quality assurance provisions, including the specifications for the tests to evaluate load-deflection and permanent-set limits. During the experimental study, the quality assurance tests were conducted on the pads of the three manufacturers. The test results were used to evaluate the effectiveness of the current specifications and provide guidance for the modification of the recommendations to better meet the performance requirements.

5.2.1. Permanent-Set Criteria

The permanent-set criteria are evaluated by testing two samples from each lot. The permanent-set values vary from 3, corresponding to a compressive stress of 500 psi, to 13, corresponding to a compressive stress of 10,000 psi. The test is conducted on a 2- x 2-inch pad as follows: (1) a 50-psi load is sustained for 5 minutes and the instrumentation is zeroed, (2) the load is increase at rate of 500 lb/min. to the target load and released, (3) the loss of height is determined as percentage of the zero-point height, (4) the next load cycle is applied to the pad within 5 minutes of release of the previous cycle.

During the experimental program, 0.75-inch and 2-inch thick samples from each manufacturer were subjected to the permanent-set criteria test. All of the samples met the criteria. These permanent-set test requirements appear to be implicitly satisfied if the bearing pad satisfies all other quality assurance measures. As a result, this test requirement is not included in the recommended modifications to the AAASHTO specifications.

5.2.2. Load-Deflection Criteria

The load-deflections tests are required on two 2- x 2-inch specimens from each lot. The deflections are measured at stress increments of 5 psi using a loading rate of 500 lb. per minute up to 2000 psi. During the experimental research program, specification tests were conducted on pad samples for 0.75-inch and 2-inch thick pads supplied from each manufacturer. The results are presented in figures 5.1 through 5.3.

Within the specification, a table of the required stress-deflection response is provided for different ranges of thickness. For this study, the deflection requirements were translated to strain. The minimum and maximum strain limits are presented in figures 5.1 through 5.3. The limits are indicated with solid circular markers on each figure.

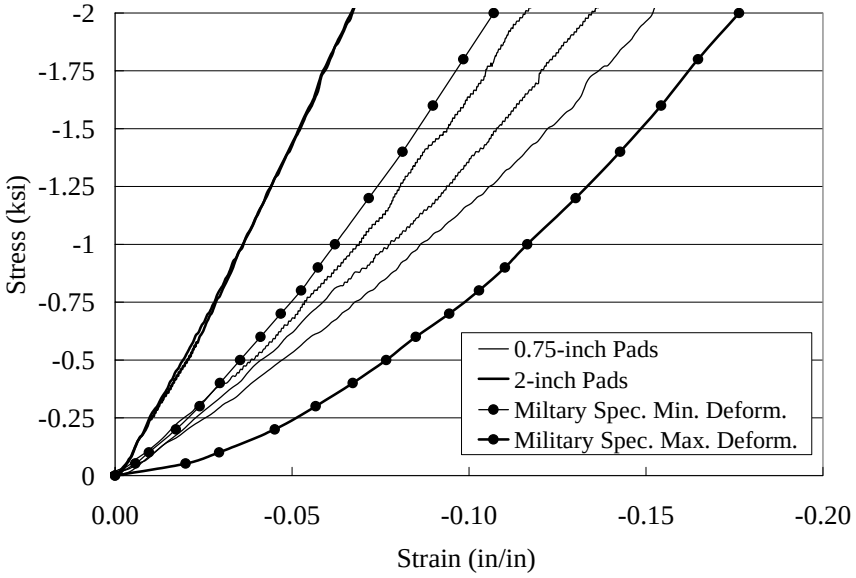

Figure 5.1. Evaluation of Manufacturer A Pads

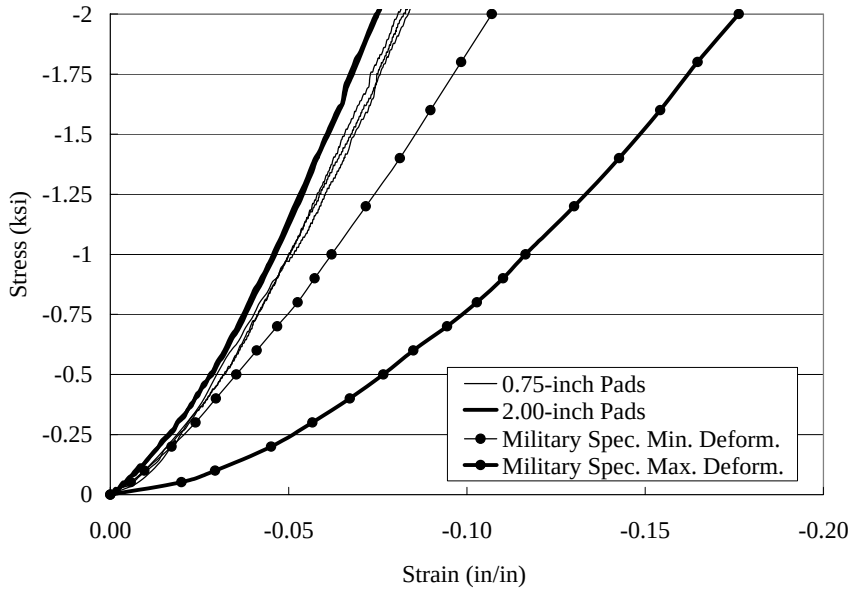

Figure 5.2. Evaluation of Manufacturer B Pads

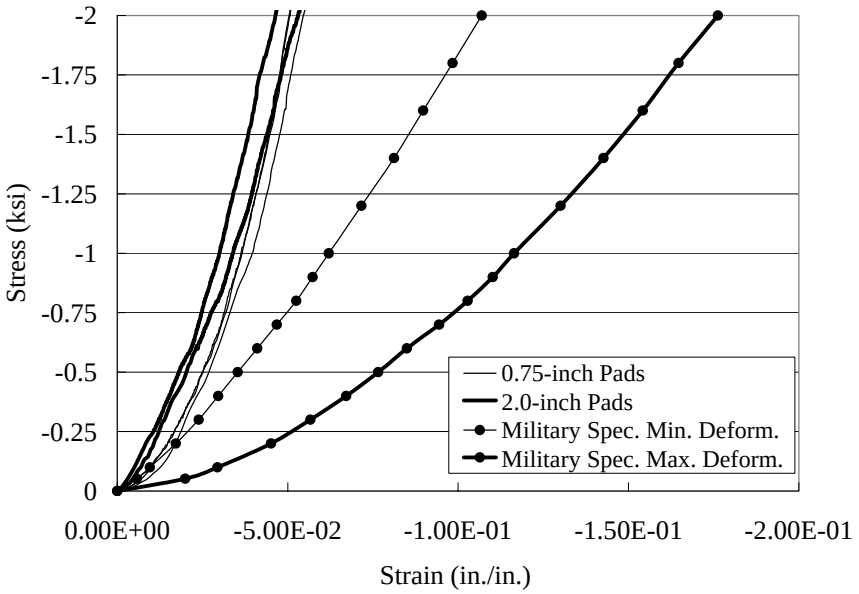

Figure 5.3. Evaluation of Manufacturer C Pads

All the pads tested had smaller strains than that allowed by the maximum-deformation limit. The results show that only the Manufacturer A pads fell within both of the specified limits. The remaining specimens failed to meet the minimum deformation limit.

The experimental research study showed that the minimum and maximum deformation limits have a strength influence on the pad performance. If the pad is too flexible, excessive deformations can result under the sustained load, which may affect bridge serviceability. In addition, there is a strong relationship between the stiffness of the pad and the failure strain, as shown in Figure 2.14. Therefore, pads that are very stiff (E_3 values that exceed 40 ksi) have small strain capacities and will not meet the rotation performance criteria. As a result, rotations of the load-deflection criteria are maintained within the proposed design recommendations.

5.2.3. Recommended Provisions for Quality Assurance

Currently the material requirements specified in the AASHTO LRFD Bridge Design Specification on Joints and Bearings Related to Elastomeric Pads (Section 14.7.6) does not provide guidance for testing to ensure engineering performance. The previous discussion indicates that modifications to the current Military Standard are necessary. The following recommendations are proposed.

1. Thickness limits: The proposed modifications to the specification, including design expressions, are based on the experimental testing program described herein and in the reference report by Roeder, Lehman, and Larson (2001). Therefore, the recommended quality assurance and design provisions are applicable to bearing pads up to 2 inches in total thickness. This limit is stipulated because experimental verification of CDP behavior is available only within this range. Thicker pads may perform adequately, but this study provided no evidence to evaluate this issue. Furthermore, thicker pads are less likely to be required with the increased compression and rotation capacity permitted by this work.
2. Stiffness testing requirements: It is recommended that guidelines for testing for quality assurance be provided in the AASHTO (and other applicable) Design Specification. Modified stiffness limits (relative to the Military Standard) are proposed. A testing protocol that is similar to the Military Standard is recommended. A minimum of two samples, 2 by 2 inches with the full sheet thickness, is to be tested. The test specimens must be conditioned for 4 hours at room temperature, $70^{o}F \pm 10\ ^{o}F$. Each specimen shall then be loaded in compression, perpendicular to the direction of lamination, where the origin of deflection and compressive strain measurements shall be taken at a compressive stress of 5 psi. The load shall be increased at a steady rate of 500 pounds per minute until the compressive load reaches 8000 pounds, and the load rate shall then be increased at a rate of up to 10,000 pounds per minute until failure of the specimen. Both the load and deflection shall be recorded during the test up to a load of 8000 lb. The specimen shall be loaded to a compressive stress of 10,000 psi without fracture or other failure. The average compressive strain of the specimens for that lot, at an average compressive stress of 2,000 psi, shall not be less than 0.07 in/in nor shall it be greater than 0.15 in/in. The entire lot shall be rejected if the CDP specimens fail to satisfy these test criteria.

   This range of strains is provided because all the pads that met these limits provided acceptable performance in this research program. Furthermore, all pads that failed

these design limits would not provide satisfactory performance with the proposed specification provided in Appendix A.

5.3. DESIGN RECOMMENDATIONS

The test results were used to develop design recommendations for each load or deformation category. Several design expressions are provided at the end of each chapter. The following summarizes the design expressions and suggested modifications to the AASHTO Bridge Design Specifications. A draft of the modified specification is provided in Appendix A.

5.3.1. Compression

CDP are designed to meet stress and deflection limits. Currently, the average compressive stress on CDP is limited to 1.5 ksi. A stiffness of 10 ksi is used to check deflection limits. The experimental research showed that the 1.5-ksi stress limit is too limiting, and the 10-ksi stiffness is too small. The following recommendations are made:

1. The average stress shall not exceed 3 ksi. The stress range shall not exceed 2 ksi. These limits are derived from Figure 2.18 to provide long-term serviceability and durability of CDP.

2. The stiffness of CDP is highly nonlinear. It is recommended that manufacturer-specific test data be used to provide a more accurate estimate of CDP stiffness. In lieu of this pad-specific test data, a secant modulus value of 30 ksi is recommended. The secant stiffness value range from 20 to 40 ksi. The recommended stiffness is an intermediate values of the measured 3-ksi secant modulus values for the Manufacturer A and B pads (pads that meet the revised quality control specification). A lower estimate of the secant stiffness will result in a more conservative estimate of the compressive-strain rotation limit. A higher estimate will result in a more conservative estimate of the uplift rotation limit.

3. The calculation of total compressive deflection of the pad must include the creep effects due to the sustained load. The experimental data indicated that for the range of the expected level of the sustained (DL) stress, a creep amplification factor of 2 is

recommended. Therefore, the total long-term deflection, Δ, may be calculated as follows:

$$\Delta = \frac{\sigma_{ll} - \sigma_{ll\_s}}{E_3} + 2\frac{\sigma_{ll} + \sigma_{ll\_s}}{E_3} \qquad \text{(Eq. 5.1)}$$

where E_3 = 30 psi in lieu of manufacturer specific data, σ_{ll} is the stress due to the live load, $\sigma_{ll\text{-}s}$ is the stress due to the portion of the live load that is sustained, and σ_{dl} is the dead load stress, all in ksi.

5.3.2. Shear

CDP are stiff in shear. The current AASHTO LRFD design specifications do not provide stiffness estimates in shear. In lieu of other experimental data, the shear modulus of CDP may be estimated as:

$$G = 2\sigma_s \geq 2ksi \qquad \text{(Eq. 5.2)}$$

The maximum shear stress is limited by the coefficient of friction. Study of the boundary conditions indicates that a reliable coefficient of friction value is:

$$\mu_s = 0.15 \qquad \text{(Eq. 5.3)}$$

5.3.3. Rotation

The current rotation design limits are based on limits on the compressive stress resulting from the maximum rotation. Experimental results indicated that the maximum rotation and the rotation range strongly influence performance, and the maximum rotation is determined by the maximum strain, not stress. The following expressions for the design of CDP for rotation are proposed:

1. Maximum strain: The experimental results indicated that pad failure (or fracture) is determined by the maximum compressive strain capacity of the pad. The limiting compressive strain is 0.20 inch/inch and the total strain, including the axial stress and rotation effects, can be estimated using Equation 5.4.

$$\varepsilon_T = \varepsilon_c + \frac{\theta_s L}{2 t_p} < 0.20 \qquad \text{(Eq. 5.4)}$$

where $E_c = \delta_s/\varepsilon_c$, where E_c is conservatively estimated to be 20 ksi in lieu of more accurate data for the specific bearing pads.

2. The maximum rotation and the rotation range that a CDP is subjected to determine the severity of delamination, or serviceability, damage. Figure 3.9 shows that both must be restricted to prevent excessive pad deterioration.

   The maximum rotation is limited to:

$$\theta_s = 0.8\frac{2t_p\varepsilon_c}{L} \qquad \text{(Eq. 5.5)}$$

   The rotation range is limited to:

$$\theta_L = \left(\frac{0.4t_p\varepsilon_c}{L}\right) \qquad \text{(Eq. 5.6)}$$

   where the limit shown in Figure 3.9 is reduced to account for additional rotation cycles (above the range of cycles used in the experimental program) that may occur over the lifetime of the pad.

3. In lieu of manufacturer-specific test data, the stiffness of CDP in rotation may be approximated as follows:

$$K_\theta = \{4.5 - 2.2\ S + 0.6\ \sigma_s\}\frac{E_c\ I}{t} \qquad \text{(Eq. 5.7)}$$

   where E_c = 30 ksi in lieu of more manufacturer-specific test data.

5.4. DESIGN EXAMPLE

To provide a better understanding of the proposed design limits, a design example is provided. The pad area and thickness are determined by using the compressive and rotation stress limits, respectively. In the example, it is expected that a PTFE sliding-surface will be used to accommodate the shearing deformations, and therefore, the shear provisions are not used.

Given

The dead and live load stress are as follows:

P_{dl} = 75 kips P_{ll} = 50 kips

The maximum rotation and rotation range are

θ_s = 0.02 rad θ_{ll} = 0.005 rad

Design for Compression

Using the limits on the maximum compressive stress and the stress range, the pad area is determined as follows:

$$\frac{(P_s = P_{dl} + P_{ll})}{A} \le 3ksi \rightarrow A \ge 42in^2$$

$$\frac{(P_{ll})}{A} \le 2ksi \rightarrow A \ge 25in^2$$

Try a 5-in. x 9-in. pad (w = 5 in. perpendicular to axis of rotation).

Design for Rotation

The pad thickness is controlled by the rotation design limits as expressed by equations 5.4-5.6. Maximum thickness resulting from these equations controls the design.

Maximum Strain

Express Equation 5.4 in terms of pad thickness. Note minimum value of E_c (= 20 ksi) was used to calculate ε_c.

$$t_p = \frac{\theta_s L}{2(\varepsilon_{cr} - \varepsilon_c)}$$

$$t_p \ge \frac{0.02 * 5}{2 * (0.2 - \frac{125}{(45 * 20)})} \rightarrow t_p \ge 0.82in.$$

Maximum Rotation

Express Equation 5.5 in terms of pad thickness.

$$t_p = \frac{\theta_s L}{1.6(\varepsilon_c)}$$

$$t_p \geq \frac{0.02 * 5}{1.6 * \frac{125}{(45 * 20)}} \rightarrow t_p \geq 0.45 in.$$

Rotation Range

Express Equation 5.6 in terms of pad thickness.

$$t_p = \frac{\theta_L L}{0.4(\varepsilon_c)}$$

$$t_p \geq \frac{0.005 * 5}{0.4 * \frac{125}{(45 * 20)}} \rightarrow t_p \geq 0.14 in.$$

Design Solution

Use a 5-in. x 9-in. x 1-in. pad with 5 in. perpendicular to the axis of rotation. Note that it is easier to achieve the rotation limits with a rectangular pad, and design aids (e.g., spreadsheets) should be developed to favor CDP plan aspect ratios that exceed 1.

CHAPTER 6
SUMMARY AND CONCLUSIONS

6.1. SUMMARY

Cotton duck bearing pads (CDP) are sometimes used to support loads and accommodate movements in bridge design. CDP are preformed elastomeric pads consisting of thin layers of elastomer interlaid with fabric, and they are manufactured under military specifications with limited guidance from the AASHTO. Because of limited research on CDP, the AASHTO design recommendations do not fully optimize CDP design. To improve engineering design provisions, CDP bearing pads were evaluated experimentally, and the data were used to establish design models for predicting this behavior, to determine the variation in behavior expected with different bearing pad manufacturers, and to develop design recommendations.

CDP bearing pads from three different manufacturers were tested, and the test program included dynamic and static (or monotonic) tests of bearings in shear, compression, and rotation. An initial study, sponsored by Arkansas State University, evaluated the behavior of pads from a single manufacturer. This research studied two additional manufacturers and is a follow-up study of that earlier research program. Forty-four static compression tests, 17 cyclic compression tests, and ten long-duration (creep) compression tests were completed. Seventeen static rotation tests and 28 dynamic rotation tests were performed. Ten static shear tests and eight dynamic shear tests were performed. In general, the static tests were used to evaluate strength, stiffness, deformation limits, and general pad behavior. The dynamic tests examined durability and performance under repeated loading and deformation.

The intermediate and final damage states from these tests were as follows:

- Category A - No observable damage.
- Category B - No damage other than secretion of oil or wax.
- Category C - Delamination of CDP layers.
- Categories D and E - Fracture, cracking or splitting.

These damage states were used to develop a design method to ensure the serviceability and durability of the pads.

The results of this test program were used to develop design recommendations, which are discussed in earlier chapters and synthesized in Chapter 5. In addition, Appendix A includes a draft of proposed wording for modification of the AASHTO LRFD Specifications to include these design recommendations. A design spreadsheet has also been developed in Microsoft EXCEL to facilitate the design. This spreadsheet is separate from this report.

6.2. CONCLUSIONS AND RECOMMENDATIONS

A number of conclusions were drawn from this research. Some of the more important conclusions include the following:

- CDP tolerates large compressive stresses, significant bearing rotation, but limited shear deformation. These capacities depend on the stiffness and deformation capacity of the CDP. The limited shear capacity is frequently overcome by the addition of a PTFE sliding surface.
- The stiffness and deformation capacity of the CDP varies from manufacturer to manufacturer. Quality control testing, as discussed in Chapter 5, is needed to assure that the bearing pad provides adequate performance.
- The maximum compressive strain limit, ε_{CR}, of CDP is approximately 0.25 or larger if the bearings are manufactured to the quality control standards presented in this report. Given the average ε_{CR} and the standard deviation of that value, a strain limit of 0.2 is proposed as a statistically reliable limit for combined rotation and compression.
- Serviceability limits for bearings in compression are primarily manifested as delamination of elastomer layers or secretion of oil and wax from the bearing pads. A maximum compressive stress limit of 3000 psi for maximum dead plus live loads and a maximum stress limit of 2000 psi for live loads are recommended to control delamination.
- CDP bearing pads are quite stiff, and stiffness parameters are defined for compression, rotation, and shear deformation. Furthermore, CDP bearing pads

are subject to creep deformation, and they do not fully recover the instantaneous strain on unloading. Approximate design limits suggest that the residual strain on unloading will be approximately 20 percent to 25 percent of the maximum instantaneous compressive strain. Long-term creep strains are approximately 100 percent of the short duration strain under long-term loading at the stress levels commonly used in design.

- The rotational capacity of CDP is limited by the compressive strain limit under combined short duration loading and uplift of the bearing pad. As a result, the strain limit noted above is directly applied to the combined compression and rotation design requirements.
- Uplift causes delamination and reduced service life. Uplift damage depends upon the maximum total rotation as well as the rotation range caused by the live load variation. Separate rotation limits are provided for these conditions.
- Maximum rotation is limited to 80 percent of the theoretical uplift rotation, and the rotation range caused by design live loads is limited to 20 percent of the theoretical uplift rotation. These limits are imposed to control delamination. They are related to uplift, but they are smaller than the theoretical uplift because the research shows that strain is not fully recovered after unloading of these bearing pads.
- Shear deformation caused by translational bridge movement is limited for CDP bearing pads because interlayer splitting occurs at larger shear strains. As a consequence, the shear strain due to translational movement is conservatively limited to approximately 10 percent.
- Bearing pad stiffness is defined for compression, shear, and rotation. Compressive stiffness appears to be fairly independent of the shape factor and is a highly nonlinear function of the compressive strain/stress. A simplified, secant stiffness value is proposed for use in design. The shear stiffness depends on the level of the compressive stress, but a minimum stiffness of 2 ksi is defined. The rotational stiffness depends on the shape factor and the level of the compressive stress.

- PTFE sliding surfaces are commonly used to accommodate translational movements in CDP bearing pads because of the above shear strain limit. However, the coefficient of friction must be low enough to prevent excess shear deformation of the pad and to prevent slip of the pad under this friction load. The tests suggest that the coefficient of friction between CDP and steel load surfaces is 0.15 or larger. PTFE employs compressive bearing stress limits to control creep and cold flow, and these bearing stress limits will likely limit the bearing pad stress if the PTFE is not properly confined.
- Stiffness, strength and strain or deformation capacity varies widely among manufacturers. This variation appears to be related to elastomer compound and manufacturing methods. Quality control measures were developed (see Chapter 5) to assure that CDP bearing pads fall within the acceptable bounds required by the design recommendations. Certification testing as defined in the specification proposals (see Appendix A) is needed if these design provisions are to be successfully used in practice.

Appendix A

Proposed LRFD Specification and Commentary

The following definitions will need to be added to 14.3 Notation

K = rotational stiffness of CDP bearing pads (moment per radian of rotation) (14.7.6.3.5.2)
t_p = total pad thickness for CDP bearing pads (14.7.6)
ε_T = total maximum compressive strain due to combined compression and rotation (14.7.6.3.5.2)
ε_c = total maximum compressive strain due to compression from total live and dead load (14.7.6.3.5.2)

14.7.6 Elastomeric Pads

14.7.6.1 GENERAL

The provisions of this article shall be taken to apply to the design of;

- plain elastomeric pads, PEP;
- pads reinforced with discrete layers of fiberglass, FGP;
- Steel-reinforced bearings; and
- Cotton duck bearing pads, CDP, with closely spaced layers of cotton duck fabric and manufactured and tested under compression in accordance with Military Specification MIL-C-882.

Layer thicknesses in FGP may be different from one another. For steel-reinforced elastomeric bearings designed in accordance with the provisions of this section, internal layers shall be of the same thickness and cover layers shall be no more than 70 percent of the thickness of internal layers.

The shape factor for FGP and PEP pads and steel-reinforced elastomeric bearings covered by this article is determined as specified in Article 14.7.5.1.

The shape factor for CDP shall be based upon the total pad thickness, t_p.

14.7.6.2 MATERIAL PROPERTIES

The materials shall satisfy the requirements of Article 14.7.5.2 except that the shear modulus shall be between 0.080 and 0.250 KSI and the nominal hardness between 50 and 70 on the Shore A scale, and shall conform to the requirements of Section 18.2 of the AASHTO LRFD Bridge Construction Specifications. This exception shall not apply to steel-reinforced elatomeric bearings designed in accordance with the provisions of this section.

The shear force on the structure induced by deformation of the elastomer in PEP and FGP shall be based on a G value not less than that of the elastomer at 73^{O}F. Effects of relaxation shall be ignored.

CDP is manufactured to Military Standards MIL-C-882E except that this specification supersedes those provisions where provided. The cotton duck reinforcement shall be either a two ply cotton yarn or a single ply 50-50 blend cotton-polyester. The fabric shall be have a minimum tensile strength of 150 lb/inch width when tested by the grab method. The filling count shall be 40 ± 2 threads per inch, and the warp count shall be 50 ± 1 threads per inch thickness. The CDP provisions included in this section are only applicable to bearing pads up to 2 inches in total thickness.

A lot of preformed CDP is defined as a single sheet that is continously formed to a given thickness except that a single lot shall not exceed 2500 pounds of material. A minimum of 2 samples from each lot shall be tested. The samples shall be 2 by 2 inches with the full sheet thickness. The test specimens shall be conditioned for 4 hours at room temperature $70^{o}F \pm 10\ ^{o}F$. Each specimen shall then be loaded in compression, perpendicular to the direction of lamination. The origin of deflection and and compressive strain measurements shall be taken at a compressive stress of 5 psi. The load shall be increased at a steady rate of 500 pounds per minute until the compressive load reaches 8000 pounds, and the load rate shall then be increased at a rate up to 10,000 pounds per minute until failure of the specimen. The load shall be recorded during the test, and the deflection shall be recorded until the compressive load reaches 8000 lbs. The specimen shall be loaded to a compressive stress of 10,000 psi without fracture or other failure. The average compressive strain of the specimens for that lot shall at an average compressive stress of 2 KSI shall not be less than 0.07 in/in nor shall it be greater than 0.15 in/in. The entire lot shall be rejected if the CDP specimens fail to satisfy these test criteria.

14.7.6.3 DESIGN REQUIREMENTS

14.7.6.3.1 Scope

-------- No change to this article ---------

14.7.6.3.2 Compressive Stress

At the service limit state, the average compressive stress, σ_s, in any layer shall satisfy:

- for PEP

$$\sigma_s \leq 0.80 \text{ KSI} \qquad (14.7.6.3.2\text{-}1)$$

- for FGP

$$\sigma_s \leq 1.0\ G\ S \leq 0.80 \text{ KSI} \qquad (14.7.6.3.2\text{-}1)$$

- for CDP

$$\sigma_s \leq 3 \text{ KSI} \qquad (14.7.6.3.2\text{-}3)$$

and

$$\sigma_L \leq 2 \text{ KSI} \qquad (14.7.6.3.2\text{-}4)$$

In FGP, the value of S used shall be that for the greatest distance between the midpoint of double reinforcement layers at the top and bottom of the elastomer layer.

14.7.6.3.3 Compressive Deflection

In addition to the provisions of Article 14.7.5.3.3, the following shall also apply:

Inlieu of using specific product data, the compressive deflection of FGP should be taken as 1.5 times the deflection estimated for steel-reinforced bearings of the same shape factor in Article 14.7.5.3.3.

For CDP, the instanteous deflection shall be determined by

$$\delta = \frac{\sigma_s}{E_c} t_p \qquad (14.7.6.3.3\text{-}1)$$

The compression modulus, E_c, shall be taken as 30 ksi for short term deflections in the absence of other more rationally determined information for the CDP bearing pads. Creep deflections shall be considered for permanent or long term loading. Long term deflections, including creep, shall be estimated multiplying instanteous deflections due to long term loads by 2.0.

The initial compressive deflection of a PEP or in any layer of a steel-reinforced bearing at the service limit state without impact shall not exceed $.07h_{rt}$.

14.7.6.3.4 Shear

The horizontal bridge movement shall be computed in accordance with Article 14.4. The maximum shear deformation of the pad, Δs, shall be taken as the horizontal bridge movement, reduced to account for the pier flexibility and modified for construction procedures. If a low friction sliding surface is used, Δs, shall be taken as the deformation corresponding to first slip.

The provisions of Article 14.7.5.3.4 shall apply, except that the pad shall be designed as follows:

- for PEP and FGP:

$$h_{rt} > 2\,\Delta_s \qquad (14.7.6.3.4\text{-}1)$$

- for CDP:

$$h_{rt} > 10\,\Delta_s \qquad (14.7.6.3.4\text{-}2)$$

The shear modulus, G, for CDP may be conservatively estimated as

$$G = 2\,\sigma_s \qquad (14.7.6.3.4\text{-}3)$$

but G shall not be less than 2 ksi.

14.7.6.3.5a Rotation

------ No Change in this section ----------

14.7.6.3.5b Rotation of PEP

------ No Change in this section ----------

14.7.6.3.5c Rotation of CDP

The maximum compressive strain due to combined compression and rotation of CDP, ε_T, shall not exceed

$$\varepsilon_T = \varepsilon_c + \frac{\theta_s L}{2 t_p} < 0.20 \qquad (14.7.6.3.5c\text{-}1)$$

where

$$\varepsilon_c = \frac{\sigma_s}{E_c} \qquad (14.7.6.3.5c\text{-}2)$$

Rotation shall be limited so that

$$\theta_s = 0.80 \frac{2 t_p \varepsilon_c}{L} \qquad (14.7.6.3.5C\text{-}3)$$

and

$$\theta_L = 0.20 \frac{2 t_p \varepsilon_c}{L} \qquad (14.7.6.3.5C\text{-}4)$$

where

σ_s = service average compressive stress due to total load associated with the maximum rotation (psi)

L = length of a CDP bearing pad in the plane of the rotation (inch)

t_p = total thickness in CDP pad (inch)

θ_L = maximum rotation of the CDP pad due to live load only (RAD)

θ_s = maximum service rotation of the CDP pad due to total load and tolerances (RAD)

The rotational stiffness of CDP bearing pads, K, shall be defined as

$$K = \{4.5 - 2.2\ S + 0.6\ \sigma_s\} \frac{E_c I}{t_p} \qquad (14.7.6.3.5C\text{-}5)$$

where

I = second moment of area about the centroidal axis of the bearing pad which is normal to the plan of rotation

14.7.6.3.5d Rotation of FGP and Steel Reinforced elastomeric Bearings

------ No Change in this section ----------

No changes in sections 14.7.6.3.6 and later

Commentary

C14.7.6.1

Elastomeric pads have characteristics which are different from those of steel reinforced elastomeric bearings. PEP is weaker and more flexible because the pad is restrained from bulging by friction alone, (Roeder and Stanton 1986, 1983). Slip inevitably occurs, especially under dynamic loads, causing larger compresive deflections and higher internal strains in the elastomer.

In pads reinforced with layers of fiberglass, the reinforcement inhibits the deformations found in plain pads. However, elastomers bond less well to fiberglass, and the fiberglass is weaker and more flexible than steel, so the fiberglass pad is unable to carry the same loads as a steel reinforced bearing (Crosier et al. 1979). Fiberglass pads have the advantage that they can be cut to size from a large sheet of vulcanized material.

Pads reinforced with closely spaced layers of cotton duck typically display high compressive stiffness and strength, obtained by the use of very thin elastomeric layers. However, the thin layers also give rise to high shear and rotational stiffness, which could lead to higer stiffness than found in layered bearings. These increased shear and rotational stiffnesses lead to larger moments and forces in the bridge and reduced movement and rotational capacity of the bearing pad. As a consequence CDP is often used with a PTFE slider on top of the elastomer pad (Nordlin et al. 1970).

C14.7.6.2

The elastomer requirements for PEP and FGP are the same as those required for steel reinforced elastomeric bearings.

CDP is made of elastomers with hardness and properties similar to that used for PEP and FGP. However, the closely spaced layers of duck fabric reduce the indentation and increase the hardness of the finished pad to the 85 to 95 durometer range. CDP is manufactured from standards with are derived from military specifications. Extensive research programs on CDP provided by 3 major manufacturers was completed (Lehman, Roeder and Larson 2003). This research shows that CDP frequently do not satisfy the full requirements of the military specification, because manufacturers do not consistently perform the required verification tests. As a result, important design requirements for CDP are restated from the original military specification here to assure that bridge engineers are aware of and verify these minimum requirements, since the these requirements are essential to the good performance of the bridge bearing pad. The tests and strain limits are also required by military specifications, but the limits used here are somewhat different than the military specification, because research shows that the wider acceptance limit will result in good pad performance. Research has also shown that pads that fall outside these stress and strain limits do not provide good performance and will not achieve the requirements outlined in this specification. CDP has a shape factor effect, and small test pads are normally more flexible than normal bearing pad geometry. However, the shape factor effect is much less pronounced than that observed with steel reinforced bearings, PEP of FGP.

C14 7.6.3.1

---------- N0 change to this article ----

C14.7.6.3.2

The compressive stress limits from CDP are based upon serviceability limit states, and stiffness and behavior is less sensitive to shape factor but very sensitive to manufacturer. The certification test requires that 2x2 pads tested from each lot of material exceed 10 ksi, and research shows that this will assure that normal sized pads can also exceed that minimum resistance. An extensive test program (Lehman, Roeder and Larsen 2003) of CDP shows that total compressive stress must be limited to 3 KSI, because delamination may occur at higher stress levels. In addition, the stress range associated with variable loads must be limited to 2 KSI to control this delamination. CDP do not fail under monitonically compressive stress values that are significantly larger than this stress limit. Dramatic failure may occur with pads that satisfy the quality control acceptance criteria of this specification, when the maximum compressive strains exceed approximately 0.25. However, bearing pads which meet the strain and stiffness limits which are provided in 14.7.6.2 will not achieve this failure strain under pure compressive load.

The reduced stress limit for steel-reinforced elastomeric bearings designed in accordance with these provisions is invoked in order to allow these bearings to be eligible for the less stringent test requirements for elastomeric pads.

C14.7.6.3.3

The compressive deflection with PEP and FGP will be larger and more variable than those of steel reinforced elastomeric bearings. Appropriate data for these pad types may be used to estimate their deflections. In the absence of such data, the compressive deflection of a PEP and FGP may be estimated at 3 and 1.5 times the deflection estimated for a steel reinforced elastomeric bearing of the same shape factor in Article 14.7.5.3.3.

The compressive deflection of CDP is less variable as a function of size and geometry than steel-reinforced elastomeric bearings, but is even more variable as a function of manufacturer. CDP is typically stiff in compression. The shape factor may be computed but it has a different meaning and less significance to the compressive deflection than it does for FGP and PEP. As a result, the maximum compressive deflection for CDP can be estimated based upon an average compressive strain. An extensive research study (Lehman, Roeder, and Larsen 2003) shows that E_c variese between 20 and 40 ksi for CDP bearing pads that meet the acceptance criteria of 14. 7.6.2. This modulus is a secant modulus at 3 ksi, since this secant modulus represents the range of service loads expected for these bearing pads. The 30 ksi estimates represents a simple intermediate limit that approximates the behavior under the full range of service conditions. However, research has shown that the stiffness varies from manufacturer to manufacturer and by different manufacturing methods. Therefore, it is permissible to use an value of E_c that was rationally determined from experiments performed on the product used for the specific bridge bearing pad application. This rational determination may be made by obtaining an average secant modulus of stress-strain curve between the stress levels of 0.1 and 3 ksi from the material certification tests described in 14.7.6.2.2. The 0.1 ksi lower stress limit is proposed to avoid the uncertainties caused by initial seating of the bearing pad

under compressive load. The 3 ksi upper stress limit is proposed as an upper limit for serviceability of CDP bearing pads.

C14.7.6.3.4

The deformation in PEP and FGP are limited because these movements are the maximum tolerable for repeated and long-term strains in the elastomer. These limits are intended to ensure serviceable bearings with no deterioration of performance and they limit the forces that the pad transmits to the structure.

In CDP, the shear deflection is limited to only 1/10 of the total elastomer thickness. There are several reasons for this limitation. First, experiments show that CDP may split and crack at larger shear strains. Second, CDP has much larger shear stiffness than that noted with steel reinforced elastomeric bearings, PEP and FGP, and so the strain limit assures that CDP pads do not cause dramatically larger bearing forces to the structure than do other bearing systems. Third, the greater shear stiffness means that relative slip between and CDP pad and the bridge girders is likely, and the slip may lead to abrasion and deterioration of the pad as well as other serviceability concerns. Slip may also lead to increased costs because of anchorage and other requirements. Finally, CDP pads are harder than PEP and FGP, and so they are very suitable for the addition of PTFE sliding surfaces to accommodate the required bridge movements. As a result, CDP with large translational movements are invariably designed with PTFE sliding surface.

The shear modulus, G, for determination of the bearing pad resistance is defined as the larger of Eq. 14.7.6.3.4-3 and 2 ksi. These stiffness results fit well with the observed experimental behavior.

C14.7.6.3.5a

------ No Change in this section ----------

C14.7.6.3.5b

------ No Change in this section ----------

C14.7.6.3.5c

Rotation and combined compression and rotation of CDP are controlled by compressive strain limits and delamination requirements. Compressive strains are used rather than shear strains because the closely space cotton duck layers restrict the apparent material stiffness for the Poisson effect. Experiments show that CDP that meets the testing requirements of 14.7.6.2.2 will not suffer a serious fracture or failure until a combined compressive strain exceeds 0.25. Creep strains do not contribute to this fracture potential. Design equation 14.7.6.3.5c-1 limits this compressive strain to 0.2, because the design is made with service loads, and research shows that the 0.20 strain limit is sufficiently far from the average failure strain to assure a β factor of 2.5 for LRFD design. To provide a more conservative estimate of the compressive strain, a minimum E_c value of 20 ksi is recommended in the calculation of ε_c.

Delamination due to rotation is associated with uplift or separation between the bearing pad and the load surface. Experiments show that this delamination is related to both the range of cyclic rotation occuring during the life of the bridge, and the maximum total rotation. Delamination does not result in a fracture or immediate failure of the bearing pad, but it results in a significant reduction in the bearing service life. Cyclc rotation associated with live loads represents the more severe delamination problem, and Equation 14.7.6.3.5c-3 provides this design limit. Rotational fatigue experiments show that delamination does not occur if the cyclic rotation does not exceed 0.3 $\frac{2\, t_p\, \varepsilon_c}{L}$. However, the cyclic fatigue tests were necessarily limited to 6,000 to 60,000 cycles because of the long time required to complete fatigue tests. As a result, the design live load is considered to be a large design load that may occur several million times during the life of the bridge, and a larger design load (1.5 time the design live load) are used to evaluate this delamination fatigue limit. Equation 14.7.6.3.5c-3 results from this work.

Research also shows that delamination is also influenced by maximum rotation level. CDP do no recover all of their compressive deformation after unloading, and Equation 14.7.6.3.5c-2 recognizes approximately 20% residual compressive strain and limits uplift due to the maximum rotation in recognition of the delamination potential.

The rotional stiffness is provided for CDP in Equation 14.7.6.3.5C-5. When rotation is multiplied by K, the product is a estimate of the moment developed in the bearing pad and transferred from the substructure to the superstructure. The moment is of interest for many bearing types, but it is of more critical interest to CDP, because moveable CDP bearing pads are normally designed with PTFE sliding surfaces to develop the translational movement capacity. The presence of moment in the bearing pad results in edge bearing stress ($\approx \frac{M\, L}{2\, I}$ where I is the moment of area of the PTFE bearing surface) in addition to the average compressive stress. The edge bearing stress is severely limited for unconfined PTFE. As a result, this may require that reduced average compressive stress be used with CDP bearings that employ PTFE sliding surfaces (say σ_T less than 1.5 or 2 ksi) or the PTFE surface may be confined within a steel plate bonded to the CDP.

The compressive strain limits used in design CDP are larger than those tolerated in steel reinforced bearings, but they have been justified by experimental results when the CDP meets the requirements of this specification. This does not suggest that CDP is generally superior to steel reinforced bearings. A well designed steel reinforced bearing is likely to provide superior long term performance to that noted with CDP, but CDP can be designed and manufactured quickly and may provide good performance under a range of conditions.

C14.7.6.3.6 and later

------ No Change in these sections ----------